# Antal Kerpely Doctoral School of Materials Science and Technology

*Foam glass production and characterization based on waste materials: container glass, cathode ray tube glass, and aluminium dross*

A Dissertation Submitted in Partial Fulfillment of the Requirements for the Degree of Doctor of Philosophy in Ceramics Engineering as a Part of Stipendium Hungaricum Scholarship in Material Science and Technology

By

**Meriem Sassi**

Supervisor

**Dr. Andrea Simon, Associate Professor**

Head of the Doctoral School

**Prof. Dr. Valéria Mertinger**


Institute of Ceramic and Polymer Engineering

Faculty of Materials and Chemical Engineering

University of Miskolc

Miskolc, Hungary

# Contents

# List of figures

# List of tables

# Chapter 1

# Introduction

Increasing energy efficiency and lowering the energy consumption of buildings have become very relevant in the last decades. One of the directions for solving this problem is to minimize the energy used in space heating and cooling, by enhancing the thermal insulation efficiency of materials used in building construction [1].

As a material for thermal insulation, reed panels were popular during the 19th century, though their hygroscopicity was poor, later on, bituminous coatings increased their flammability. Edward Perry [2] invented mineral wool insulation in Wales in 1840 for pipes and machine insulations to reduce their heat loss and reduce the risk of accidents, but the production was discarded due to the harmful effects on workers. In the 1870s and 1880s, trials to upgrade the thermal insulation qualities of ceramic bricklaying elements were conducted. Unfortunately, its insulating capacity was not as good as expected and it had poor mechanical strength. In the 1931s, an experiment to produce foam glass took place using silica, combustible material (lignite, coal, wood), and foaming agents (hydrochloric acid, sodium hydroxide solution) at 1500°C. It is considered one of the best thermal insulation materials. It is durable and chemical resistant. In 1932, the Mendeleev Institute of Moscow developed another method to create foamed glass by mixing finely powdered glass with calcium-carbonate ($CaCO_3$) as a foaming agent and firing at 850°C [2]. Many patents were granted at the same time which increased the uncertainty about the initial creator of foam glass. It was in 1934 that a laboratory technician at the Pittsburgh Plate Glass & Corning Glass Works (Pennsylvania, USA) used finely powdered silica, borax, and zinc oxide in an attempt to create additional pores in the foam by adding different foaming agents (air, water-vapor). The production of commercial foam glass started in 1943, in Port Allegany (Pennsylvania, USA) [2]. After the 1950s, new thermal insulation materials were introduced like polyester foam (PES) and polyethylene foam (PE). In the 1970s, new kinds of foams appeared such as phenolic foam (PF) and formaldehyde foam (UF) while melamine foam (MF) was invented in the 1990s [2]. Eco-friendly foams, present a revolutionary product in diverse fields, whether it is metallic, polymeric, or ceramic foams. Nowadays, the industrial revolution and the extensive production of solid waste revert the exhaustion and depletion of natural resources causing an increase in the ecological problems

and the costs of the mineral raw materials which explains the elevated unit price of the commercial foam glass [1].

Converting waste material into functional products or partially replacing raw materials with waste is a key component from the economic and ecologic point of view. A clear understanding of the types, quantities, and characteristics of the waste will improve waste management strategies and green processing. Waste materials can be categorized into different types depending on the origin, aspect, and characteristics of the materials. The easiest way is to classify it into biodegradable wastes and non-biodegradable wastes. Biodegradable materials are usually organic waste that can be decomposed by microorganisms. Non-biodegradable wastes are usually divided into recyclable and hazardous waste. Recyclable waste can be transformed into new functional products such as paper, glass, and metals. Hazardous waste includes items harmful to the fauna and flora and requires special handling and proper disposal. It contains materials that are toxic, reactive, corrosive, and flammable, usually generated by chemical plants, heavy and light manufacturing, manufacturing of petroleum and coal products, agricultural chemicals (pesticides, fertilizers), power plants, mineral extraction, and processing [3]. Besides, hazardous waste also comes from our daily products like batteries, electronics paints, pharmaceutical products, and cosmetics. According to the United Nations Environment Program (UNEP), we produce 400 million tons of hazardous waste each year - almost 13 tons a second [4]. Other than harming nature and animals, some elements in the waste can adversely affect humans, causing damage to DNA, reproductive problems, and birth defects [4]. Meanwhile, the disposal costs of those materials are too high and require special handling and sealing especially with the limited number of facilities dealing with them [4].

The best strategy to manage hazardous waste safely and effectively is to incorporate them into building material fabrication. The research below will ensure the production of foam glass from 100 % waste material where two kinds of hazardous waste were incorporated. The goal is to reduce the production price and increase the insulation capacity to produce affordable and reliable insulating material without neglecting environmental protection.

Foam glass was successfully made based on container glass material (cullet), cathode ray tube (CRT) glass, and aluminum dross. The physical and chemical characteristics were examined with a special focus on the effect of the foam glass composition on compressive strength, microstructure, density, water absorption, and thermal conductivity. This was done without ignoring the chemical stability of the final product due to the hazardous aspects of the raw materials (CRT glass and aluminum dross). The lifespan and durability of the foam glass were evaluated under normal and critical conditions.

## 1.1. State of the art

Foam glass is an ultra-light material insulating material with high chemical stability where density and texture can vary depending on the initial chemical composition. Foam glass produced by manufacturers has compressive strength ranging between 0.6 to 1.0 MPa, low density (120-160 kg/m$^3$), low thermal conductivity (0.04-0.07 W/m·K), and low water absorption ($\leq$ 5-6 kg/m$^2$ after 28 days) [5] [6] [7]. The basic components of foam glass - primarily glass and foaming agents - are mixed and heated above the softening point of the glass. Then, the foaming agent decomposes and releases gaseous products, which drive the expansion of the glass [8] [9].

Foam glass is well known for the construction of the foundations of an energy-saving Passive House. It has great insulation characteristics and resistance to moisture. It helps remove the need for an extra layer of alternative insulating materials such as expanded polystyrene. In addition, it reduces friction angle for the construction of houses on gradients, and difficult terrain [10] [11]. It is used too in pavements, roads, harbour areas, bridge embankments, ramps, and culvert foundation work by reducing the load on the subsoil as well as reducing the horizontal load on structures in the vicinity [12] [13] [11] [14]. Foam glass aggregate is designed to keep its structural bulk lightening properties for a minimum of fifty years [11]. The use of foam glass in pipe trenches can reduce the need for maintenance work as well as increase the structure´s operational life. If zinc-coated pipes are employed a geotextile or other type of membrane should be used in between the pipe and the foamed glass [11].

**Basic raw materials**

Foam glass is primarily composed of up to 98% glass powder. The original glass foam composition was formulated using virgin glass only. Currently, there are several foam glass production plants that are using up to 98 wt% post-consumer glass waste. EU-28 Market trade in glass waste increased from roughly 250 000 t/month in 2002 to approximately 350 000 t/month in 2007 and to 430 000 t/month in 2013 [15]. Glass exports are considered minor (4% of the exported volume). By comparing the European glass production volume (30 Mt/year) with the European glass cullet market (9 Mt/year), we can estimate that a third of the total glass production would be reusable as cullet.

In terms of glass waste pricing, fluctuations are observed, but it stays generally between 40 and 50 pounds per tonne. Cullet market prices differ according to the colour of the glass, without considering the price of the sorting and treatment process. From Figure 1 we can see that clear recovered glass has a higher price, while mixed glass can sometimes have a negative price.

Another factor affecting the prices is the initial sorting by citizens. For example, British and German residents tend to sort glass containers by colour before placing it in the receptacles provided for collection [15].
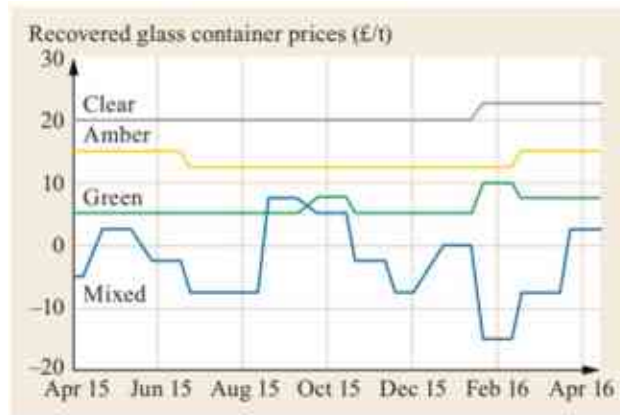


**Figure 1.** Recovered glass container price according to colour [15]

The most common waste glasses are hollow glass and flat glass. Hollow glass is referred to as container glass. It is used as packaging mostly in food, beverages, perfumes, and medicine. The production volume is about 20Mt/year. Firstly, the glass ceramics in the post-consumer waste glass should be removed as it causes imperfection in the final product. Secondly, glass waste must be sorted to separate the glass objects according to colour or apply chemicals to eliminate the dyes. The recycling rates of the glass containers in Hungary is estimated to be around 36% in 2014 (Figure 2) [15].



**Figure 2.** Recycling rates for glass containers in EU28 in 2014 [15]

Flat glass comes from construction and demolition waste (C&D), automotive glass, and appliances. The production volume of flat glass can reach 8-10Mt/year. Unlike container glass, flat glass needs more than a simple sorting and a colour unification. Flat glass is usually covered with a PVB (polyvinyl butyral) sheet which can change the redox behaviour of the melt in the furnace [15].

**Optional additives of foam glass**

Different materials can be introduced to produce foam glass and the main objective is usually to determine the optimal load-bearing, chemical stability, and microstructure of the product [16]. Qian et al. [17] announced that the mixture of 89 wt% coal fly ash and 6 wt% $CaCO_3$, sintered at 1150 °C, gives foam glass with high compressive strength up to 80.3 MPa. Zhang et al. [18] used incineration waste of bottom ash, fly ash, and pickling sludge with the aid of $CaCO_3$ to synthesise foam glass. The pore morphology and distribution of the foam structure was investigated. The best composition ratio of bottom ash to fly ash to obtain a uniform pore size distribution was determined to be 7/9. Zipeng et al. [19] presented a statistic analysis of glass foam products made by fly ash, glass powder, sodium carbonate ($Na_2CO_3$) as a foaming agent, trisodium phosphate ($Na_3PO_4 \cdot 12H_2O$) as foam stabilizer (to prevent the coalescence of the gas bubbles), and boron nitride (BN) as releasing agent (to avoid other materials bonding to the surfaces). They concluded that the thermal insulation of the foam glass material was directly influenced by the porosity. Cosmin et al. [20] used calcium sulphate as a foaming agent in form of plaster waste mixed with glass waste where the amount of plaster waste varied from 3.03 wt% to 15.79 wt%. The shape and size of the pores were analysed using an optical microscope in reflected light. The microporous structure of the foamed glasses depends on the foaming agent amount. The optimal quantity of calcium sulphate was 5.88 wt%, leading to a homogenous microstructure having uniformly sized pores (around 50 μm). Higher amounts of foaming agents cause inhomogeneous microstructure with irregular pores. The apparent density of the obtained foam glasses was measured using the liquid saturation method with vacuum and water as a working liquid. For the glass foams obtained using windowpanes wastes, the apparent density and the apparent porosity of the foam glasses ranged between 0.47-0.71 g/cm³ and 20.19-54.54%, respectively. When bottle glass wastes were used as precursors, depending on the amount of foaming agent, the apparent density and the apparent porosity ranged from 0.51 to 0.72 g/cm³ and 18.77-51.75%, respectively. Due to the large amount of titanium tailing waste, Xi et al. [7] tried to use it to synthesize foam glass mixed with glass waste, foaming agent $Na_2CO_3$ (0–3 wt%) and fluxing agent $B_2O_3$ (0–3 wt%). The sintering temperature is considered low (760–790 °C) and the sintering time is between 10 to

40 min. Thermal dilatometer, X-ray diffraction, and heat flow methods are used to investigate thermal conductivity, crystallinity, and thermal expansion coefficient. In addition to apparent density and compressive strength, pore structure also affects thermal conductivity and thermal expansion coefficient [7]. Shi et al. [21] also used high titanium blast furnace slag with glass waste, and aluminium nitride (AlN) as a foaming agent. As they increased the AlN content, the pore size distribution became homogeneous. Jing Li et al. [22] used mixtures of 33.3 wt%-43.3 wt% fly ash and recycled glass from a float glass factory, with 0.5 wt% SiC as a foaming agent, and 9-11wt% $Na_2CO_3$ as a fluxing agent. The mixtures were fired at 865–915 °C temperature range with 15 min residence time at the peak temperature. König et al. [23] investigated gas-releasing reactions of carbon and manganese oxides ($MnO_2$, $Mn_2O_3$, and $Mn_3O_4$) during the foaming process using thermogravimetry coupled with mass spectrometry. Foaming process is negatively affected by $MnO_2$ because it increases the temperature of the foaming. The carbonaceous foaming agent burns before the glass particles sintering, resulting in open pores. In oxidizing atmospheres, $Mn_2O_3$ should replace $MnO_2$, and in oxygen-free atmospheres, $Mn_3O_4$ should replace $MnO_2$. Robson Couto et al. [24] produced foam glass from soda-lime glass waste using sodium hydroxide as foaming agent. Ru Ji et al. [25] [26] used mineral wool waste and recycled glass from building construction and demolition as raw materials. The outcomes of the sintering temperature and the composition of the foams on the properties of foam glass were inspected. Some other materials were involved along with glass waste like geopolymer, metakaolin by direct foaming using $H_2O_2$ (chemical pore-forming agent). Samples heat-treated in the temperature range 700–900 °C were subjected to secondary foaming, due to the decomposition of hydrated species [27]. Arriagada et al. [28] proved that a higher porosity and smaller pore size could contribute to higher mechanical strength and lower thermal conductivity by reducing the particle size of the foaming agent and by increasing the foaming temperature. König et al. [29] prepared foam glasses by heating a mixture of waste flat glass, foaming additives (carbon and $Mn_3O_4$), and $TiO_2$ as a nucleation agent. The samples contained larger open cells (>0.1 mm), and smaller closed cells (<0.1 mm), mostly located in the cell walls. The average pore size, excluding the closed cells, was determined to be 0.59 mm. Rincon et al. [30] produced foam glass from a mixture of glass and fayalite slag by alkali activation of glass suspension firstly foamed by mechanical stirring then sintered. The slag determined a 'dilution' of the calcium silicate hydrated compounds, responsible for low-temperature hardening of glass/slag suspensions and attributable to an alkaline attack of the soda-lime glass fraction. This product can be used in electromagnetic shielding insulation. Guo et al. [31] used red mud, an alkaline leaching waste as raw material for the preparation of glass

ceramic foams. The results of the mineralogical analysis and the microscopic examination showed that the use of red mud affected the mineralogical characteristics and structure of the produced foams. Taoyong et al. [32] prepared foam glasses by utilizing lead-zinc mine tailings, fly ash, and red mud as the major component. The optimal porosity, compressive strength, and chemical stability of glass ceramic foam were achieved at the sintering temperature of 980 °C. In another research, Taoyong et al. [33] used polymetallic ore tailings as the main raw material synthesize foam glasses through partial vitrification, without any foaming agent. The foaming behavior, the effect of sintering temperature, and fly ash addition on the cell structure were investigated. Tulyaganov et al. [34] used a sheet glass cullet along with SiC powder as a foaming agent. Adding 1 wt% of the alkali earth aluminosilicate glass powder improved the sinterability and increased the compressive strength of the foam glass due to the formation of a well-packed honeycomb structure with an optimal distribution of pentagonal and hexagonal shaped cells. Luo et al. [35] prepared foam glass using coal fly ash. Before sintering, the coal fly ash was prepared by soaking in an alkali activation that coated particles with a layer of hydroxysodalite crystals. The alkali-activated fly ash underwent a self-foaming reaction during sintering. The leaching toxicity tests proved that the hazardous heavy metals are within the glassy phases during sintering. Taoyong et al. [36] produced foam glasses from coal gangue, fly ash, and silica sand as raw materials without adding any agents. The microstructure and some physical properties of the foams were investigated. They conducted that adding silica sand resulted in closed porosity. Abdel-Gawwad et al. [37] synthesized foam glass using lead glass sludge with the addition of ($CaCl_2$) and sodium hydroxide (NaOH) through chlorination processes and sintering (750–950 ºC). Pb-stabilization has been deeply investigated. In the process lead will transform into insoluble ganomalite phase. More important adding NaOH and $CaCl_2$ improved the foaming process and stabilized Pb-leaching.

While powder glass was mostly the main component in the previous research, Khater et al. [38] used solid industrial wastes, namely, blast furnace slag (10 to 90 wt%) and ceramic sludge (90 to 10 wt%) with the addition of limestone and sand. Crystalline phases, density, porosity, and dielectric properties of the resulting porous material were investigated.

Moreover, Zhai et al. [39] presented a molecular insight into the foaming mechanism where the foaming effects of dextrin and carbon, and different carbon allotropes on the morphology and the physical and mechanical properties were studied. 1 wt% carbon black is more suitable to create smaller pores in favorite of the stability of the foams.

One of the most frequently used materials in foam glass production is the cathode-ray tube glass (CRT). CRT glass comes from computer monitors and TV sets. The replacement of

cathode ray tube screens by flat panel displays such as liquid crystal display (LCD), plasma display panels (PDP), and light emitting diode (LED) displays increased the electronic waste dramatically [40] [41]. CRT can be black-and-white (monochrome) or colour. The monochrome CRT contains a front panel or the screen and a funnel that attaches the panel to the neck covering the electron gun. The colour CRT is similar to the monochrome CRT, except a tiny sheet of metal positioned behind the glass panel called a shadow mask is added (Figure 3) In a television or a computer monitor, the CRT weighs around 65% of the overall weight and is composed of 85% glass, of which 65% is the front panel, 30% is the funnel, and 5% is the neck glass. The front panel is mainly composed of barium-strontium silicate glass (up to 12% barium oxide and up to 12% strontium oxide) while the funnel and the neck are made of lead silicate glass with almost 25% lead oxide in the funnel and 40% in the neck [42] [43] [44]. The lead oxide content in CRTs varies from 5 kg to 3 kg [15]. Besides, the inside of the CRT is coated with phosphor, cadmium, and other metals (strontium, antimony, barium, europium, selenium, etc.). Lead can cause the risk of dispersing poisonous substances during remelting making CRT recycling difficult and requiring special safety handling. Managing this problem is critical from the viewpoint of creating functional WEEE treatment systems [42]. Herein, CRT glass recycling technologies could be classified as a closed-loop recycling (glass-to-glass, old CRT glass to new CRT glass) and open-loop recycling (glass-to-products) [40]. The emergence of new display devices caused a decline of CRT need and closed-loop recycling is no longer considered effective recycling. The industrial focus has shifted to open-loop recycling.
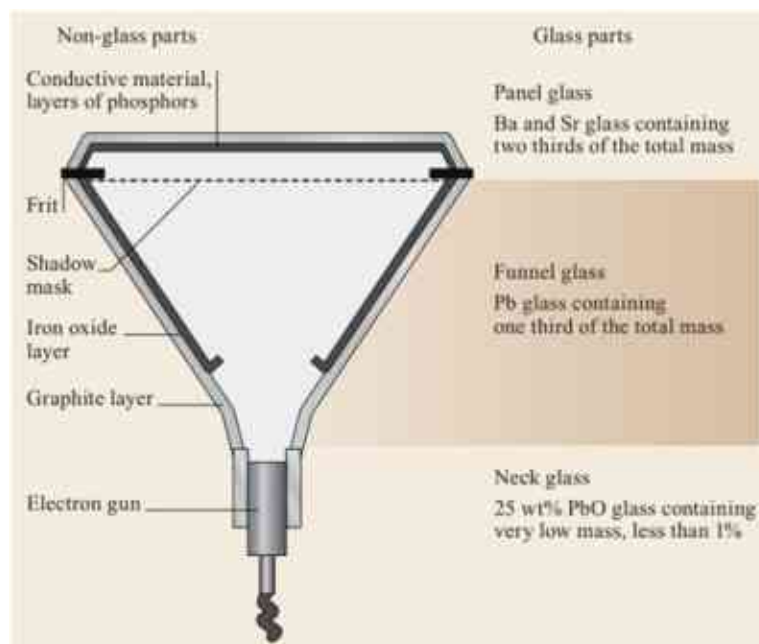


**Figure 3.** Representation of CRT constituents [15]

In building materials and other fields like glass base materials, radiation protection materials, and low-cost adsorbent materials, CRT glass can be directly used as a secondary material without considering the lead content [40]. Otherwise, lead can be extracted and treated by three methods: pyrometallurgy, hydrometallurgy [45], and mechanical activation [40]. CRT glass can be added into the raw materials to produce a variety of building materials, such as foam glass, glass-ceramic brick, and concrete materials [46] [47] [48] [49] [50] [51] [52] [53]. König et al [54] focused on studying the close and open cells in foam glasses made with waste CRT panel and soda-lime-silica glasses with the addition of carbon black, and manganese or iron oxides. The closed-porous foams were prepared from CRT panel glass mixed with 0.44 wt% carbon and 5.97 wt% $Mn_3O_4$ while the open-porous samples were prepared from 33 wt% container glass, 67 wt% flat glass, 0.33 wt% carbon, and 4.45 wt% $Fe_2O_3$. The XRD analysis of the foam glass showed that the sample with the soda-lime glass contained a larger number of crystals than the sample with the CRT glass that proved the stability of the CRT glass. They concluded that the type of porosity played an important role in the application of foamed glass. For thermal insulation applications, the porosity must be closed, while open porosity is preferred for acoustic insulation. In an older study, König et al. [23] Tried $CaCO_3$ as a foaming agent. The influences of powder preparation, $CaCO_3$ concentration and foaming temperature and time on properties of the foam glass were highlighted. The main results focus on the influence of $CaCO_3$ concentration and the milling time of the glass–$CaCO_3$ mixture to obtain a homogeneous closed porosity. Østergaard et al [55] used CRT panel-$Mn_3O_4$–C–alkali phosphate system to produce glass foam. The addition of alkali phosphates lowered the glass transition temperature, at the same time increasing the density and the ratio of open pores. In their recent work, Østergaard et al [56] used CRT panel glass, manganese oxide, and carbon as foaming agents to produce foam glasses. They applied high-speed synchrotron X-ray tomography to detect the change in the pore structure during the foaming process, quantify the foam structure and porosity dynamically, and create a 3D model of glass foams to predict the porosity dependence of the thermal conductivity. Another method to synthesize foam glass is to apply high gas pressure (5–25 MPa) using Ar or $N_2$ during the sintering of cathode ray tube CRT pellets at 640 °C then cool down to room temperature [57]. The minimum density appointed to samples sintered at a gas pressure of 15–20 MPa. The samples exhibited a closed pore structure. The thermal conductivity of the glass foams decreased with decreasing foam density [57].

Aluminium dross is produced by the secondary aluminium industry during aluminium scrap. Aluminium dross may contain 15-30 wt% aluminium oxide, 30-55 wt % sodium chloride, 15-

30 wt % potassium chloride, 5–7 wt % metallic aluminium, and impurities (carbides, nitrides, sulphides, and phosphides). Due to these impurities, it is classified as toxic and hazardous waste, it should be handled under the current legislation. It is prohibited to landfill in most of the European countries and it should be recycled and processed correctly by considering the environmental impact [58] [59]. Aluminium can be produced through a long primary process from the bauxite ore or directly from recycling of aluminium scrap [60].

Primary aluminium production steps are bauxite mining, alumina production, and electrolysis. Four identified processes used in alumina production with different recovery rates: the Bayer process, the Sinter process, the combined Bayer–Sinter process, and the Nepheline-based process. Primary aluminium production generates a high amount of waste, red mud, estimated to be over 120 million tonnes per year in the world [58]. As a rough estimation, the global aluminium dross generation are more than four million tons per year [61].

Compared to primary aluminium production, recycling of aluminium products is more effective regarding the economic and environmental aspects where it needs as little as 5% of the energy and emits only 5% of the greenhouse gas. The scrap feed is a complex combination of all types of aluminium scraps such as beverage cans, foils, extrusions, turnings, and cast metal [58].

Aluminium dross composition varies depending upon the operation of the plants. Three major types of aluminium dross are classified concerning their average metallic content [62]: white dross (50–70 % Al) or "skimming", black dross (30–50 % Al), and salt cake (5–10% Al). The so-called "white dross" comes from skimming the molten aluminium without salt cover. Black dross is issued from the secondary smelter may contain aluminium metal (10–20%), a salt-flux mixture (40–55%), and aluminium oxide (20–50%) [58]. On the other hand, the salt cake is a non-metallic residue with a usual composition of 5–7% residual metallic aluminium, 15–30% aluminium oxides (corundum ($\alpha$-$Al_2O_3$), spinel ($MgAl_2O_4$), and diaoyudaoite ($NaAl_{11}O_{17}$)), 30–55% sodium chloride, and 15–30% potassium chloride, fluorides (cryolite ($Na_3AlF_6$), fluorite ($CaF_2$), and Sodium fluoride (NaF)), and impurities such as carbides, nitrides, sulphides, and phosphides [63] [58] [61]. To describe the process of salt flux formation, an oxide film structure over the metallic aluminium is expelled away from the liquid aluminium, at the point when the liquid aluminium interacts with climatic oxygen [63]. Salt flux is added to prevent the oxidation of aluminium at the outer surface of the melt. It facilitates agglomeration and separation of the metal, furthermore, enhances metal recovery. It improves the heat transfer to the metal and carry-on contaminants, such as oxides, nitrides, carbides [64] [58].

Aluminium dross is a non-biodegradable waste that remains in the ground for a long-time-interval and causes environmental and public health problems [64]. It has an extreme impact on the flora and fauna and is classified as toxic and hazardous waste according to the European Catalogue for Hazardous Wastes [59]. It can contaminate groundwater and salinate soil, causing health complications such as lung and bladder cancer, respiratory problems, neurological disorder, nausea, vomiting, and coughing (H5: substances and preparations which, if they are inhaled or ingested or if they penetrate the skin, involve limited health risk) [59]. It is as ''highly flammable'' (H3-A: substances and preparations which, in contact with water or damp air, evolve highly flammable gases in dangerous quantities), and ''leachable'' (H13: Substances and preparations capable by any means, after disposal, of yielding another substance) leading to the formation of toxic, harmful, explosive, poisonous and unpleasant odorous gases, such as $NH_3$, $CH_4$, $PH_3$, $H_2$, $H_2S$, etc [59].

Several attempts to recycle aluminium dross were conducted [65] [62] [66]. One way is the pyrometallurgical and hydrometallurgical routes [67] [68] [62] [69] [70] [71]. The convenience of these methods is the generation of non-metallic waste besides additional treatment for removing AlN [72]. Another alternative way is to apply the dross directly in the generation of the valuable products as an additive for the synthesis of composites, alloys, derivative compounds of aluminium, aluminium-alumina refractories, refractory coatings [5], glass ceramics [73] [74] [69] [75], geopolymer [64], as a clay replacement in lightweight aggregate [76], cement clinker production [64], as catalyst support for glycerol dry reforming [77], as a partial replacement for sand in sandcrete blocks [60], and as reinforcement for composite production., etc. The abundance and presence of $\alpha$-$Al_2O_3$ and $MgAl_2O_4$ in aluminium dross favours the production of refractories with insulating properties at high temperatures (1000°C and above) [65]. Furthermore, aluminium dross is used to generate gaseous products, such as high pure hydrogen [78] [64] [79] [80], ammonia, and the development of compounds like sulphates or tamarugite [81] [62].

**Initial particle size of the raw materials**

A direct relationship exists between the fineness of the initial raw materials and the pore diameter of the glass foam owing an even degree of the materials dispersion [82]. As a result, it can influence the density of the resulting foams where finer particle size leads to a foam with a lower density (Figure 4).
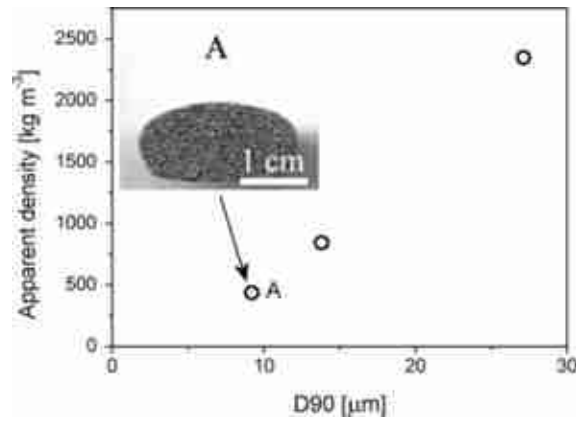
**Figure 4.** Effect of the particle size of the powder mixture on the apparent density of the foam glass samples prepared with 1 wt% of carbon at 820°C for 5 min [83]

**Foaming process**

To optimize the glass product, the heating rate must be controlled. Large cracks develop through the glass mass if the temperature rises rapidly. In the other hand, it is undesirable to use overly slow heating rate because prolonged isothermal heating could lead to prematurely gas generation. For uniform temperature distribution, a larger sample should be heated at a slower rate. Usually, the suitable heating rate is 5-10°C per minute (Figure 5) [82] [84].
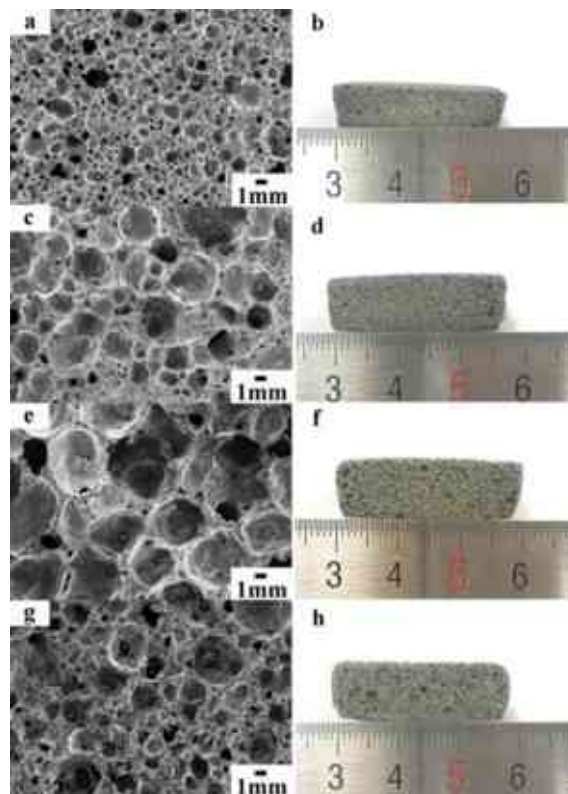


**Figure 5.** Cross-sectional views of foam glass prepared at different sintering times a and b) 10 min, c and d) 20 min, e and f) 30 min, g and h) 40 min (temperature: 780 °C, $Na_2CO_3$ content: 2 wt%, $B_2O_3$ content: 2 wt%) [7]

Densities continuously decrease during gas release. Upon finishing this stage, the foam gradually collapses due to coalescence of the pores. This resulted in a decrease in the surface energy of the system [82] [84]. It is possible to lock in the obtained structure and the evolved gas by rapidly cooling below the foaming temperature and slightly above the annealing range. To eliminate any residual stress, a very low cooling rate is required throughout the glass transformation range. There is some shrinkage of the cells during cooling due to a drop in pressure inside the cells, and this results in tensile stresses as well [82].

Choosing the right foaming temperature is crucial in the production of foam glass. A direct relationship exists between the viscosity of the glass and its foaming temperature. The foaming temperature is determined by a combination of two factors: viscosity, which determines the foam stability, and the internal cell structure. The pores must be homogeneous and regular in size and shape, and their walls must be as thin as possible [82]. When the foaming temperature is high, the melt viscosity is low, and the structure can't be controlled since bubbles rise to the top (as in glass fining). On the opposite side, when the temperature is extremely low, the glass viscosity becomes higher, which makes the gas expansion difficult and as a result the volume increases slowly. Because the separating walls are not completely formed, there is residual porosity that increases water absorption, causing the high absorption of the foam glass [82]. Usually, the foaming temperature of the foam glass ranges from 800 °C to 900 °C (Figure 6).
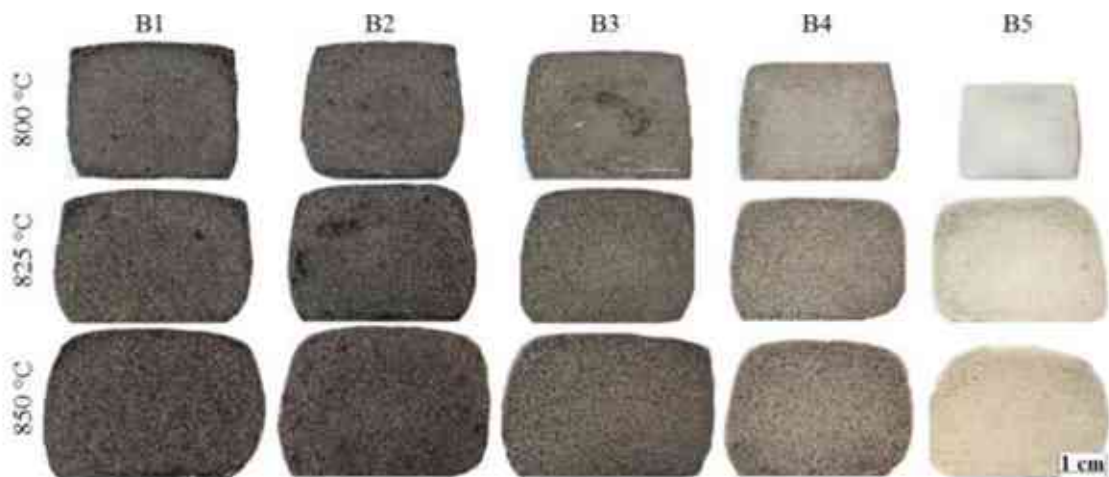


**Figure 6.** Effect of the sintering temperature on the foam glass [5]

There are two types of foaming agent that can be used: the oxidation-reduction carbonaceous blowing agents (including starch, glycerol, soot, anthracite, graphite, etc.), and the result is called "black" foam glass. The second case is the use of neutralization inorganic foaming agents in the form of carbonates, boron and phosphorus oxides, resulting "white" foam glass. Some components of glass, especially $SiO_2$, $B_2O_3$ and $P_2O_5$, are the acidic component in the neutralization reaction, and the foaming agent, which is usually an alkaline-earth metal

carbonate, is the alkaline component (Table 1). This group is no longer used in modern industry with a small exception because of the high-water absorption of such products, on average about 70% by volume [5]. The gas discharge when the glass is liquid to form a foam can be expressed with a simple reaction, for example, for limestone:

$$CaCO_3 + SiO_2 = CaSiO_2 + CO_3 \tag{1}$$
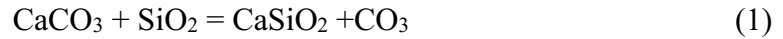
The thermal decomposition of limestone takes place simultaneously with the neutralization reaction, depending not only on the temperature, but also on the partial pressure of carbon dioxide in the foam glass cells. Colorless glass usually produces weight foam glass while colored glass produces foam glass of various colors [5].

Foam glasses are usually produced using the redox technology. The reduction component of the glass is usually $SO_3$, the reducing foaming agent is carbon or an organic substance containing it. The reaction of the foam glass formation can be represented by the following equation:

$$glass\text{-}SO_3 + 2C \rightarrow glass\text{-}S^{2-} + CO + CO_2 \tag{2}$$
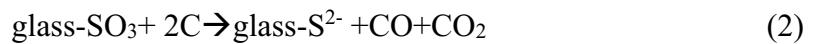
Due to the great influence of the carbon dispersion on the porous structure uniformity, an addition of a material rich in carbon, such as solutions of an organic readily decomposable substance (for example, sugar or glycerol) can produce fine-dispersed carbon during thermal processing and improve foaming. Carbon can be better distributed in the foaming mixture and, therefore, can be used in smaller quantities. Additionally, it is important to take into consideration that carbon in fine-grained forms is highly inclined to oxidation. Since the use of dense forms or foaming in a furnace with non-oxidizing atmosphere in real production is difficult, the introduction of materials carbon that envelop the carbon particles and prevent its premature oxidation is necessary [5]. In some cases, not only the amount and type of foaming agent will affect the foaming process but also combining two or more foaming agents. For example, Liu et al. [85] investigated the effect of combining two foaming agents, calcium carbonate and graphite. The decomposition of $CaCO_3$ at high temperature will generate $CO_2$ which reacts with graphite. By increasing the oxidation of graphite, foam growth will be increased, and pores will be stabilized.

**Table 1.** Summary of foaming agents used for the elaboration of glass foam [15]

| Category | Foaming agent | Mechanism |
|---|---|---|
| Metal carbonates/sulfates | $Na_2CO_3/CaCO_3/MgCa(CO_3)_2$ (dolomite)/$Na_2SO_4/CaSO_4$ | Reactive/thermal decomposition |
| Metal oxides | $Mn_xO_y/Fe_xO_y/Cr_xO_y/PbO$ | Redox reaction in melt |
| Nitrides | $AlN/TiN/Si_3N_4$ | Redox reaction |
| Carbonaceous | SiC<br>Carbon<br>Water glass<br>Virgin glass | Surface reaction<br>Solid-gas reaction<br><br>Redox reaction |

**Chemical stability evaluation**

Because of the hazardous characteristics of this material, a chemical stability test should take place. Cosmin et al [20] studied the hydrolytic and chemical stability of foam glasses made with recycled glass wastes and plaster wastes from used ceramic casting molds as a foaming agent. The hydrolytic stability of the foam glass was determined according to ISO 719-1985 using 2 grams of glass, kept for 60 min in 50 ml de-ionized water at 98°C. A volume of 25 ml of the obtained solution was titrated against 0.01 mol l$^{-1}$ HCl solution. The volume of HCl needed for neutralization is recorded to express the equivalent $Na_2O$ extracted. The hydrolytic stability of the porous glasses qualifies them as HGB1-HGB3 (borosilicate glass and regular soda-lime glass resistance) glasses having a good resistance toward water aggressively. The apparent porosity greatly affects the hydrolytic stability of the glass foams by increasing the surface exposed to the water chemical aggressively. The chemical stability is determined by measuring the ion extraction using leaching tests performed according to the American Extraction Procedure Toxicity Test leaching procedure. The de-ionized water was used as a leaching fluid (solid to liquid ratio was 1/10). Foam glasses were crushed to a particle size of less than 9.5 mm, subsequently dried in an oven at 110°C for 24 h.

The ions leached after 28 days were $Na^+$, $Ca^{2+}$, and $Mg^{2+}$. The presence of $Ca^{2+}$ in these glass foams was considered important due to its increased sensibility at humidity exposure. The leachability of $Ca^{2+}$ after 28 days was lower than 0.735% of the total $Ca^{2+}$ present in the studied glasses. A quasilinear dependence between the amount of plaster waste used and the $Ca^{2+}$ extracted can be established for both glass wastes used, suggesting that the $CaSO_4.2H_2O$ is the main vector for the $Ca^{2+}$ present in the glass foam.

**Chemical durability appraisal**

An insulation material's performance can be adversely affected by the chemical environment in which it is exposed. Foam glass should be resistant to all kinds of liquid and vapor chemicals to ensure long-term performance.

When selecting an insulation system, chemical durability is often one of the most significant factors. Chemical absorption does more than destroy an insulation mechanically and impair its thermal performance, it also increases the risk of fires and structural corrosion. Chemical attacks can be caused by acid rain, salt air, spills from adjacent equipment, or from the insulated installation system itself [86]. Each insulation system has weaknesses, for example:

- Polymer foam such as phenolic and polyolefin materials can withstand high and very low temperature (-50 °C to 85 °C). These foams, however, are significantly deteriorated by most solvents and reagents. It is therefore necessary to avoid using them in applications that will require exposure to incompatible solvents and reagents [86].

- Despite being inert, glass fiber insulation is usually coated with organic binders that can be destroyed by chemicals. Additionally, it is capable of wicking or absorbing potentially hazardous materials. Further, the ability to absorb flammable liquids can increase fire risk [86].

- Calcium silicate and perlite are usually used too as insulation but due to their higher absorption rate an auto-ignite could occur when interacting with oxygen at a specific temperature [86].

The universally well-known chemical resistance of glass let as think to use the same start up material for insulation which led to foam glass with high durability.

# 1.2. Critical issues in foam glass research and production

Knowledge gap 1

Based on the literature review, flat glass is used mainly to produce foam glass. However, millions of tons of jars are disposed of each year due to defects or not having the required specifications. Is it possible to use container glass to produce foam glass products? Does it need any special pre-treatment? Does the particle size of the powder glass affect the foaming glass production? If so, which particle size will give the optimal properties?

Knowledge gap 2

To deal with the rising generation of waste, researchers incorporated industrial waste into foam glass such as fly ash, titanium tailing, red mud, mineral wool waste, geopolymer, metakaolin, fayalite slag, and coal gangue. In those papers, the foaming temperature was selected arbitrarily

either in the range of 700 to 900°C as it is the basic interval of foam glass manufacturing [87] or by trying several different temperatures depending on the foaming agent's decomposition temperature. Is there an accurate method to determine the exact foaming temperature?

Those waste materials used, necessitate adding a foaming agent such as calcium carbonate, silicon carbide, carbon, and manganese oxides. Is it possible to make foam glass with optimal properties using 100 % waste materials? Is there any waste material that can act as one of the main components of foam glass, as a foaming agent, and as a stabilizer?

Knowledge gap 3

Using CRT glass in foam glass manufacturing was reported to produce mostly closed pores and better glass stability. Comparatively, container glass develops open pores as a result of partial crystallization, and the author believes this weakens the stability of foam glass [54]. This is contradictory to the well-known which is crystalline solids have a more stable particle arrangement than amorphous solids. In another study, container glass generated mostly closed pores [88]. What is the relationship between the crystallinity and the stability of foam glass? What about the pores resulting from combining CRT and container glasses? Does container glass exhibit open or closed pores? Does using different CRT glass particle size influence the properties of the foam glass? How to investigate the interaction of the added alkaline cations with the glass structure?

Knowledge gap 4

Adding aluminium dross to produce foam glass is a novel aspect of the recycling of this waste material that started to see the light in 2021 in fewer papers [73] [74] [69] [75]. El-Amir et al. investigated the effect of AlN on the foaming process by adding 2.5 to 7.5 aluminium dross at a specified temperature between 900 and 1000 °C. The density was quite high (0.43 g/cm$^3$), and the cells varied from 0.045 to 0.27 mm [75]. Aluminium dross composition varies depending on the scarp. The aluminium nitride acts as a foaming agent, but some aluminium dross may not have aluminium nitride. Can aluminium dross, a hazardous industrial waste, be used as an additive in foam glass production? In what amount it can be added? Will hazardous components affect the properties of foam glass? Aluminium nitride is used as a foaming agent in literatures [89] [73] is it applicable in this study as well? What is the effect of salt content in the dross? What about the other component of the dross? Can the effect of adding aluminium dross on foam glass differ depending on the original source and composition of the dross? Is the product (i.e., the foam glass) eligible for safety regulations?

Knowledge gap 5

Investigating the foaming process is the main direction to produce foam glass with optimal characteristics. The most conventional method is to experiment with different foaming temperatures and rates based on the decomposition temperature of the foaming agent. The foaming rate is generally reported to be from 5 °C/min to 10 °C/min. A common method in the literature to better understand foaming kinetics is to use thermogravimetric analysis to detect spikes indicating gas release due to pores bursting. Another way is to apply high-speed synchrotron X-ray tomography to investigate the pore structure evolution during foaming [90]. This method is expensive and is not available in most university laboratories. Is there an effective method to determine the foaming behaviour of the foam glass? Is the foaming temperature will be the same as the sintering temperature? What is the effect of the foaming temperature on the foam glass structure? How to evaluate the cellular structure of the foam glass? Does the resultant viscosity affect the structure and porosity of the foam glass or other factors may interfere?

Knowledge gap 6

As was seen above foam glass can be made from a large variety of waste materials that can contain hazardous impurities. It is indeed necessary to perform a toxicity test to determine the chemical stability of the final product. A well-known example is CRT glass which contains a high amount of lead. Although most papers describing the use of CRT glass to fabricate foam glass do not address this issue, it is essential to be aware that hazardous materials can be leached from the final product causing dangers to the environment. Essentially, in order for a product to see the light and reach the European market, certain requirements must be met. These requirements begin with reviewing the product's compliance with standardized conditions, its labelling, and its declarations of conformity. What is the most appropriate toxicity test for foam glass since there is no specific test? Do hazardous elements from CRT glass remain stable in foam glass? does the final product compile with the European regulations? Is the lead stabilized in the foam glass? where it is located (in the amorphous phase or in the crystalline phase)?

Knowledge gap 7

Similar to the chemical stability test, the chemical durability test is neglected while it is critical to estimate the foaming aging process of the foam glass. It is only confined to foam glass companies like Foamit® and FOAMGLAS®. There is no specific aging test for foam glass, but a variety of tests were used for glass (ISO 719-1981, DIN 12111, USP-111). The aging test of the foam glass made by soda lime and aluminosilicate glasses was carried out by FOAMGLAS® company [86]. It has been shown that cellular glass has the same chemical

durability as Type III pharmaceutical packaging glass under the US and EU Pharmacopoeia procedures [86].

 In the absence of a specific aging test for foam glass, which test can be used to estimate its durability? What is the effect of adding aluminium dross and/or CRT glass on foam glass durability? What is the predicted life span of the final products?

# Chapter 2

# Effect of dross content and CRT glass particle size

## 2.1. Materials and experimental procedures

### 2.1.1. Materials and samples preparation

The raw materials used to produce foam glass in this work were container glass (collected from household), CRT glass (provided by Daniella Ipari Park Ltd., Debrecen, Hungary), and secondary aluminium slag (produced by Arconic-Köfém Mill Products Hungary Ltd., Szekesfehervar, Hungary). The metal and salt content of the as-received dross was removed by Kekesi et al. [91] with the following method. After melting the aluminum slag to recover the molten metals, the remaining dross was crushed, milled, and washed three times with distilled water to dissolve and eliminate the salt content. Container and CRT glasses were milled and sieved under 70 and 63 μm particle size, respectively. CRT glass was sieved to two separated particle sizes 63 and 32 μm. In the mixtures, container glass was the basic component. In addition, 5 and 10 wt% CRT glass (from each particle size) and 10, 20, or 30 wt% dross was added to the container glass (Table 2). Mixtures having both 32 and 63 μm CRT glass (5-5 or 10-10 wt %) were prepared as well (Figure 7). Moreover, 2 wt% silicon carbide was admixed as a foaming agent and 3 g from each mixture was poured in a stainless-steel mold then pressed under 11 MPa for 10 s into a cylindrical shape (diameter = 20 mm, height = 16 mm). Five samples from each mixture were prepared. The samples were sintered in an electric chamber furnace at different temperatures (determined through the heating microscope) with a heating rate of 5°C/min and a holding time of 10 min.
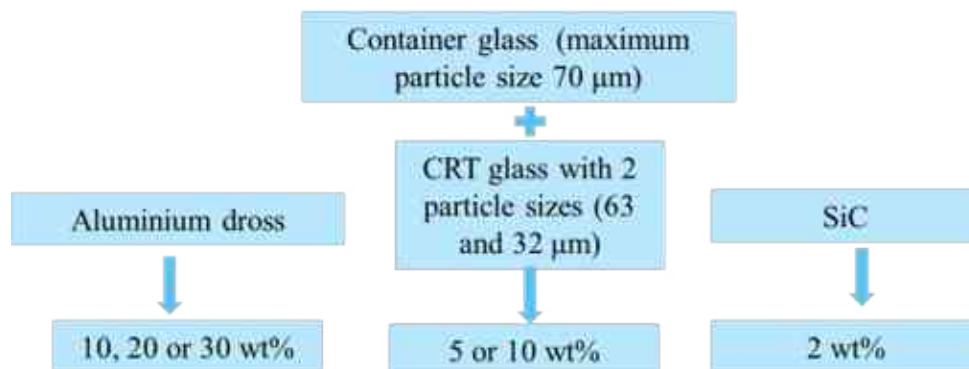


**Figure 7.** Raw materials process

**Table 2.** Composition and foaming temperature of the mixtures

| Sample code | Composition (wt%) | | | | | Foaming temperature (°C) |
| --- | --- | --- | --- | --- | --- | --- |
| | Dross | SiC | CRT63 | CRT32 | Bottle glass | |
| **BG** | | 2 | | | 98 | 960 |
| **5CRT63/10D** | 10 | 2 | 5 | | 83 | 965 |
| **5CRT63/20D** | 20 | 2 | 5 | | 73 | 897 |
| **5CRT63/30D** | 30 | 2 | 5 | | 63 | 890 |
| **10CRT63/10D** | 10 | 2 | 10 | | 78 | 915 |
| **10CRT63/20D** | 20 | 2 | 10 | | 68 | 894 |
| **10CRT63/30D** | 30 | 2 | 10 | | 58 | 880 |
| **5CRT32/10D** | 10 | 2 | | 5 | 83 | 965 |
| **5CRT32/20D** | 20 | 2 | | 5 | 73 | 887 |
| **5CRT32/30D** | 30 | 2 | | 5 | 63 | 875 |
| **10CRT32/10D** | 10 | 2 | | 10 | 78 | 900 |
| **10CRT32/20D** | 20 | 2 | | 10 | 68 | 890 |
| **10CRT32/30D** | 30 | 2 | | 10 | 58 | 887 |
| **5CRT32-63/10D** | 10 | 2 | 5 | 5 | 78 | 915 |
| **5CRT32-63/20D** | 20 | 2 | 5 | 5 | 68 | 897 |
| **5CRT32-63/30D** | 30 | 2 | 5 | 5 | 58 | 880 |
| **10CRT32-63/10D** | 10 | 2 | 10 | 10 | 68 | 880 |
| **10CRT32-63/20D** | 20 | 2 | 10 | 10 | 58 | 870 |
| **10CRT32-63/30D** | 30 | 2 | 10 | 10 | 48 | 872 |
| **BG/10D** | 10 | 2 | | | 88 | 897 |
| **BG/20D** | 20 | 2 | | | 78 | 862 |
| **BG/30D** | 30 | 2 | | | 68 | 896 |
| **5CRT63** | | 2 | 5 | | 93 | 970 |
| **5CRT32** | | 2 | | 5 | 93 | 960 |
| **10CRT63** | | 2 | 10 | | 88 | 947 |
| **10CRT32** | | 2 | | 10 | 88 | 955 |
| **5CRT32-63** | | 2 | 5 | 5 | 88 | 950 |
| **10CRT32-63** | | 2 | 10 | 10 | 78 | 922 |

In Table 2, the first number indicate the wt % of CRT, then the particles size of CRT glass of D90=32μm or D90=63 μm. The number before D means the presence of 10, 20 or 30 wt% dross in the mixtures and BG (=base glass) means samples with container glass powder (without CRT).

## 2.1.2. Characterization methods

The chemical composition of the raw materials was determined as follows: The composition of the container and CRT glasses was analyzed X-ray fluorescence spectrometry (XRF) instrument (Rigaku SuperMini 200). The hazardous elements in CRT glass were determined by using an inductively coupled plasma mass spectrometry (ICP-OES) (Varian 720 ES spectrometer). The mineral composition of the dross was identified by X-ray powder diffractometry (XRD) (Rigaku Miniflex II) and quantified by Rietveld fitting. Raw powders were sent to the scanning electron microscopy (Zeiss EVO MA10) to identify their morphological and microstructural features.

The powder mixtures were admixed and then analyzed by a heating microscope (MicrOvis, Camar Elettronica) to determine the exact foaming temperature for sintering. The samples were pressed (with approximately 5 mm height and 2 mm diameter) using the mold kit of the microscope and placed on an 8 × 10 mm sized alumina sheet and moved into a furnace where the sample's silhouette change in function of temperature is registered to identify the beginning of sintering, softening, sphere, half-sphere, and melting temperatures. The temperature, where the sample reached the maximum height, is determined as the foaming temperature.

After sintering in an electric chamber furnace, the samples were cut into cubic shapes where bulk density, microstructure, thermal conductivity, water absorption, and compressive strength were determined.

The bulk densities of the samples were calculated as the mass per volume (g/cm$^3$). The microstructure of the foams was characterized with an optic microscope (C. Zeiss Discovery V.12) by measuring the cell sizes and wall thicknesses. The cell size indicates the length (diameter) of a cell between the opposite walls. The wall thickness indicates the width of the cell wall measured perpendicularly to the edges of the wall. The statistic was made in a total of 15 measurements for each sample, where the cell size and wall thickness results were divided into six interval grades: $d \geq 3$ mm, $2$ mm $\leq d < 3$ mm, $1$ mm $\leq d < 2$ mm, $0.5$ mm $\leq d < 1$ mm, $0.1$ mm $\leq d < 0.5$ mm, and $0.01$ mm $\leq d < 0.1$ mm [59]. Thermal conductivity was measured by a C-Therm TCi using the Modified Transient Plane Source Method (which conforms to ASTM D7984) [92]. A momentary constant heat source is applied to the sample by a single-sided, interfacial heat reflectance sensor. The measurement pulse is usually between 1 and 3 seconds. Thermal conductivity and effusivity are measured directly to generate an understanding overview of the heat transfer of the samples [92].

Water absorption was measured with method B under Hungarian standard MSZ EN 1217 B. Samples were boiled in distilled water for four hours and soaked for 24 hours then the water absorption was calculated as follows:

$$Water\ absorption\ (\%) = \frac{m_{wet} - m_{dry}}{m_{dry}} * 100 \tag{3}$$

$M_{dry}$: dry weight of the sample (g), $M_{wet}$: weight of the sample directly measured after soaking (g)

Compressive strength was measured using an Instron universal testing instrument on cubic shaped samples with an average cross section of $12.5 \times 12$- and 14-mm height. The samples were loaded with a force perpendicular to their surfaces.

## 2.2. Results and discussion

### 2.2.1. Raw material characterization

In this work, the container glass is used as a base material and abbreviated as BG. The particle shape and size of the raw materials are presented in Figure 8. Container glass (BG), CRT glass, and α-SiC particles have angular and prismatic shapes with rigid surfaces. Aluminium dross particles have an irregular shape and rough surfaces.



|  (A)  |  (B)  |  (C)  |  (D)  |
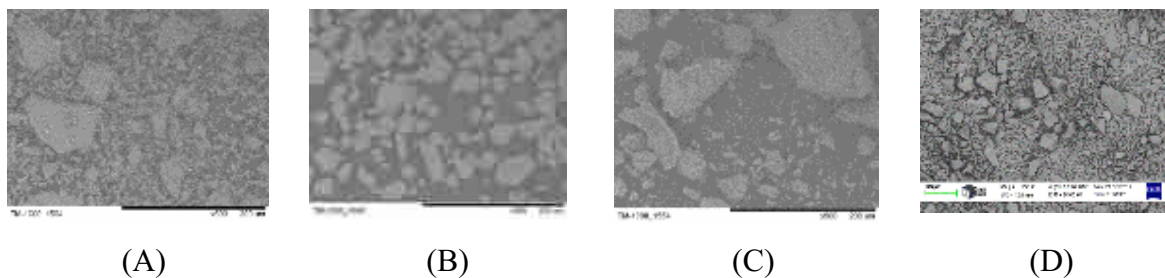
**Figure 8.** Morphological analysis of bottle glass (A), silicon carbide (B), aluminium dross (C) and CRT (D)

The chemical composition of the container glass and CRT glasses are shown in Table 3 and Table 4. The container glass is a typical soda-lime-silica glass, which mainly consists of silica, sodium oxide, and calcium oxide with minor components, such as magnesia and alumina. CRT glass has almost the same main constituents (silica, alkali oxides, alumina) with the presence of some hazardous elements (Table 4). X-ray diffractograms of the raw materials are presented in Figure 9. Aluminium dross contains a high amount of spinel with the existence of corundum, aluminium nitride, salts, and aluminium hydroxides (Table 5).

Treated dross contains a high content of spinel with the presence of corundum, aluminium nitride, salts, and a small percentage of aluminium hydroxides (Table 5 and Figure 9).

**Table 3.** Chemical composition (wt%) of container glass powder and CRT (ICP analysis)

| Oxides | $SiO_2$ | $Na_2O$ | $K_2O$ | CaO | MgO | $Al_2O_3$ | $Fe_2O_3$ | $Cr_2O_3$ | $TiO_2$ | MnO | $SO_3$ | $P_2O_5$ | BaO | $ZrO_2$ |
|---|---|---|---|---|---|---|---|---|---|---|---|---|---|---|
| BG | 71,5 | 12,5 | 0,72 | 8,75 | 2,44 | 1,75 | 1,15 | 0,066 | 0,034 | 0,022 | 0,21 | 0,009 | 0,068 | 0,007 |
| CRT | 55.9 | 5.96 | 5.49 | 0.52 | 0.21 | 1.7 | 0.21 | - | 0,005 | 0,005 | | 0.005 | - | - |

**Table 4.** Hazardous elements (ppm) in CRT glass (XRF analysis)

| Element | Cu | Zn | Pb | Rb | As | Cr | Co | Ni | Sr | Ba | Zr |
|---|---|---|---|---|---|---|---|---|---|---|---|
| **ppm** | 45 | 1891 | 1071 | <10 | 53 | 93 | <10 | 143 | 3.6 | 7.2 | 5.7 |
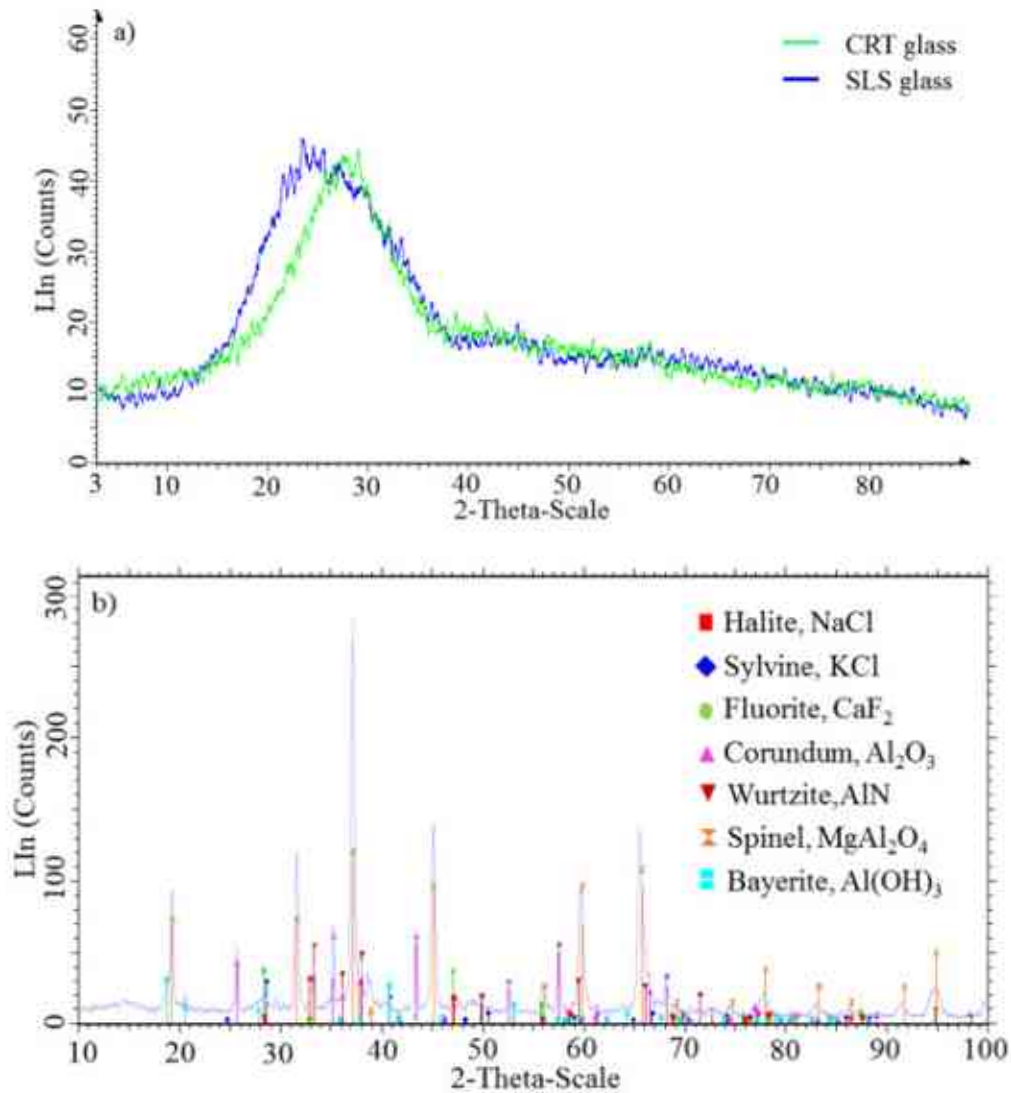


**Figure 9.** X-ray diffractograms of the raw materials (a) SLS and CRT glass; (b) aluminum dross

29

**Table 5.** Composition of aluminium dross (XRD analysis)

| Formula | Phase name | Amount, wt % |
|---|---|---|
| $MgAl_2O_4$ | Spinel | 68.14 |
| $Al_2O_3$ | Corundum | 17.59 |
| AlN | Wurtzite | 8.57 |
| $Al(OH)_3$ | Bayerite | 1.9 |
| $CaF_2$ | Fluorite | 1.72 |
| NaCl | Halite | 1.51 |
| KCl | Sylvine | 0.33 |

### 2.2.2 Sintering and foaming behavior

Using a heating microscope, the exact foaming temperature of the mixtures was determined. Foaming temperature is defined as the temperature associated with the maximum height of the foam. The sintering curves of the mixtures are shown in Figure 10. The overall foaming process of the mixtures can be observed in the Annex A (Figure A1). Dross-containing mixtures have a lower foaming temperature and a higher foaming height, while dross-free mixtures show a higher foaming temperature and a lower foaming height. The sample containing 20 wt% dross exhibits the greatest foaming intensity. The dross decreased the foaming temperature and enhanced the foaming process. The latter is due to the self-foaming mechanism of dross, according to Zhang et al. [89]. This foaming is based on releasing gaseous products ($NH_3$, $N_2$, and NO) between 800-920°C according to the following equations [73]:

$$2AlN + 3H_2O = Al_2O_3 + 2NH_3 \qquad (4)$$
$$4AlN + 3O_2 = 2Al_2O_3 + 2\,N_2 \qquad (5)$$
$$4AlN + 5O_2 = 2Al_2O_3 + 4NO \qquad (6)$$
$$4NH_3 + 5O_2 = 4NO + 6H_2O \qquad (7)$$
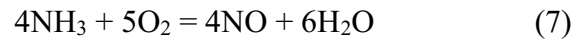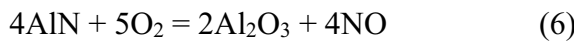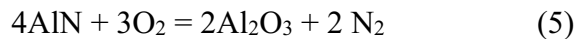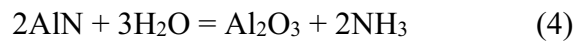
Ewais et al [21] found that AlN decomposed between 850-950°C as follows:

$$2AlN(s) \rightarrow 2Al(s) + N_2\,(g) \qquad (8)$$
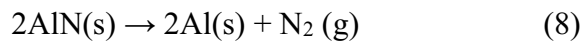
In the glass industry, salts (fluorite, halite, and sylvine) are used to reduce silica glass's melting temperature, which may contribute to the decreasing foaming temperature. Mixtures with the container and CRT glasses have similar sintering curves. Due to the similarity of viscosity of lead glass and commercial soda-lime-silica glass ($10^2$ to $10^{15}$ poises) [93], adding CRT glass by itself did not affect remarkably the foaming height but slightly reduced the foaming temperature of the container glass (Figure 10 a) due to the lower melting point of lead glass.

At the same time, adding CRT to dross improved the foaming height compared to mixtures with only container glass and aluminium dross.

There is no pronounced difference between the foaming behaviour of the mixtures with 63 µm particle size of the CRT glass and the mixtures with 32 µm (Figure 10 c,d). Combining the two-particle sizes of the CRT may decrease the foaming height. Filling the voids between the different particles may occur when using two different particle sizes which will reduce the amount of oxygen in the sample leading to limiting the oxidation reactions taking place during sintering (Figure 10 e).
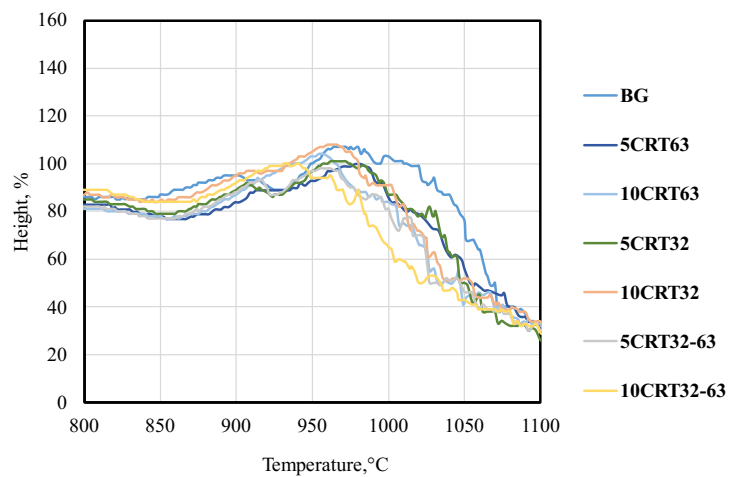


a
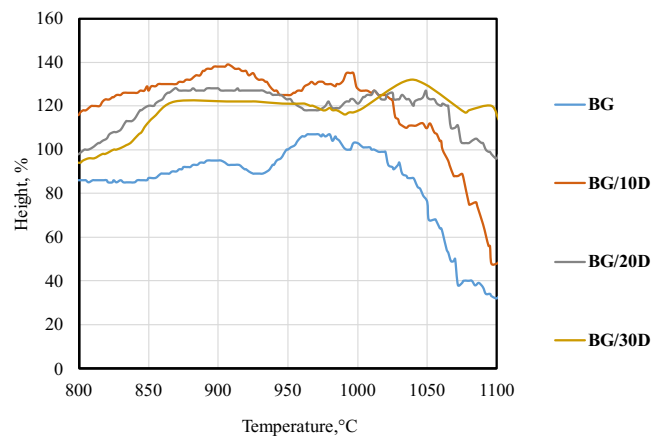


b
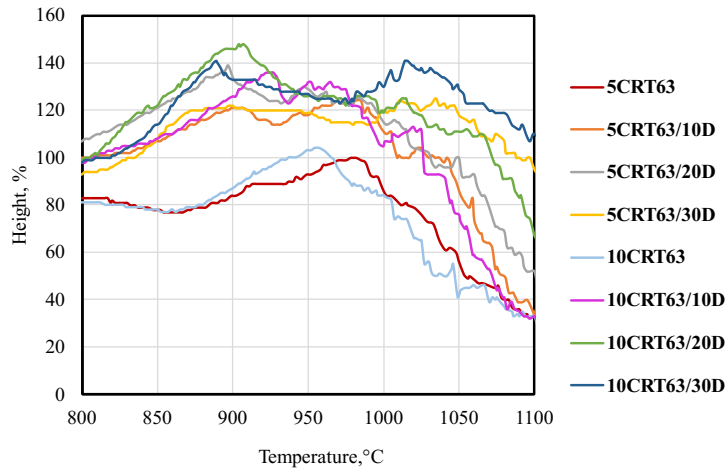
c
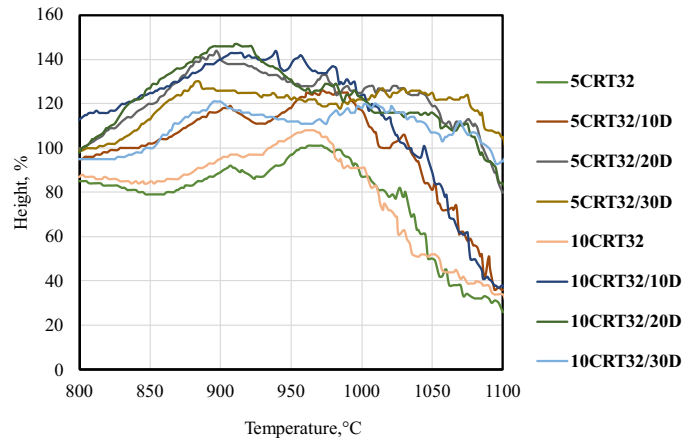


d
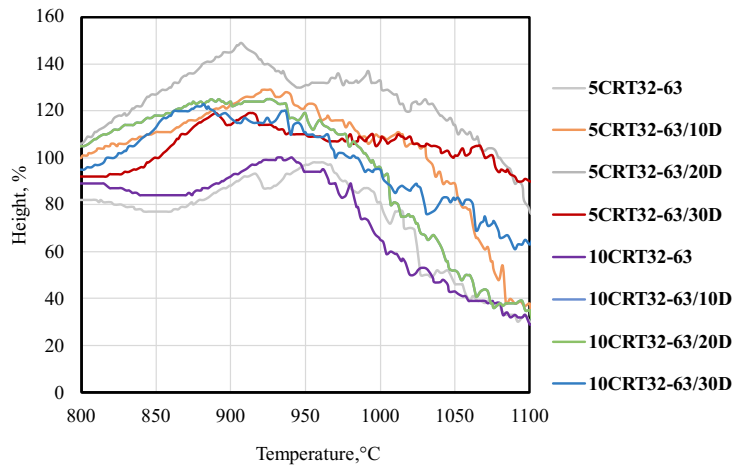


e

**Figure 10.** Heating microscopy curves of dross free mixtures (a), CRT free mixtures (b), dross and CRT glass (particle size 63µm)  mixtures (c) dross and CRT glass (particle size 32 µm) mixtures (d), and dross and CRT with two particle sizes 63 and 32 µm mixtures (e)

The oxides that form the glass can be categorized into three groups: network forming, modifier, and intermediate. The basic units of glass structure (silica tetrahedron) are formed by network-forming oxides (e.g., $SiO_2$). Modifiers alter the structure of the network by entering the voids of the network. They can change the angle and position of the bonds [73]. Intermediate oxides can be built into the glass network and modifiy it as well. Dross contains both modifier (MgO) and intermediate ($Al_2O_3$) oxides. Si-O-Si bonds are replaced by Si-O-Mg-O-Si bonds when the dross is added to container glass, forming aluminate tetrahedra instead of silicate tetrahedra. In addition, $Al_2O_3$ increases the glass melting point. In contrast, PbO, BaO, and SrO (components of CRT glass) lower the melting point. Additionally, PbO can be incorporated into glass networks as an intermediate oxide. Pb-based units replace additional silicate tetrahedra when CRT glass content increases. The formed PbO bonds, however, are weaker than the Si-O bonds due to the larger atomic or ionic radius of Pb atoms [73].

In the work of Ben Kacem et al. [94], Raman spectra were used to study the structure and properties of lead silicate glasses and melts. A strong decrease in glass transition temperature and viscosity is observed with increasing PbO content. This is highly correlated with the network depolymerization of the silicate network with the creation of non-bridging oxygens replacing bridging oxygens. As the content of the network modifier increases, the difference between adding $Na_2O$ and PbO to the glass transition temperature (Tg) decreases, and the effect on the glass transition temperature becomes more significant. Due to this, the foaming temperature may be lowered in samples containing CRT glass and dross and the viscosity increased, allowing gas bubbles to form, thereby increasing the foaming height [89] [75] [95]. Samples with CRT glass and dross at the same time mostly cover this range. Boosting the foaming process is accomplished by lowering the softening (melting) temperature and enhancing the decomposition of AlN in the dross [73].

### 2.2.3. Microstructure analysis

The microstructural analysis of the foam glasses was conducted on the cubic-shaped samples (Figure 11 to Figure 17). Figure 11 presents glass foam with container glass where the effect of adding aluminium dross in different amounts can be seen. Foam glass with only container glass had thin walls with an average cell size of around 1.5 mm. By adding 10 wt% of aluminium dross (BG/10D), the cells become wider (average 2.22 mm), and the wall thickness decreases. Adding 20 wt% dross will slightly decrease the cell's size and gives wider wall thickness distribution. Samples with 30 wt% dross have a uniform structure with smaller cells. Samples BG, BG/10D and BG/30D have almost the same value for the most frequent wall

thickness while samples BG/10D have the narrowest distribution. A larger cell size and smaller wall thickness lead to better thermal resistance but smaller compressive strength.
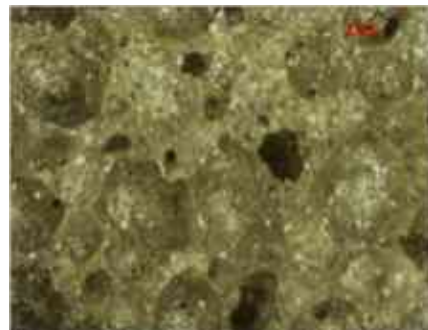


BG



BG/10D



BG/20D



BG/30D
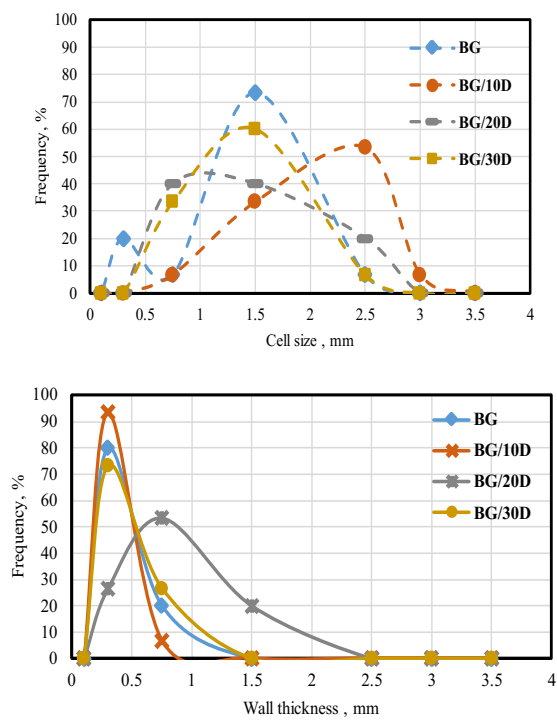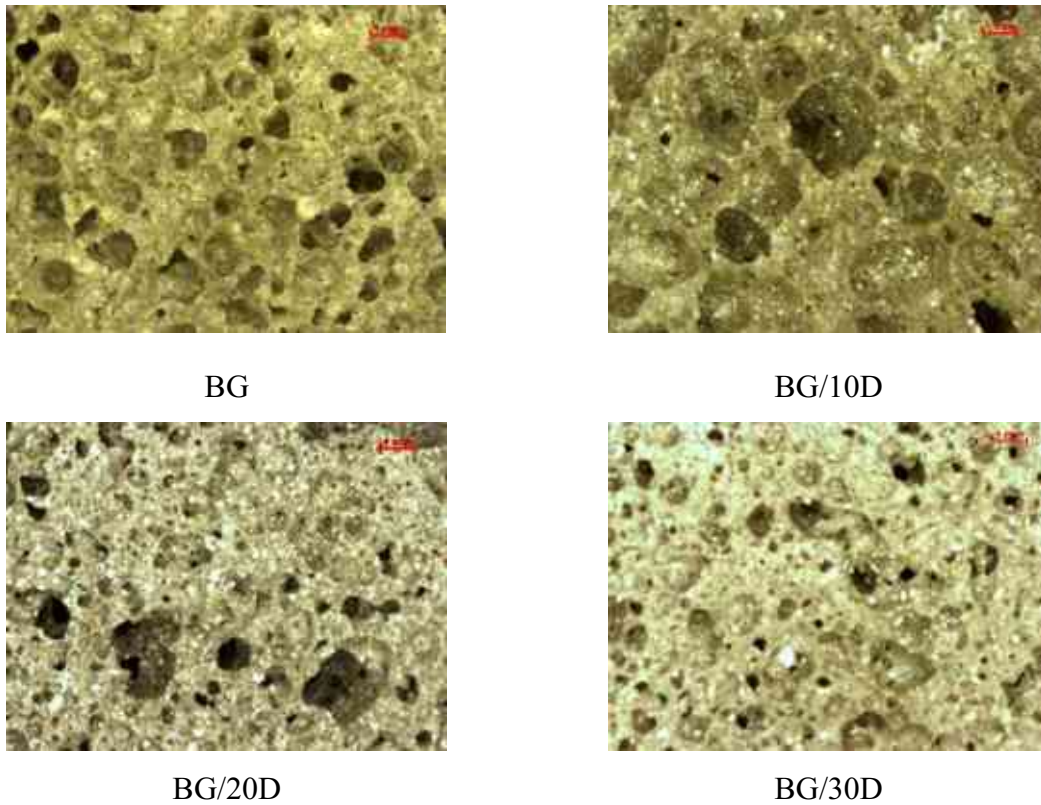




**Figure 11.** Micrographs (scale 1mm), cell size distribution, and wall thickness of foam glasses made by container glass and aluminium dross (0, 10, 20, 30 wt% dross)

Figure 12 presents foam glasses with container glass, CRT, and aluminium dross. The CRT particle size used in this section is 63 µm. Samples with 5 wt CRT and container glass powder (5CRT63) have almost the same average cell size as the foam glass with only container glass. The structure of the cells is more homogenous with round and oval shapes. While gradually adding 10 wt% aluminium dross, samples start to have more of a binomial cell size distribution (1.5 mm and 3 mm) with a homogeneous wall thickness distribution close to 0.25 mm (5CRT63/10D). Samples with 20 wt% dross have a more homogeneous cell size, with the most frequent value close to 1.5 mm, and a wider wall thickness distribution ranging from 0.25 to 2.5 mm (5CRT63/20D). With 30 wt% dross, the cells are becoming smaller while the wall thickness is still wide-ranged.
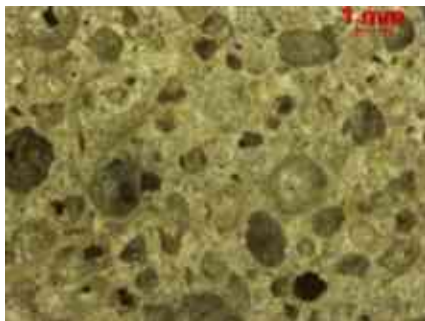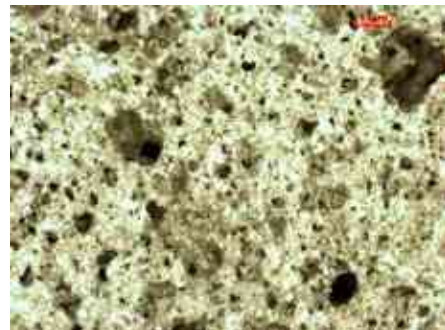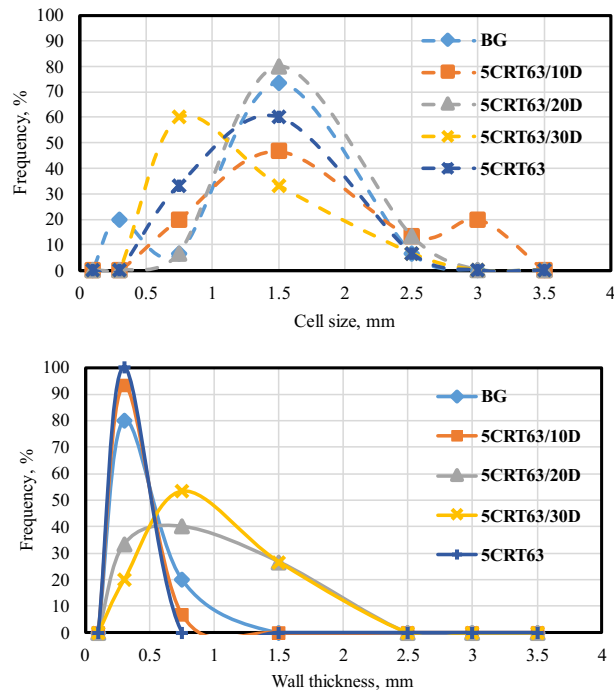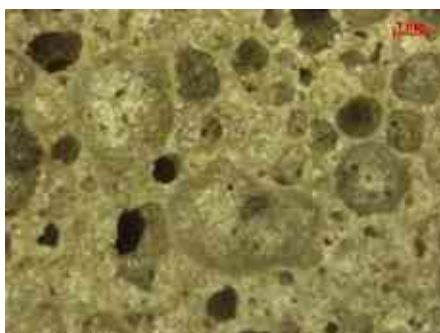


5CRT63



5CRT63/10D
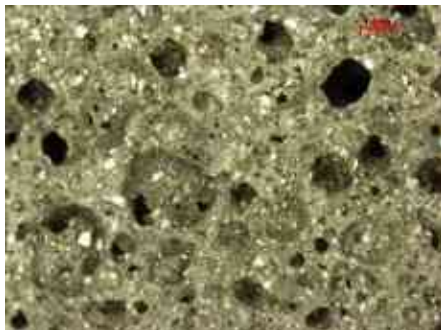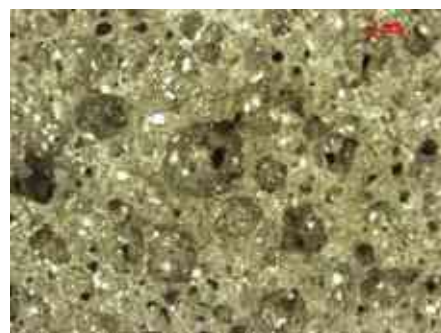


5CRT63/20D



5CRT63/30D

**Figure 12.** Micrographs (scale 1mm), cell size distribution, and wall thickness of foam glasses with 5 wt% CRT and aluminium dross (0, 10, 20, 30 wt% dross)

Figure 13 shows the results of samples in which the CRT content is increased to 10 wt%. Foam glass containing CRT and container glass has the same cell structure with slightly wider cells. Increasing the CRT glass content from 5 wt% to 10 wt% gives a more homogeneous structure of the foams. Adding aluminium dross created more diversified cell shapes due to the boosted effect of the foaming process leading to cell growth and coalescence. Glass foams containing 20 wt% dross (10CRT63/20D) have bimodal distribution with cell sizes varying from 0.25mm to 3.5 mm and a wider wall thickness. Samples with 30 wt% of dross show narrower cells (0.25mm) and wider wall thickness (10CRT63/30D).
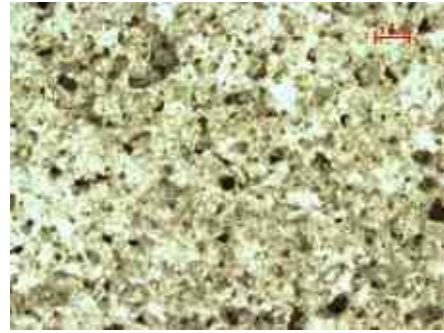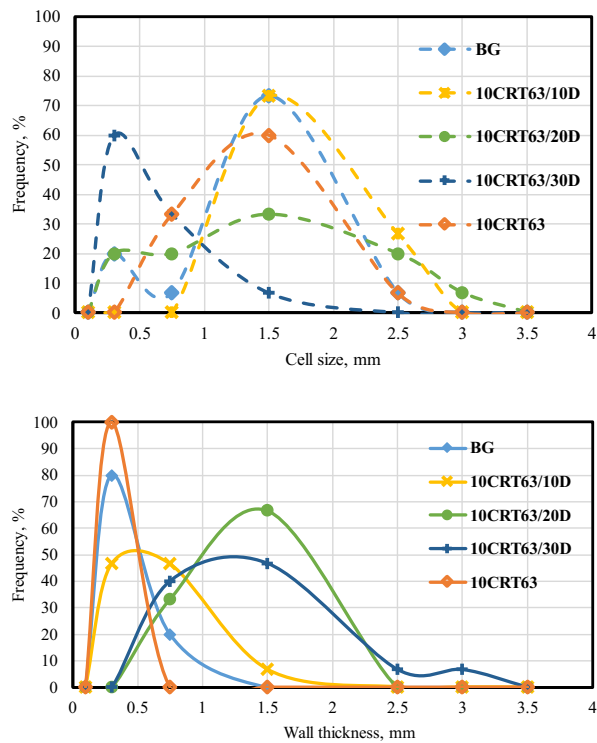


10CRT63



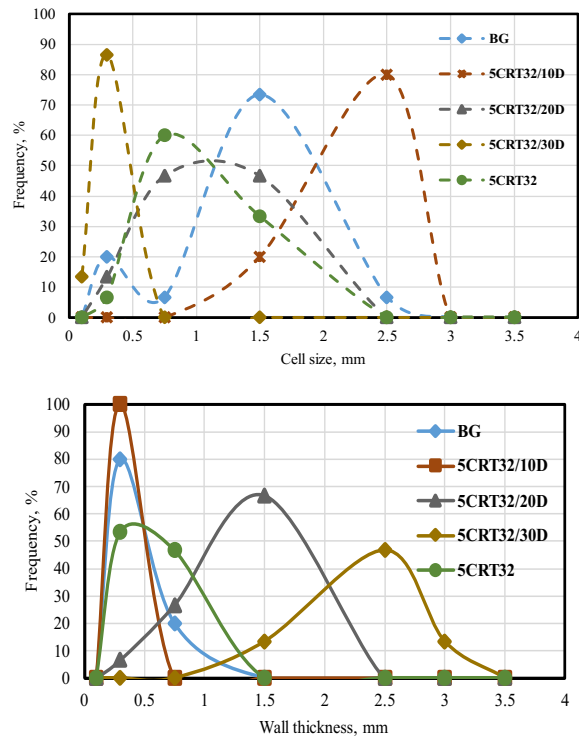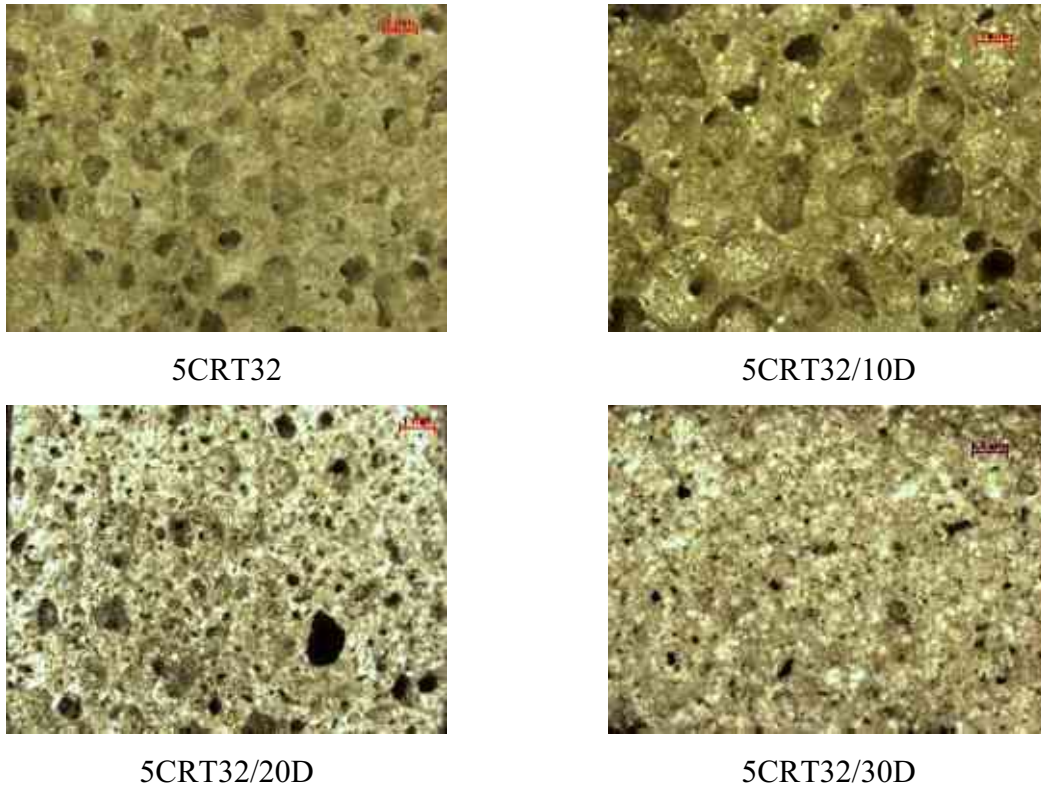10CRT63/10D
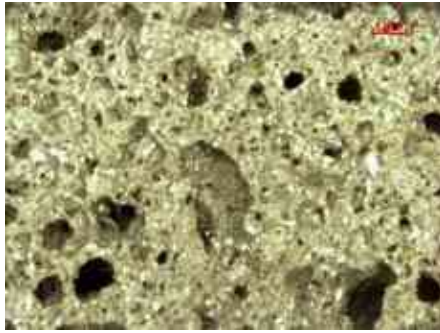
10CRT63/20D            10CRT63/30D





**Figure 13.** Micrographs (scale 1mm), cell size distribution, and wall thickness of foam glasses made with 10 wt% CRT63 and aluminium dross (0,10, 20, 30 wt% dross)

Figure 14 presents foam glasses with CRT 32 μm particle size. Samples with 5 wt% CRT and container glass exhibit slightly smaller cell sizes and wider wall thicknesses compared to glass foam made from only container glass powder without a pronounced change in the shape of the cells. By adding 10 wt% (5CRT32/10D) aluminium dross the average cell size becomes 2.5 mm with wall thickness close to 0.25 mm. With increasing the dross content to 20 wt%, the cell size decreases to 1 mm and keeps decreasing by adding 30 wt% dross to reach 0.2 mm (5CRT32/30D).

**Figure 14.** Micrographs (scale 1mm), cell size distribution, and wall thickness of foam glasses made with 5 wt% CRT32 and aluminium dross (0, 10, 20, 30 wt% dross)

Increasing the amount of CRT (32 μm particle size) to 10 wt% gives a bigger cell compared to container glass (Figure 15). Samples with 10 wt% dross (10CRT32/10D) exhibit the same
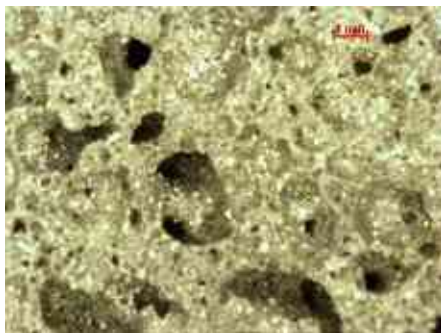
behavior as samples having only container glass powder (BG). Adding 20 wt% aluminium dross decreases the cell size and the wall thickness (10CRT32/20D). As I concluded before, 30 wt% dross decreases the cell size and increases the wall thickness with the presence of intercell in the wall (10CRT32/30D).
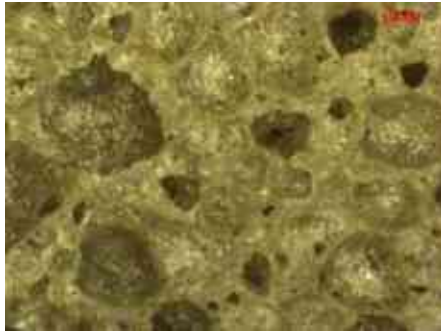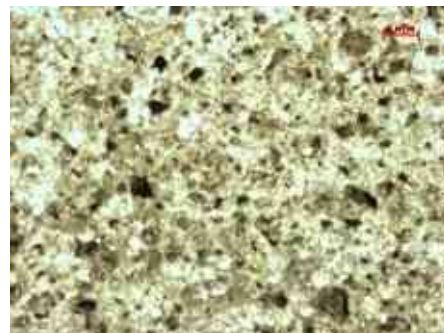


10CRT32
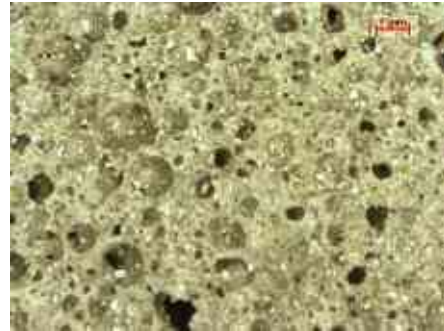


10CRT32/10D



10CRT32/20D



10CRT32/30D

**Figure 15.** Micrographs, cell size distribution and wall thickness of foam glasses made with 10 wt% CRT32 and aluminium dross (0, 10, 20, 30 wt% dross)

Figure 16 presents glass foam containing two particle sizes of CRT (32 and 63 μm), 5 wt% from each type. The mixing gives the nonhomogeneous distribution of cells (5CRT32-63). This heterogeneity slightly decreases by adding 10 wt% aluminium dross (5CRT32-63/10D). Glass foam with 20 wt% (5CRT32-63/20D) has the most frequent cell size of 1.5 mm, which decreased later by adding 30 wt% of dross (5CRT32-63/30D).



5CRT32-63



5CRT32-63/10D



5CRT32-63/20D
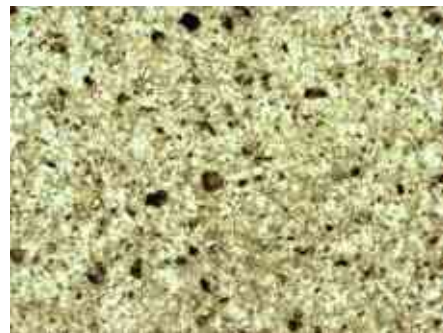


5CRT32-63/30D

**Figure 16.** Micrographs (scale 1mm), cell size distribution, and wall thickness of foam glasses made with 5 wt% CRT32-63 and aluminium dross (0, 10, 20, 30 wt% dross)

Finally, the CRT glass content was increased to 20 wt% (10 +10 wt% 63 and 32 μm particle size mixed together). Foam glass with 20 wt% of CRT glass has half of the cell size around 1.5 mm (10CRT32-63) and almost 100% of the wall thickness is equal to 0.2 mm. Inserting 10 wt% of aluminium dross (10CRT32-63/10D), the most frequent cell size ranges from 1 to 2.5 mm with an irregular polygon shape. Adding 20 wt% of dross, the cell size distribution becomes bimodal, with two peaks at 1.5 and 3 mm by (10CRT32-63/20D) and the walls become thicker. Using 30 wt% of dross (10CRT32-63/30D), 60% of cells are close to 1.5 mm (Figure 17).



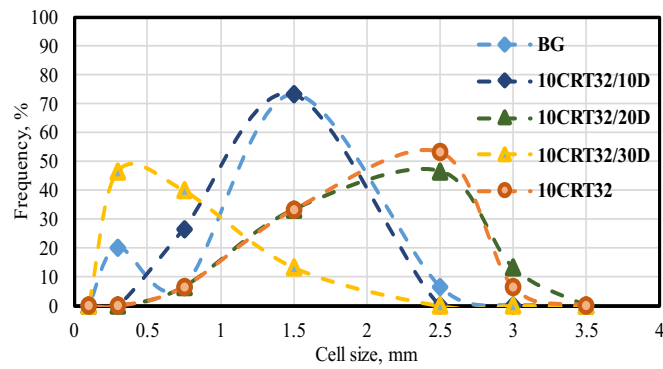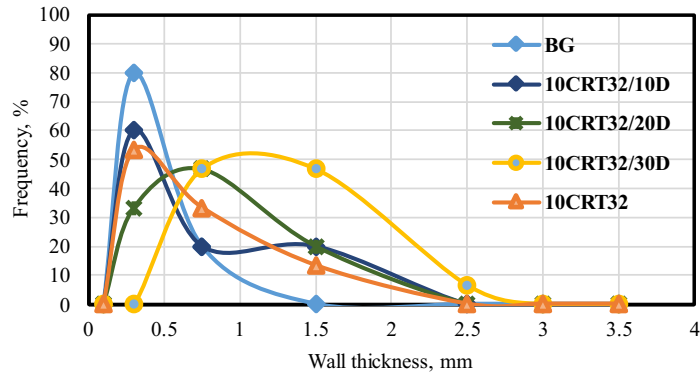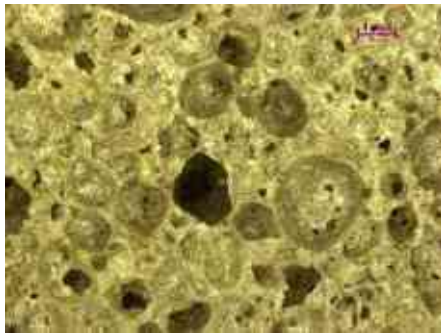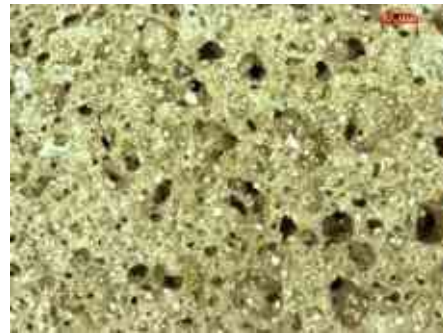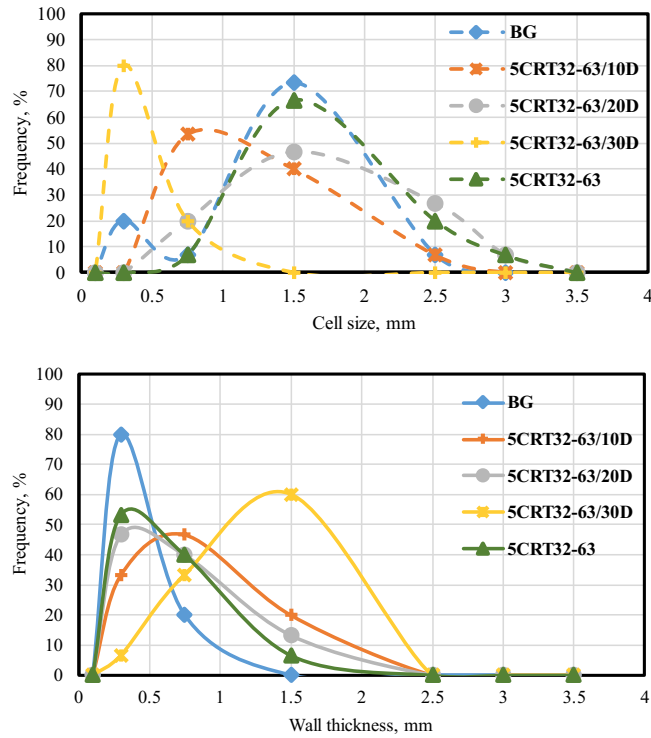10CRT32-63                                    10CRT32-63/10D

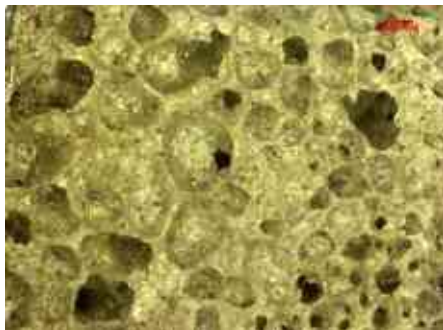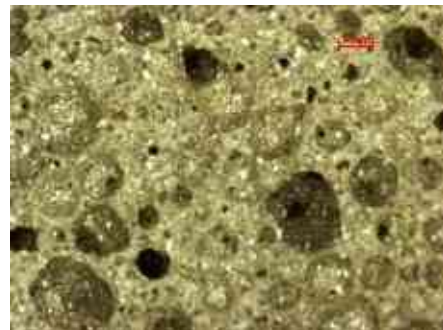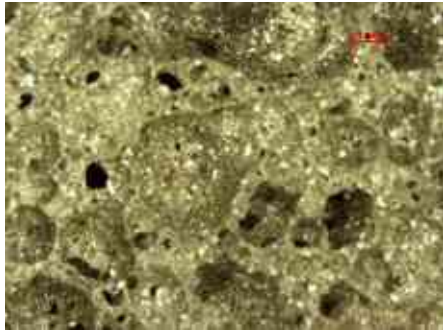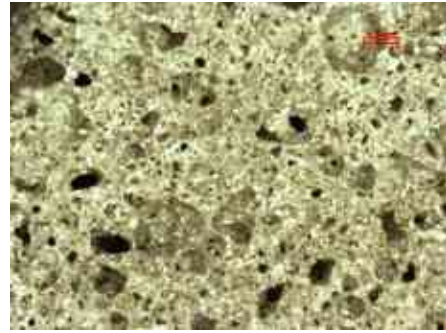10CRT32-63/20D                    10CRT32-63/30D
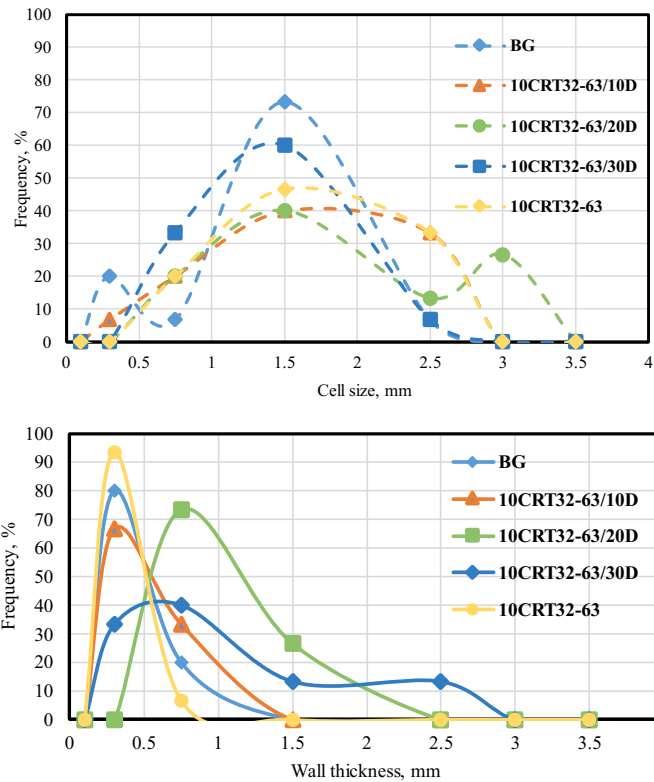




**Figure 17.** Micrographs (scale 1mm), cell size distribution of foam glasses made with 10 wt% CRT32-63 and aluminium dross

Overall, dross-free samples had thin walls with medium average cell size (1.11–1.4 mm). The shape of the pores ranges from round through oval to irregular polygons. Both open and closed pores were formed in the structure. Adding aluminium dross causes an increase in the cell size, with heterogenous structure. Round-shaped pores indicate a viscous environment formation while oval and irregular-shaped pores indicate a boasted foaming process resulting in their growth and coalescence. The densest microstructures with diversified shaped pores were detected in foams with 30 wt% dross. It is due to the increase in aluminium content which will

lead to a slight increase in the softening temperature and decelerates the liquid phase formation [96].

Figure 18 presents the elemental content of aluminium, magnesium, calcium, and sodium calculated from the XRD analysis of the composition of the raw materials. The goal is to investigate the effect of those elements on viscosity during melting. As sodium and calcium tend to destroy the bridging oxygen in the glass structure and lower the viscosity, aluminium, and magnesium increase the viscosity to create a contrariwise effect. At some point increasing the viscosity may create a dense melt which will prevent gas from expanding (Sample 10CRT63/30D). Samples with 30 wt% dross show the highest levels of aluminium and magnesium at 10 wt% and 4 wt%, respectively, whereas calcium and sodium are at their lowest levels. Cations change their position depending on the chemical composition of the glass. Elemental composition and the related variation in properties can help decide whether an ion is a former, intermediate, or modifier. For example, $[MgO_4]$ tetrahedron formation is only possible when valence compensation is obtained from the alkali ions present in the medium. In this case, Mg will act as a network former. In a soda-lime glass containing $Al_2O_3$, the $Al^{3+}$ can form $[AlO_4]$ coordination with the nonbridging oxygens and acts as a network former [96]. $Al^{3+}$ ion can take the place of $Si^{4+}$ ion in the glass structure as $[AlO_4]$ coordination resembles the $[SiO_4]$ coordination and the difference in valences is compensated by the alkali ions content. The PbO ion has the same effect and can serve as a network former, but due to its small concentration, the effect cannot be observed.
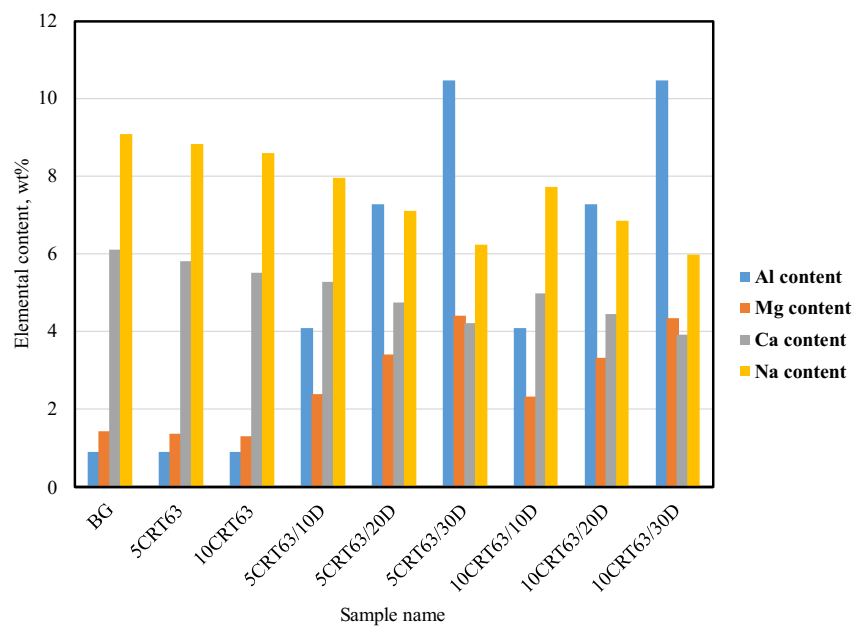


**Figure 18.** Al, Mg, Ca, and Na content in the mixtures

Overall, using a heating microscope to determine the foaming temperature is a novel and effective method. This allows saving energy and time and controlling the desired expansion of the product. For instance, aluminium dross decreased the foaming temperature and enhanced the foaming process due to the presence of aluminium nitride which decomposes and releases gaseous products ($NH_3$, $N_2$, and $NO$) [21]. Other than aluminium nitride, dross contains salts (fluorite, halite, and sylvine) which may contribute to decreasing the foaming temperature. Foam glass can be produced with optimal properties based on not only the foaming agent but also the initial raw composition and its effect on the viscosity during melting. The microstructure observation and the elemental analysis proved that adding aluminium dross can change the properties of the glass phase structure by creating bridging oxygen due to aluminium and magnesium content and consequently increasing the viscosity contrary to certain elements present in container and CRT glass (Ca, Na, Pb…) which can provoke network depolymerization and cause a decrease in the viscosity. Limiting the amount of those elements can help control the foaming process by controlling the viscosity during gas expansion.

### 2.2.4. Density

Density results are plotted in Figure 19. Foam glass made from container glass has a density of 0.23 g/cm$^3$. Adding CRT glass, the density didn't noticeably change. It is may due to the similar viscosity during melting leading to the same foaming mechanism taking place. Samples with aluminium dross have different densities depending on the amount. CRT-free (glass/dross) samples have continuously increased density with the dross content. Samples containing 5 wt % CRT glass (63 μm particle size) present an increment in the density until 20 wt% content of aluminium dross, where it starts to decrease. At the same time, the density of the samples with 10 wt% CRT glass increased with increasing dross content. Foam glass with a smaller particle size of the CRT glass has an increased density regardless of the amount of the CRT glass (Figure 19).

The average cell size is highly negatively correlated to the density of the foam glass shown in Figure 20. As the aluminium dross content increases the average cell size of the foam decreases and the density increases. The negative slope didn't change by adding 10 wt% CRT glass to container glass but slightly differed in case of adding 5 wt% CRT glass. The reverse relation between density and average cell size can be seen too in Annex Figure A2. It is due to the indirect effect of the viscosity on the foaming process. A chemical reaction occurs at a specific temperature to create gaseous products. The gas will expand depending on the viscosity of the liquid. The viscosity of the surrounding bubbles must be able to withstand the shape of the bubble without collapsing the walls in order to create a lightweight structure. Due to the high
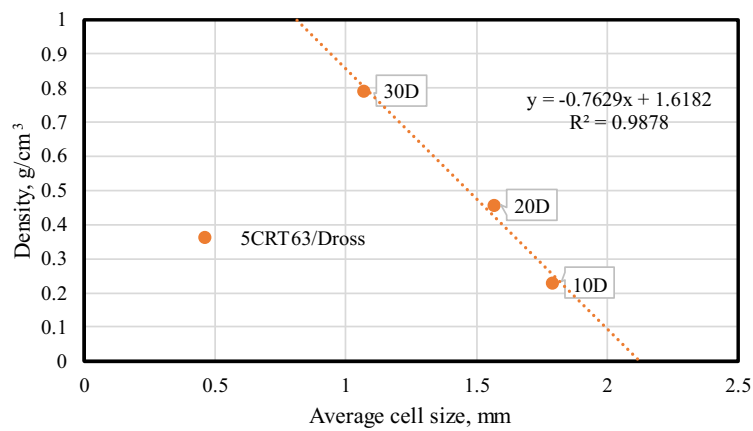
level of aluminium and magnesium in the material, the density increased, creating a very strong barrier that was virtually impossible to penetrate by the gas bubble. This can explain the high density of the foam glass with 30 wt% dross which can reach 2.5 g/cm$^3$.
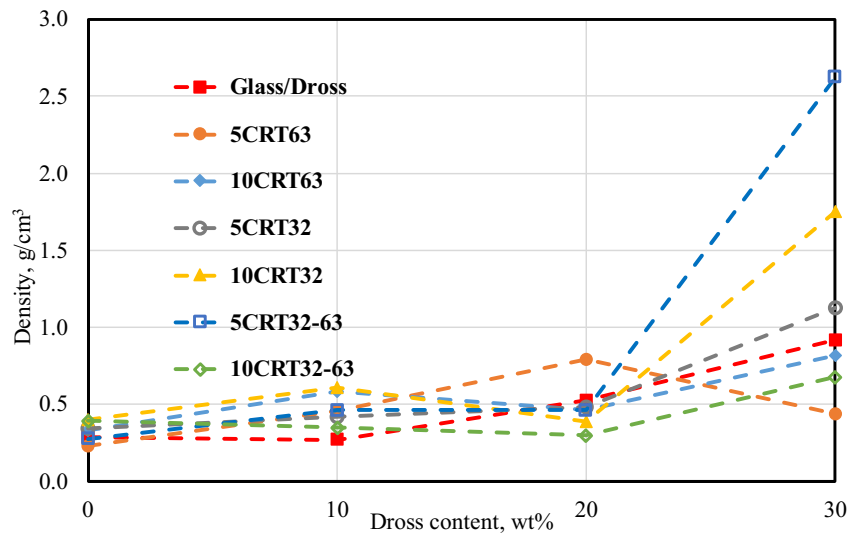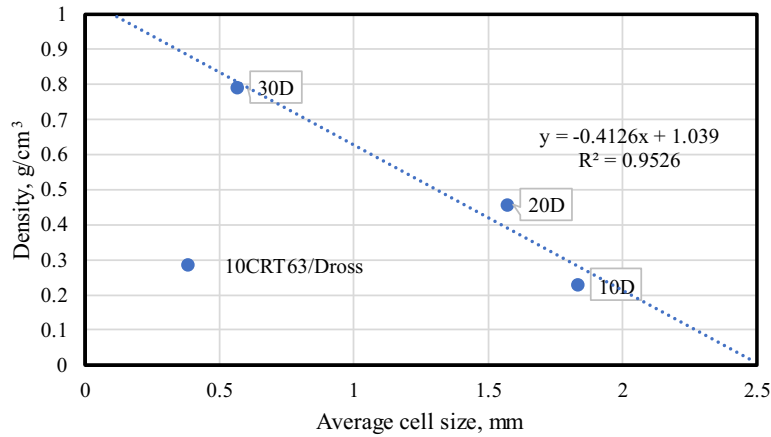


**Figure 19.** Density of the samples in function of aluminium dross content
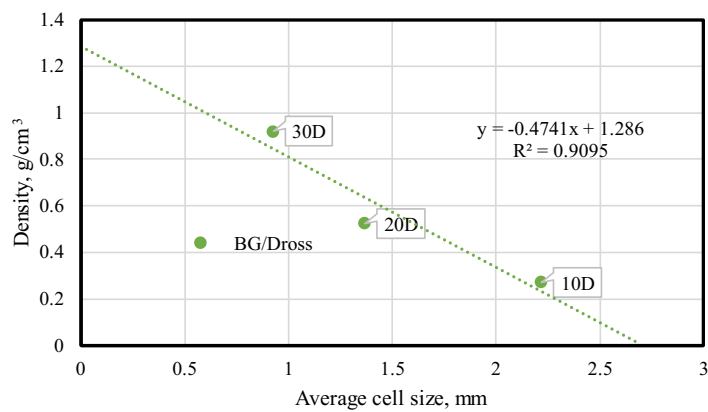


a



b

c

**Figure 20.** Density versus average cell size of CRT glass-free samples (a), container glass with 5 wt% CRT glass and dross samples (b), and container glass with 10 wt% CRT glass and dross samples (c)

### 2.2.5. Thermal conductivity

Foam glass has been widely used in many fields of heat insulation in the inner and outer walls of buildings, petroleum chemical engineering, decoration engineering refrigeration, and ground engineering. For those purposes, the thermal conductivity of the materials is important.

The data registered from the instrument for the samples are plotted in Figure 21. Thermal conductivity coefficient ranges between 0.038 and 0.07 W/mK. Mixtures 10CRT63, 5CRT32, 10CRT63-32, and 5CRT63-32 have a thermal conductivity that increases with increasing dross to 10 wt%, then starts to decrease to reach the minimum in samples containing 20 wt% dross. After that, it increases again to reach the maximum at 30 wt% dross content. 5CRT63, 10CRT32, and Glass/Dross samples have the opposite behaviour compared to other samples where the thermal conductivity reaches the minimum at 10 w% dross content and then starts to increase again.

Thermal conductivity depends on the density and size of the cells. Thermal conductivity is negatively correlated to the average cell size (Figure 22). As the average cell size increases the thermal conductivity decreases. It is generally believed that the larger the cells, the better the thermal insulation because heat waves propagate through the walls and are attenuated by air or gases. The uniformity (homogeneity) of the cells is another critical factor that affects thermal conductivity. In a sample, heterogeneous cell sizes offer better thermal insulation. The weak correlation in samples with 5 wt% CRT glass and dross can be due to the heterogeneity of the cell size.

**Figure 21.** Thermal conductivity in function of dross and CRT content
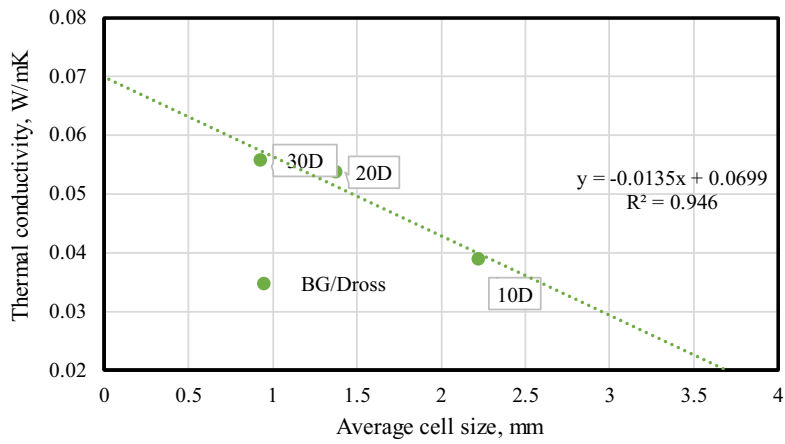


a
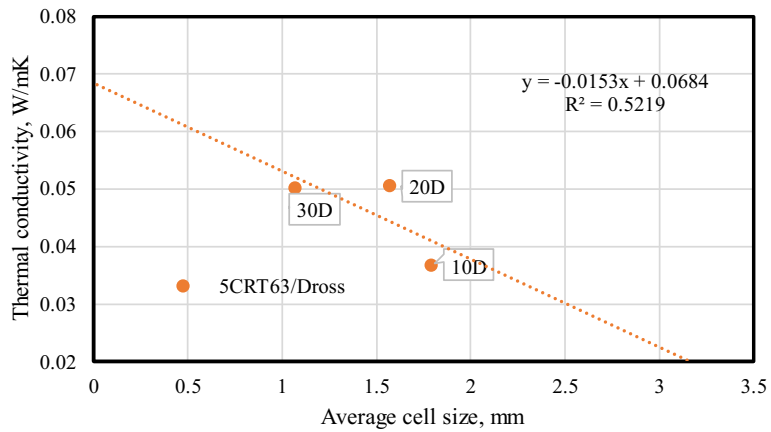


b
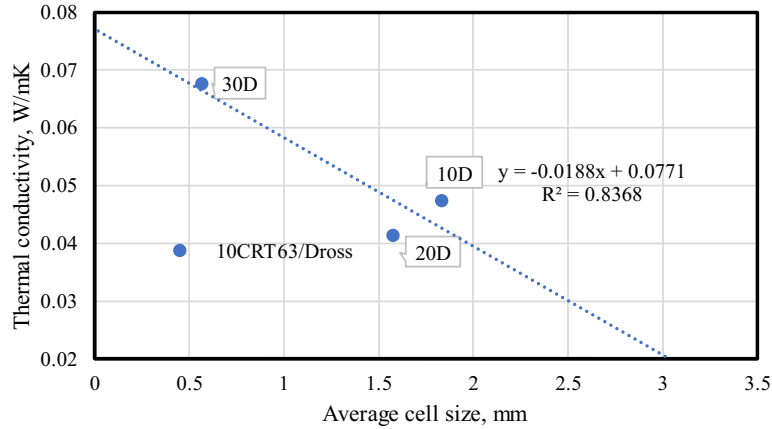
c

**Figure 22.** Thermal conductivity versus average cell size of CRT glass-free samples (a), container glass with 5 wt% CRT glass and dross samples (b), and container glass with 10 wt% CRT glass and dross samples (c)
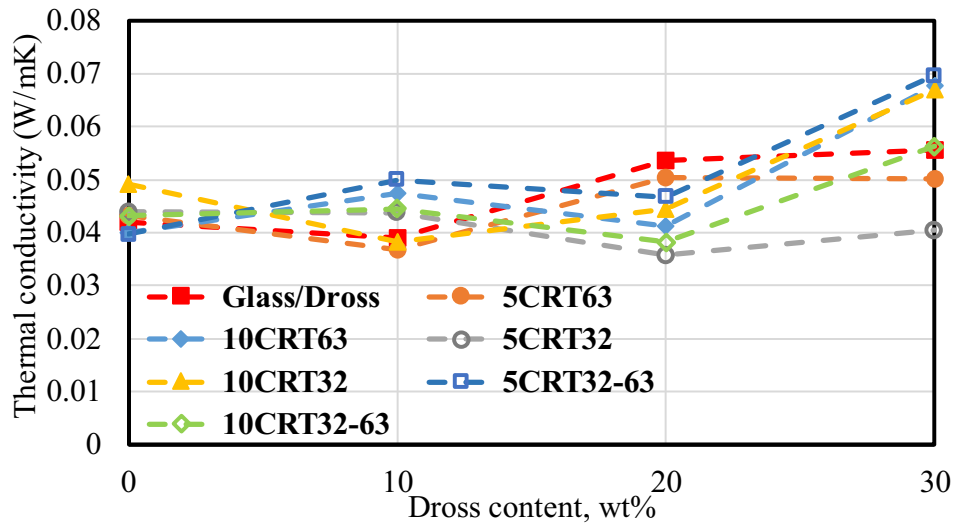
Thermal conductivity is positively correlated to the density and follows the same trend as it is seen in Figure 23. Most of the samples having high density have high thermal conductivity, as well. Especially samples with 30 wt% dross (Figure A3 and A4 in the Annex A). CRT-free samples (BG, BG/10D, BG/20D, and BG/30D), for example, show an increase in density and thermal conductivity with increasing aluminium dross content. It is due to the increase of the Al-Mg content which created more densified structure.
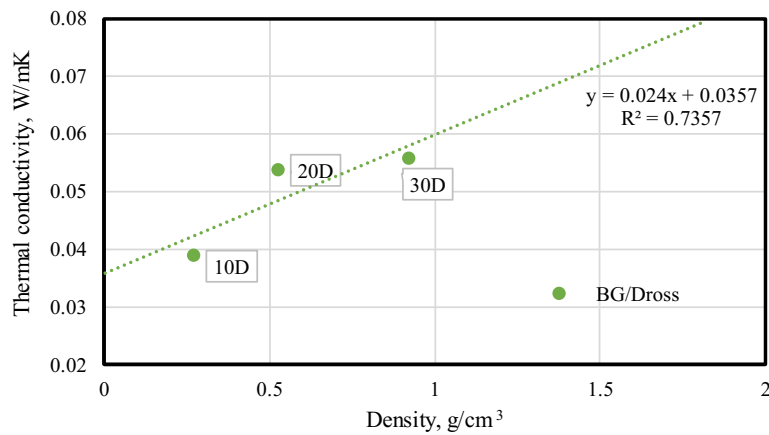


a
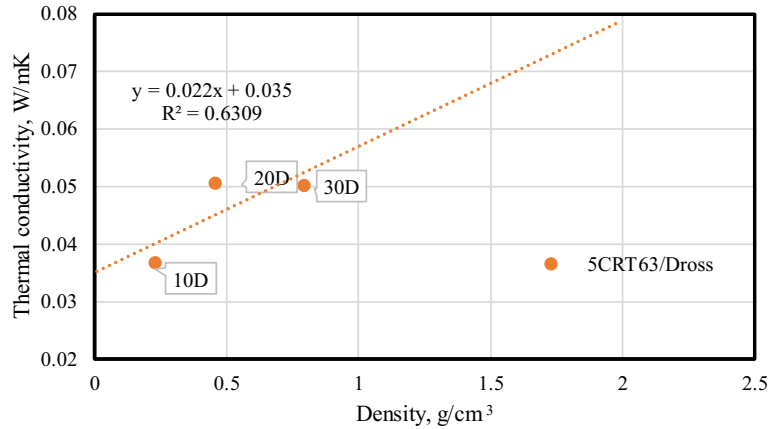
b
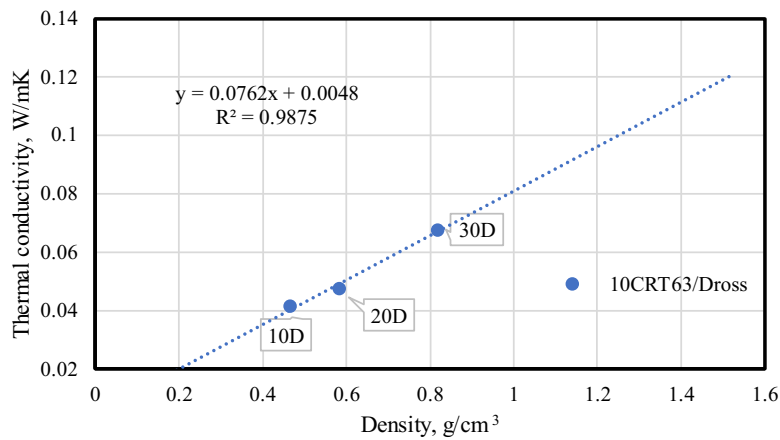


c

**Figure 23.** Thermal conductivity versus density of CRT glass-free samples (a), container glass with 5 wt% CRT glass and dross samples (b), and container glass with 10 wt% CRT glass and dross samples (c)

### 2.2.6. Water absorption

The absorption test results of the samples are given in Figure 24. Samples containing 5 and 10 wt% of CRT 63, have the same tendency with samples containing 10 wt% of CRT 32 and samples with 10 wt% CRT 63 and 32 mixtures. Those curves start to decrease to reach 10 wt% dross content then start to increase slightly with samples containing 20 wt% dross and decrease again to the minimum absorption with samples containing the highest dross 30 wt%. Water absorption of the samples containing 5 wt% of CRT32 and 5 wt% of CRT63 and 32, decreases with adding aluminium dross to reach the minimum with 30% dross content. In case of samples with container glass and dross, the absorption decreases until 20 wt% dross content then increase to reach the maximum at 30 wt% dross content.

Absorption usually depends on the porosity of the foam glass and whether the pores are closed or open. This can be determined by a porosity measurement device such as a mercury porosimeter or helium porosimeter. Both kinds of foams can be used. Foam glass with closed cells can be used as insulation in the building while open pores foams can be used in ice rings and on stadium grounds.
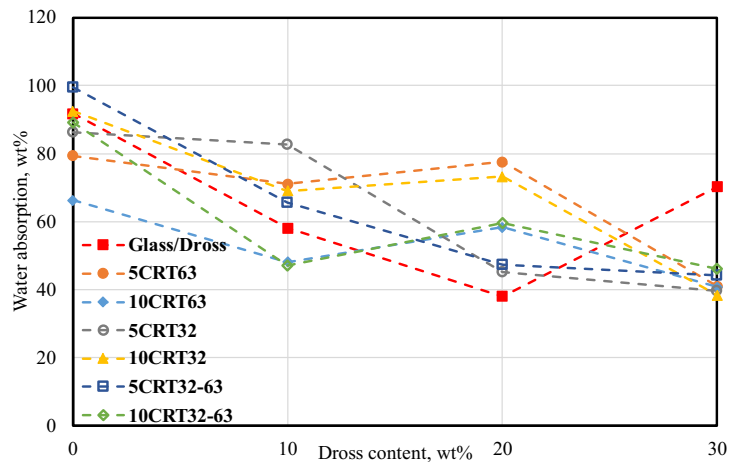


**Figure 24.** Water absorption of the foam glasses in function of dross content

## 2.2.7. Compressive strength

Foam glass can be used in complex embankment applications as filling material to reduce vertical and lateral earth pressures, and to increase slope stability. Strength properties measurement is required to be able to produce specific light material that can withstand high loads. Compressive strength test was done on the samples. It was determined by using an Instron universal testing instrument. Samples were evenly loaded with a force perpendicular to their surface. Test results are shown in Figure 25.

Samples with 10 wt% CRT particle size 63 and particle size 32, and samples with both particle sizes combined show a maximum with 10% dross, and a minimum strength when adding 20 wt% dross. For glass / dross samples, the highest strength is detected in samples with 20% dross. For samples with CRT63- 5 wt% and CRT32-5 wt%, the strength decreased to reach the minimum at 10wt% dross content then increased again to the maximum at 30 wt%.

Compressive strength depends directly on wall thickness (Figure A5). The compressive strength is positively correlated with the wall thickness. Usually, the load will be distributed evenly on the walls of the cells. The thicker the walls, the greater the load resistance. Figure 26 illustrated this. As the wall thickness increases with increasing the aluminium dross, the compressive strength will increase as well.
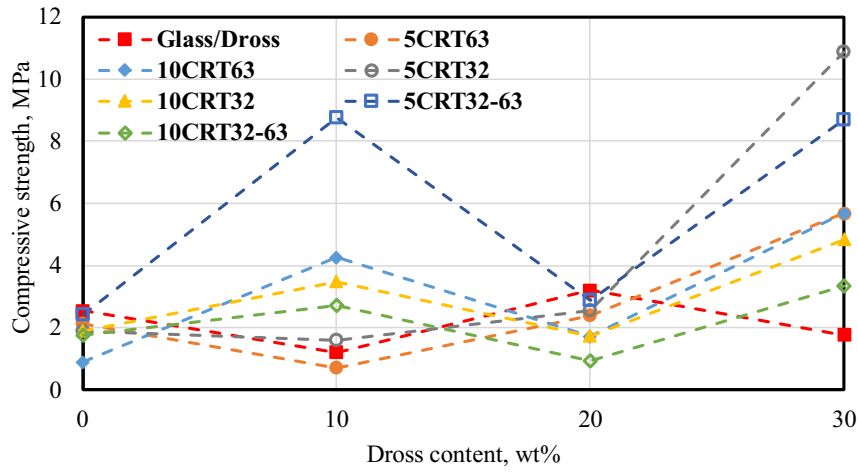
**Figure 25.** Compressive strength of the foam glass
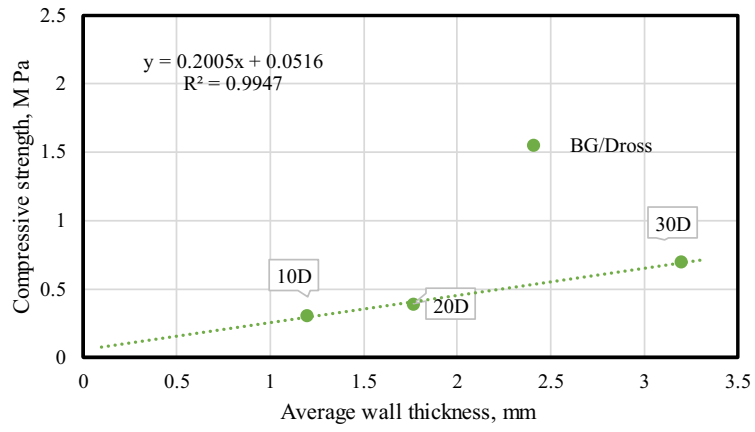


(a)
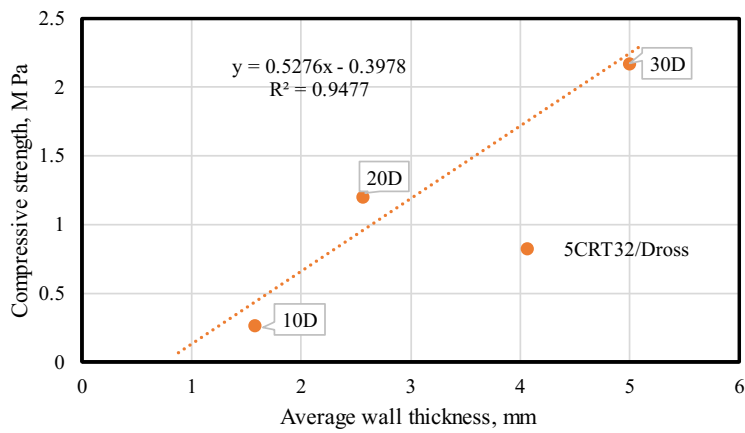


(b)
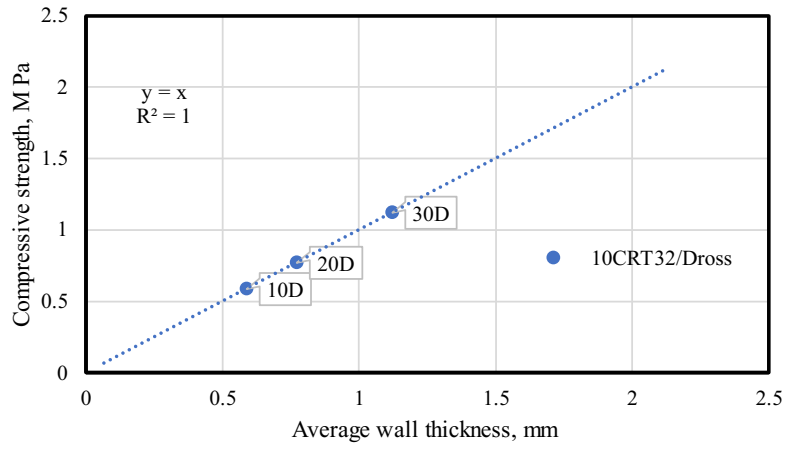
c

**Figure 26.** Compressive strength versus average wall thickness of CRT glass-free samples (a), container glass with 5 wt% CRT glass and dross samples (b), and container glass with 10 wt% CRT glass and dross samples (c)

# 2.3. Conclusions

Foam glass was successfully produced using nearly 100% waste materials: container glass material, cathode ray tube (CRT) glass (5 and 10 wt%) with two particle sizes 63 and 32 μm, secondary aluminium dross (10, 20, and 30 wt%), and silicon carbide (2 wt%). Accordingly, the following observations and conclusions were drawn from the first part of this research:

**Foaming behaviour**

Investigating the foaming process is the main direction to produce foam glass with optimal characteristics. The most conventional method introduced in the literature is to use thermogravimetric analysis or high-speed synchrotron X-ray tomography. I used a heating microscope to determine the foaming behavior, which is considered a novel and effective technique. This allows for saving energy, and time and taking control over the expansion of the final product.

**The effect of adding aluminium dross on**

Foaming process

Added aluminium dross to produce foam glass is a novel aspect of the recycling of this waste material that started to see the light in 2021 in fewer papers [73] [74] [69] [75]. Aluminium dross decreased the foaming temperature and enhanced the foaming process due to the presence of aluminium nitride which decomposes and releases gaseous products ($NH_3$, $N_2$, and NO) [97] [89]. Other than aluminium nitride, dross contains salts (fluorite, halite, and sylvine) which may contribute to decreasing the foaming temperature.

Viscosity

Magnesium and aluminium are abundant in aluminium dross, which can alter the glass phase structure by creating bridging oxygen and thereby increasing the viscosity, as opposed to certain elements in container and CRT glass (Ca, Na, Pb...) that may cause network depolymerization and decrease viscosity. At some point increasing the viscosity may create a dense melt which will prevent gas from expanding. This can be shown in the samples with 30wt% dross where the level of aluminium and magnesium reaches 10 wt% and 4 wt% respectively, whereas calcium and sodium are at lowest levels. For Mg and Al to act as network formers, tetrahedron formation is necessary to form $[MgO_4]$ and $[AlO_4]$ which resemble $[SiO_4]$ coordination allowing $Mg^{2+}$ and $Al^{3+}$ to replace $Si^{4+}$. The difference in the valence will be compensated by the alkaline content.

From the overall composition, it can be said that aluminium and magnesium should not exceed 10 wt% and 4 wt%, respectively. Therefore, the viscosity will not be overly high for the gas

bubbles to form and shape the foam glass cells. By controlling the viscosity of the melt, the cell size, density, thermal conductivity, and compressive strength can be controlled as a result.

Density

It is shown that the average cell size is highly negatively correlated with the density of foam glass. As the aluminium dross content increases the average cell size of the foam decreases and the density increases. It is due to the indirect effect of the viscosity on the foaming process. A chemical reaction occurs at a specific temperature to create gaseous products. The gas will expand depending on the viscosity of the liquid. The consistency of the surrounding bubbles must be able to withstand the shape of the bubble without collapsing the walls to create a lightweight structure. As a result of the high aluminium and magnesium content in the material, the density increased. This created a very strong barrier that was virtually impossible to penetrate by the gas bubble which can explain the high density of the foam glass with 30 wt% dross content (2.5 g/cm$^3$).

Thermal conductivity

Thermal conductivity depends on the density and size of the cells. Thermal conductivity is negatively correlated to the average cell size. As the average cell size increases the thermal conductivity decreases. It is generally believed that the larger the cells, the better the thermal insulation because heat waves propagate through the walls and are attenuated by air or gases. The uniformity (homogeneity) of the cells is another critical factor that affects thermal conductivity. In a sample, heterogeneous cell sizes offer better thermal insulation. The weak correlation in samples with 5 wt% CRT glass and dross can be due to the heterogeneity of cell size.

Thermal conductivity is positively correlated to density. Samples with high density have high thermal conductivity especially samples with 30 wt% dross.

Compressive strength

Compressive strength depends directly on wall thickness. The compressive strength is positively correlated with the wall thickness. Usually, the load will be distributed evenly on the walls of the cells. The thicker the walls, the greater the load resistance. As the wall thickness increases with increasing the aluminium dross, the compressive strength will increase too.

**The effect of CRT glass**

Particle size

Using 63 or 32 µm gives close results but combining the two sizes can decrease the foaming height and increase the density. The particle size of the different raw materials should be close

(less than 70 µm) to allow oxygen into voids to enable oxidation reaction during foaming process.

Lead content

PbO can be incorporated into glass networks as an intermediate or former oxide. Pb-based units replace additional silicate tetrahedra when CRT glass content increases. The formed PbO bonds, however, are weaker than the Si-O bonds due to the larger atomic or ionic radius of Pb atoms [73]. The effect of CRT glass will be more detailed in the second part of this research.

# Chapter 3

# Properties optimisation : Effect of dross type and CRT content

## 3.1. Experimental procedures and methods

### 3.1.1 Raw materials preparation

The first step of producing foam glass was to prepare the raw materials. Container glass was collected from households in Miskolc (white glass). The bottles were washed, cleaned and dried. Container glass was crushed and milled (in the Institute of Raw Material Preparation and Environmental Processing). The particle size of the glass powder was determined using a Horiba Laser Scattering Particle Size Distribution Analyzer LA-950. The cumulative curve shows that D95 is equal to 94 μm (Figure 27). To reach smaller size, the powder was sieved with a 63 μm sieve. CRT glass powder was provided by Daniella Ipari Park Ltd. The particle size of the CRT glass was less than 63 μm as well. Three aluminium drosses (64, X, 53) with different composition were used (produced by Arconic-Köfém Mill Products Hungary Ltd., Szekesfehervar, Hungary). The metal and salt content of the as-received dross was removed by Kekesi et al. [91] with the following method. After melting the aluminum slag to recover the molten metals, the remaining dross was crushed, milled, and washed three times with distilled water to dissolve and eliminate the salt content.

In the mixtures, container glass was the basic component. In addition, 5 to 10 wt% CRT glass and 10, 15 or 20 wt% dross was added to the container glass (Table 6 and Figure 28). This interval was selected based on the previous results. While compressive strength improved, 30 wt% dross was eliminated since it results in foam glass with the highest density and thermal conductivity. Moreover, 2 wt% silicon carbide was admixed as a foaming agent (α-SiC with particle size less than 32 μm). From each composition, 100 g was prepared. Weighted mixtures were homogenized in a laboratory mixer for 10 minutes at 300 rpm. Five grams from each mixture were poured in a stainless-steel mold then pressed under 11 MPa for 10 s into a cylindrical shape (diameter = 20 mm, height = 11 mm). 20 samples from each mixture were prepared.

After the process of admixing, the experimental powder mixtures were analysed by a heating microscope (MicrOvis, Camar Elettronica) to determine the exact foaming temperature for sintering. Test samples were prepared using the pressing mold kit of the microscope. The pressed samples (with approximately 5 mm height and 2 mm diameter) are placed on an 8 × 10 mm sized alumina sheet and moved into a furnace where the sample's silhouette change in function of temperature is registered to identify the beginning of sintering, softening, sphere, half-sphere, and melting temperatures. The temperature, where the sample reached the maximum height, was identified as the foaming and sintering temperature. The samples were sintered in an electric chamber furnace at different temperatures with a heating rate of 5°C/min and a holding time of 10 min.
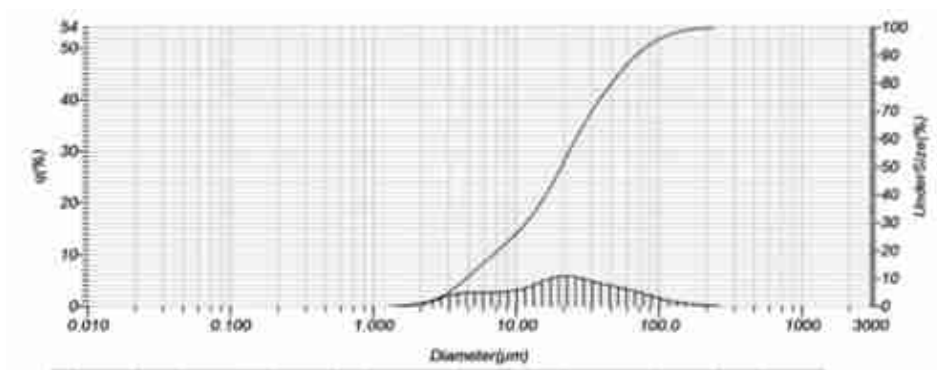


**Figure 27.** Particle size distribution of the container glass powder before sieving
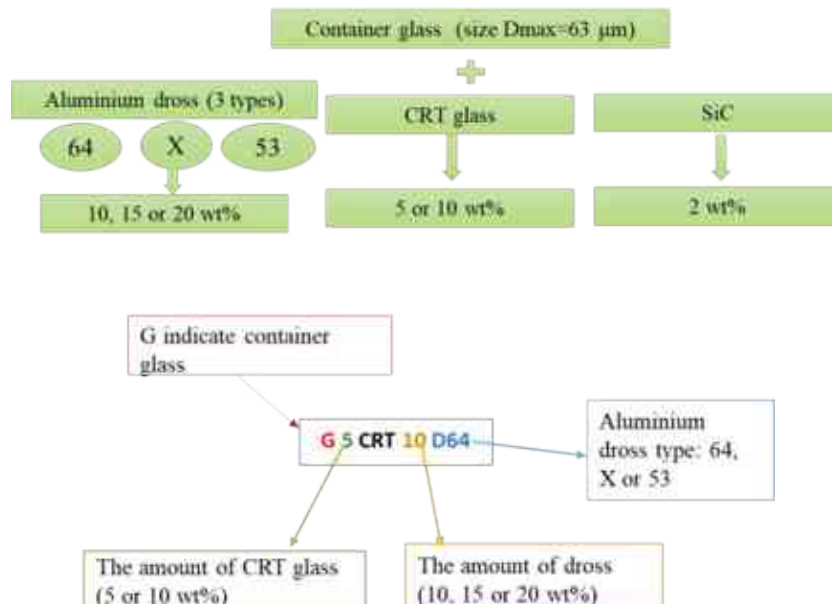


**Figure 28.** Research plan and sample name coding

**Table 6.** Composition and foaming characteristics (determined by heating microscopy) of the mixtures

| Sample code | Composition (wt%) | | | | | | Foaming temperature (°C) | Max foaming height (%) |
|---|---|---|---|---|---|---|---|---|
| | **D64** | **DX** | **D53** | **SiC** | **CRT** | **BG** | | |
| G | 0 | | | 2 | 0 | 98 | 847 | 158 |
| G5CRT | 0 | | | 2 | 5 | 93 | 849 | 160 |
| G10CRT | 0 | | | 2 | 10 | 88 | 860 | 154 |
| G10D64 | 10 | | | 2 | 0 | 88 | 869 | 160 |
| G15D64 | 15 | | | 2 | 0 | 83 | 869 | 166 |
| G20D64 | 20 | | | 2 | 0 | 78 | 864 | 165 |
| G5CRT10D64 | 10 | | | 2 | 5 | 83 | 858 | 155 |
| G5CRT15D64 | 15 | | | 2 | 5 | 78 | 869 | 156 |
| G5CRT20D64 | 20 | | | 2 | 5 | 73 | 880 | 168 |
| G10CRT10D64 | 10 | | | 2 | 10 | 78 | 860 | 168 |
| G10CRT15D64 | 15 | | | 2 | 10 | 73 | 855 | 157 |
| G10CRT20D64 | 20 | | | 2 | 10 | 68 | 859 | 150 |
| G10DX | | 10 | | 2 | 0 | 88 | 859 | 163 |
| G15DX | | 15 | | 2 | 0 | 83 | 855 | 155 |
| G20DX | | 20 | | 2 | 0 | 78 | 848 | 144 |
| G5CRT10DX | | 10 | | 2 | 5 | 83 | 859 | 161 |
| G5CRT15DX | | 15 | | 2 | 5 | 78 | 851 | 168 |
| G5CRT20DX | | 20 | | 2 | 5 | 73 | 860 | 152 |
| G10CRT10DX | | 10 | | 2 | 10 | 78 | 849 | 164 |
| G10CRT15DX | | 15 | | 2 | 10 | 73 | 845 | 169 |
| G10CRT20DX | | 20 | | 2 | 10 | 68 | 845 | 172 |
| G10D53 | | | 10 | 2 | 0 | 88 | 869 | 161 |
| G15D53 | | | 15 | 2 | 0 | 83 | 866 | 163 |
| G20D53 | | | 20 | 2 | 0 | 78 | 865 | 142 |
| G5CRT10D53 | | | 10 | 2 | 5 | 83 | 850 | 159 |
| G5CRT15D53 | | | 15 | 2 | 5 | 78 | 864 | 150 |
| G5CRT20D53 | | | 20 | 2 | 5 | 73 | 865 | 161 |
| G10CRT10D53 | | | 10 | 2 | 10 | 78 | 860 | 152 |
| G10CRT15D53 | | | 15 | 2 | 10 | 73 | 854 | 159 |
| G10CRT20D53 | | | 20 | 2 | 10 | 68 | 865 | 154 |

### 3.1.2. Investigation methods

The chemical composition of the raw materials was determined as follows: the composition of the container and CRT glasses was determined by inductively coupled plasma mass spectrometry (ICP-OES) (Varian 720 ES spectrometer) and X-Ray Fluorescence (Rikagu Supermini). The mineral composition of the dross was analyzed by X-ray powder diffractometry (XRD) (Rigaku Miniflex II) and quantified by Rietveld-fitting. The particle shape and composition of the CRT glass and aluminium dross were characterized using a scanning electron microscope (SEM) Zeiss EVO MA10.

After sintering in an electric chamber furnace, the samples were cut into cylindrical shapes (diameter = 40 mm, height = 16.5 mm) where volume expansion, water absorption, bulk density, porosity, microstructure, thermal conductivity, and compressive strength were investigated. The volume expansion coefficient was calculated as follows:

$$Volume\ expansion\ Coeff\ (-) = (V_F - V_i)/V_i \tag{10}$$

Where: $V_i$ and $V_F$ are the volume of the sample before and after firing (cm$^3$) respectively.

Density, thermal conductivity, water absorption, and compressive strength tests were conducted in the same way as in the previous part.

For the microstructure evaluation, the samples were cut, and the upper surfaces were photographed with Nikon camera. Samples were sent to the computerized tomography (YXLON CT computed tomography system scan). This method combines a series of X-ray images taken from different angles around the material and uses computer processing to create cross-sectional images (slices) of the object without destruction. As part of the microstructure characterization, selected samples were sent to scanning electron microscopy (SEM) with Zeiss EVO MA10. Coating the samples with gold was required to improve the imaging qualities. It reduces thermal damage inhibits charging and improves the secondary electron signal. The porosity, the amount of open and closed pores in the foam glass were calculated through the measurement of the skeletal density and the powder density (ground in mortar) using a Helium pycnometer (ULTRAPYC 1200e, TU Bergakademie Freiberg):

$$\phi = \left(1 - \frac{\rho_{bulk}}{\rho_{solid}}\right) \times 100 \tag{12}$$

$$\phi_{cp} = \frac{\rho_{skel}^{-1} - \rho_{solid}^{-1}}{\rho_{bulk}^{-1} - \rho_{solid}^{-1}} \times 100\ \% \tag{13}$$

$$\phi_{op} = \phi - \phi_{cp} \tag{14}$$

Where $\phi$ is the porosity of the foam glass (%), $\phi_{cp}$ is the closed porosity (%), $\phi_{op}$ is the closed porosity (%), $\rho_{skel}$ (the skeletal density) is the density of the foam structure measured by the He

pycnometer (g/cm$^3$) $\cdot$ $\rho_{bulk}$ (the bulk density) is the geometrical density calculated as the mass per volume in (g/cm$^3$), $\rho_{solid}$ (the solid density) is the density of the powder issued from grinding the foam glass in (g/cm$^3$).

In the following part, the experimental tests were conducted in TU Bergakademie Freiberg, (Institute of Glass Science and Technology and the Center for Efficient High-Temperature Processes and Materials Conversion (ZeHS)), Germany.

Fourier-transform infrared spectroscopy (FTIR) and Raman spectroscopy were used to determine the different states of the molecules in foam glass. A BRUKER-TENSOR 27 spectrophotometer was utilized to investigate Fourier transform infrared (FTIR) spectra. A RenishawInvia micro-Raman spectrometer equipped with a notch filter was used to collect Raman scattering spectra. Unfortunately, vibrational spectroscopy was not suitable as FTIR is more convenient for organic material and Raman Spectra was inadequate due to the high metal content in the foam glass tending to block spectra detection. This can be seen in Figures B1 and B2 in Annex B. Thus, the following test was conducted to identify foam glass oxides. Samples were digested with hydrofluoric acid/perchloric acid. Foam glass was first crushed. 200 mg powder was weighed, placed in a platinum bowl, and wetted with a little deionized water, 10 ml HF and 2 ml HClO$_4$ were added and heated on the hotplate. Heating is repeated with half the amount of the acids. An insoluble residue remained in all flasks. Samples were analysed with Inductively Coupled Plasma Optical Emission spectroscopy (ICP-OES), Spectroflame to determine the oxides content.

X-ray Powder Diffraction (XRD) investigation was done on the selected samples using Siemens Kristalloflex D500, and the results were interpreted by Rietveld-Method to get information on the phases appearing after sintering.

The release of soluble hazardous components after contact with water is a significant problem leading to a potential environmental hazard. A leaching test is necessary to determine the leaching properties of the material. The used test was according to EN 12457-4:2002 concerning the characterization of waste leaching compliance test for leaching of granular waste materials and sludges Part 4 which is one stage batch test at a liquid to solid ratio of 10 l/kg for materials with particle size below 10 mm (without or with size reduction). This test is usually used by FOAMGLAS® company. The samples with the highest CRT and aluminium dross content were selected for this test. Firstly, the foam glass was crushed and sieved into grain size less than 10 mm. The leaching agent (L) used is nitric acid (HNO$_3$) with 0.1 mol/l concentration. The leaching agent (L) was added so the liquid/solids ratio (L/S) will be equal to 10 l/kg ± 2% during the extraction in a non-reactive bottle. The closed bottle was placed in

a shaker for $24 \pm 0.5$ h. Excessive shaking is avoided to prevent grain size reduction. For the Liquid/Solid Separation Step, the suspended solids are set to settle for $15 \pm 5$ min. The resulted solution was filtered through 0.45 μm membrane filter and the PH was measured. The concentrations of the components of interest were later determined using ICP-OES (Spectroflame) analysis.

Despite a wide range of research on foam glasses [37] [8] [90] [26] [84] [29] [48] [24] [56], researchers tend to overlook durability tests to estimate how long a product will last before its properties deteriorate. Consequently, there is no exact test to apply on the foam glass to estimate the aging process. There are three possible tests that may be applicable on foam glass:

- The "Test specimens of autoclaved aerated concrete (AAC) or lightweight aggregate concrete (LAC) (EN 990:2002)" method consists of creating corrosive environments by applying 10 cycles of soaking in sodium chloride and drying. The target sample will be visually examined for corrosion and compared to the limit values of the relevant product standard.

- The "Test methods for thermal properties and weathering resistance of aggregates (EN 1367-8:2014)" method concerns the determination of the resistance of light-weight aggregates against disintegration. High pressure and temperature (2 MPa, 250°C) are applied on the sample for 90 min using an autoclave. The content shall be dried at 110 $\pm$ 5 °C and the weight is recorded. The final degradation is calculated as the deterioration of the weight.

- Hydrolytic resistance of glass grains at 121 °C – (ISO 720:2020 Test methods and classification) is presented as the volume of acid needed to titrate the alkali extracted per unit mass of glass. The procedure consists of placing 10 g glass in an autoclave with 50 ml distilled water under a specific thermal cycle: temperature rise from room temperature to 100°C in 20 to 30 min, temperature plateau is kept at 100 °C for 10 min then the temperature increases in the container from 100 °C to 121 °C within 20 min to 22 min. Temperature plateau is set to be constant for 30 min at 121 °C.

As the compressive strength of aerated concrete is higher than that of foam glass, the first test is not suitable for foam glass. Therefore, the last two tests are the most appropriate for foam glass. In case of FOAMGLAS® and Foamit®, the third test and the second tests are used to evaluate the lightweight aggregate. Due to the limited control of the pressure in the autoclave, the last test (ISO 720:2020) was selected. Samples with the highest aluminium dross content (20 wt%) having both 5 and 10 wt% CRT glass content were chosen to undergo this test. Firstly,

samples weighted 5 grams were placed in 25 ml of distilled water in a steel autoclave. The autoclave has a volume of 0.21 l and can withstand up to 200 bar and 250 °C. The autoclave then was placed in an oven and the thermal cycle mentioned above were loaded. When the cycle finished, the sample were left to cool down and the solution was transferred to an Erlenmeyer flask. An identical Erlenmeyer flask was prepared at the same time with distilled water (reference). 0.05 ml of methyl red indicator solution was added to each flask and titrated with the hydrochloric acid solution (0.02 mol) until the colour corresponds exactly to that of distilled water plus 0.05 ml of indicator (reference). The samples were dried and weighted, and the thermal conductivity was measured. The aging process was applied on the samples twice. Each time the listed above parameters were measured. This process is considered equivalent to 36 months in normal condition. At the same time samples were placed on the top of the building in Bergakademie Freiberg. An electronic thermometer and beaker were mounted to record the temperature change and the rainfall quantity. The deterioration in the weight and the thermal conductivity is expected to be measured after 36 months and compare it with the accelerated aging results.
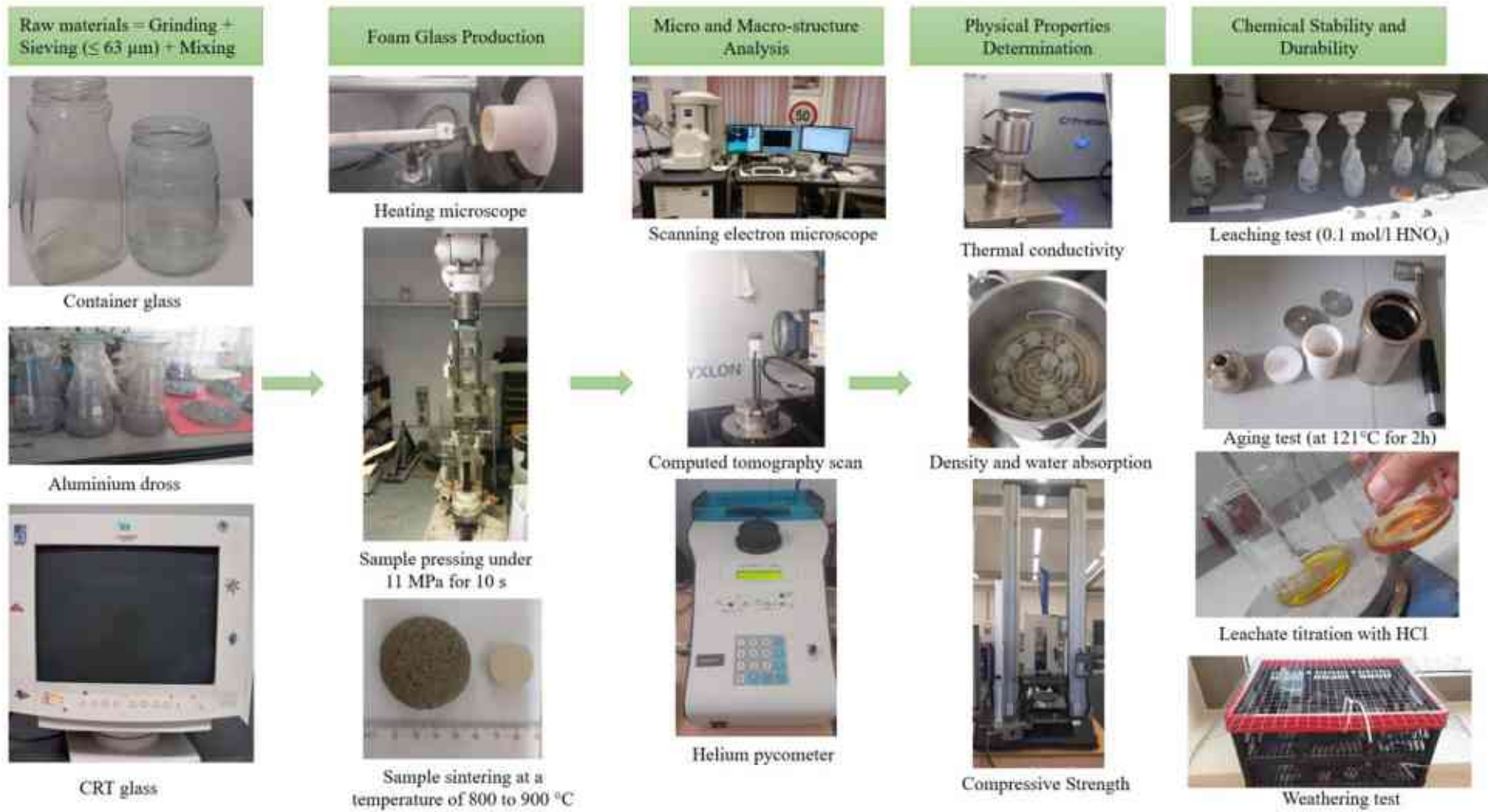
**Figure 29.** Foam glass preparation and testing steps

## 3.2. Results evaluation

### 3.2.1. Raw materials examination

The structure and morphology of the raw materials are presented in Figure 30. The SEM micrograph of the CRT glass displays polyhedral shapes with multiple planar faces. A polyhedral facet ranges from about 20 to 50 µm and has small debris surrounding it. CRT glass is mainly composed of silica, sodium oxide, and calcium oxide, with minor amounts of magnesia or alumina, similarly to container glass. However, hazardous elements such as Pb, Sr, and Ba are present in CRT glass (Table 7 and Table 8).

The structure and the morphology of the aluminium dross grains are almost the same. The predominant fractions are aluminium oxides and spinel in form of round grains and whisker crystals. The minor fraction presents the salt content with rigid and roughly structure. The mineral composition of the aluminium drosses is presented in Table 9. The phases detected are spinel ($MgAl_2O_4$), wurtzite (AlN), corundum ($Al_2O_3$), halite (NaCl), nordstrandite ($Al(OH)_3$), bayerite ($\beta$-$Al(OH)_3$), calcite, and fluorite ($CaF_2$). Dross 64 and X have high amount of wurtzite (AlN) which can play an important role in the foaming process as shown in the following equation [98] while dross 53 have the lowest amount of wurtzite 1.5 wt%.

$$4AlN(s)+3O_2(g)=2Al_2O_3(s)+2N_2(g) \tag{14}$$
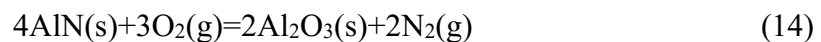
In the other hand, dross 53 has a high content of spinel that will probably enhance the compressive strength and the lowest salt content. Residual salts can play a major role in decreasing the foaming temperature. Residual aluminium may exist in form of aluminium hydroxide or aluminium oxy hydroxide, depending on the heat treatment. The most thermodynamically stable form of alumina is the $\alpha$-aluminium oxide [99] [98].

Dross X contains calcite magnesium $(CaMg)(CO_3)$, a form of calcite which is a magnesium-rich variety (not to be confused with dolomite).

a



b



c



d
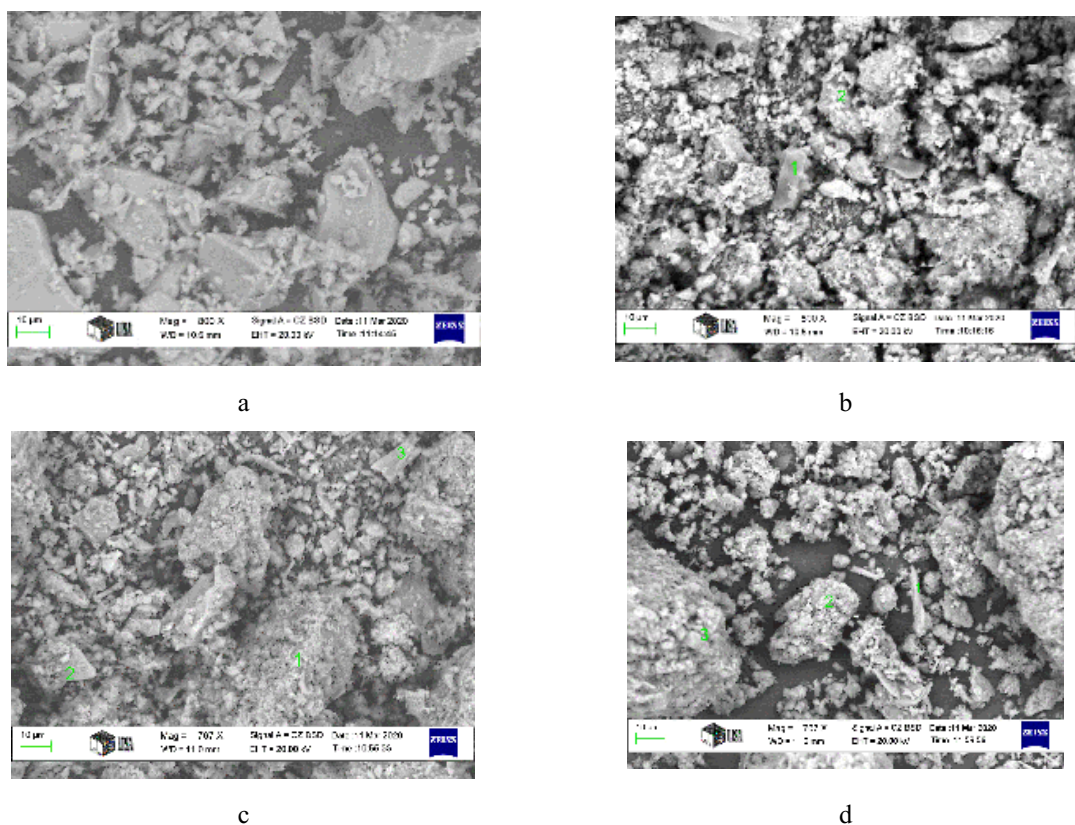
**Figure 30.** SEM micrographs of CRT glass (a), dross 64 (b), dross X (c) and dross 53 (d)

**Table 7.** Chemical composition (wt%) of container glass (BG) and CRT glass (XRF analysis)

| Sample | SiO₂ | Al₂O₃ | MgO | CaO | Na₂O | K₂O | Fe₂O₃ | MnO | TiO₂ | P₂O₅ | S | F | TOTAL |
|--------|------|-------|-----|-----|------|-----|-------|-----|------|------|---|---|-------|
| BG | 74.0 | 1.3 | 2.26 | 8.32 | 12.03 | 0.62 | 0.45 | 0.008 | 0.048 | 0.011 | 0.18 | <0.3 | 99.2 |
| CRT | 53.5 | 1.6 | 0.26 | 0.56 | 5.11 | 5.30 | 0.05 | <0.005 | 0.317 | <0.005 | 0.02 | <0.3 | 66.8 |

**Table 8.** Hazardous elements in CRT glass (XRF analysis)

| Element (ppm) | Cu | Zn | Pb | Rb | Sr | Ba | As | Cr | Co | Ni | Zr |
|---------------|----|----|----|----|----|----|----|----|----|----|----|
| CRT | 14 | 1808 | 2342 | <10 | 3.73% | 10.51% | 33 | <DL | 11 | 70 | 0.40% |

**Table 9.** Mineral composition (wt%) of the aluminum drosses (XRD analysis)

| Phase name and formula | Dross type | | |
|------------------------|------|------|------|
| | 64 | X | 53 |
| Spinel (MgAl₂O₄) | 22.54 | 23.49 | 54.76 |
| Wurtzite (AlN) | 10.65 | 19.64 | 1.5 |
| Corundom (Al₂O₃) | 6.77 | 14.18 | 12.6 |
| Nordstrandite (Al(OH)₃) | 18.01 | 11.82 | 17.03 |
| Bayerite (β-Al(OH)₃) | 39.25 | - | 8.98 |
| Calcite (Ca(CO₃)) | - | - | 2.62 |
| Calcite Magnesium (CaMg)(CO₃) | - | 7.39 | - |
| Halite (NaCl) | 8.71 | 13.58 | 1.79 |
| Fluorite (CaF₂) | | 9.9 | 0.56 |
| Sylvite (KCl) | - | - | 0.17 |
| Salts together | 8.71 | 23.48 | 2.52 |

### 3.2.2. Foaming behavior

To have the optimal foaming temperature, the samples were analysed by the heating microscope (Figure 31 to Figure 34). In all the mixtures, the foaming temperature didn't exceed 880°C with the foaming height ranges from 142 to 169 %. The size of the material affected the foaming process and proved to be more efficient than the previous study.

Using particles less than 63 µm size for container and CRT glass increased the foaming height from 150% (mixtures in the first part of the work) to 169 %. Due to the similarity of viscosity of lead glass and commercial soda-lime-silica glass ($10^2$ to $10^{15}$ poises) [93], adding CRT glass did not significantly affect the foaming height but reduced the foaming temperature (Figure 31). The foaming height of the dross-free samples is increased compared to the previous study, but still lower than the samples with dross. Samples with 10 and 15 wt% dross have the highest foaming height. Among the three-dross types added, dross 53 has the lowest foaming height (Figure 34). Adding 5 wt% or 10 wt% CRT glass content to the samples with dross gives better foaming height except for samples with dross 53. Due to the lack of AlN in the dross 53, the foaming height was lower than in case of the other two drosses. The presence of the small amount of calcite didn't compensate the role of the AlN which confirms the conclusion drawn in the chapter 2 (2.2.2 Sintering and foaming behavior): Dross-containing samples show a decrease in the foaming temperature and an increase in the foaming height, while dross-free mixtures show a higher foaming temperature and a lower foaming height. It is due to the self-foaming mechanism of the dross where aluminium nitride decomposes and releases gaseous products like $NH_3$, $N_2$, and NO at a temperature between 800-920°C [69] [75]. Samples with dross X contain high amount of salts (23.48 wt%) which help to lower the foaming temperature compared to the other two dross types due to the fluxing effect of alkali oxides. Other than salt flux, CRT glass contains lead which present in glass as bivalent $Pb^{2+}$ and usually lowers the melting temperature [100].
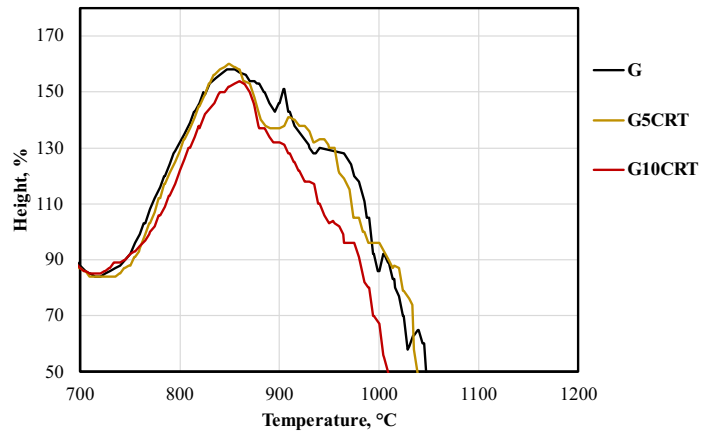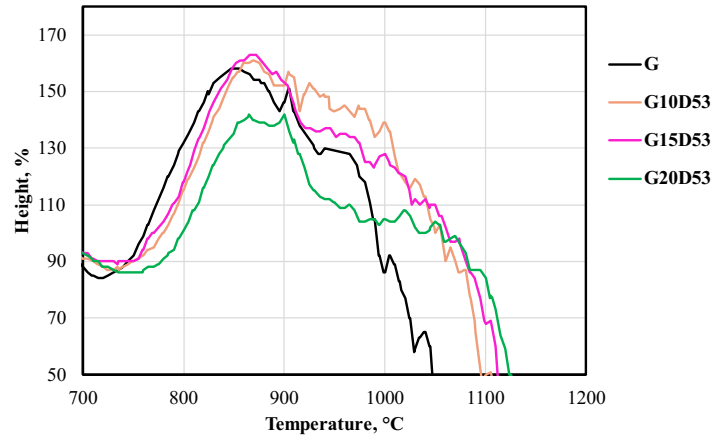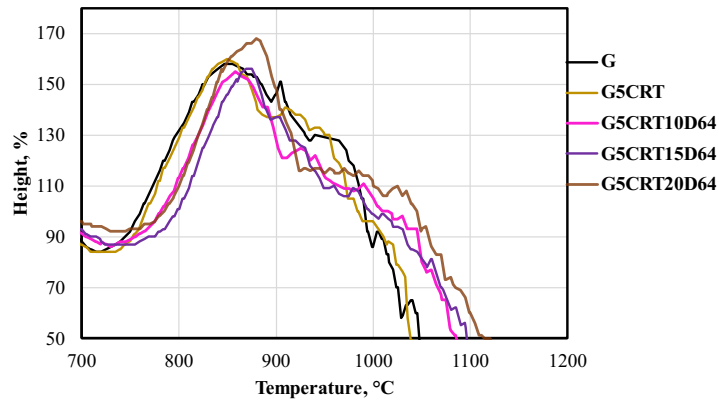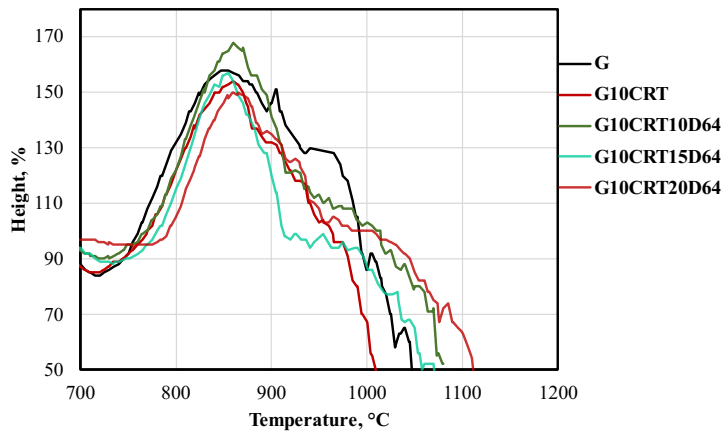
a
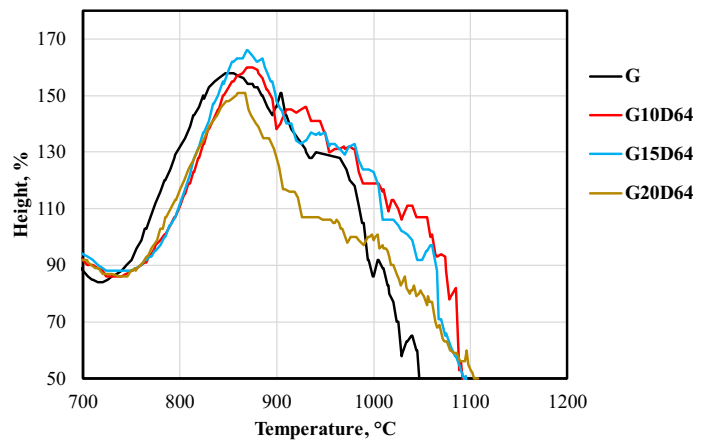


b
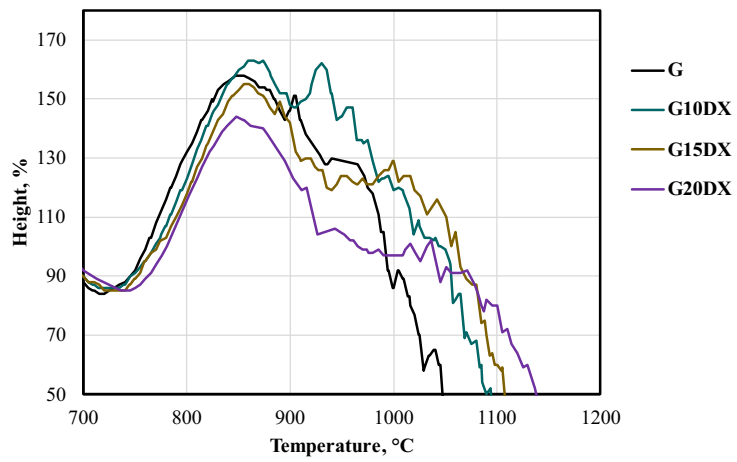


c

d

**Figure 31.** Heating microscopy curves of the samples with container glass and CRT glass (a), and CRT glass-free samples (b,c, and d)
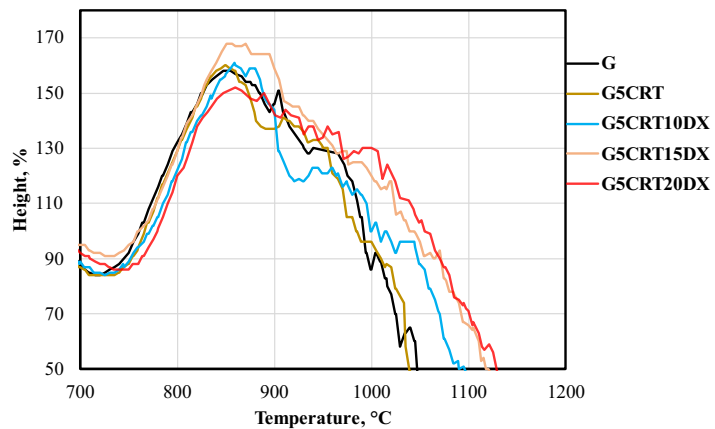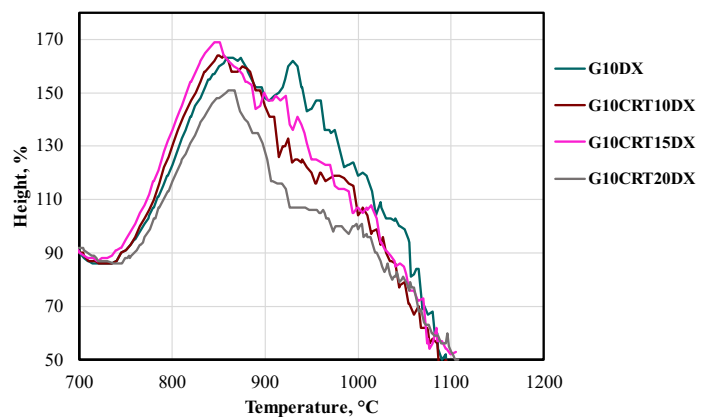


a



b

**Figure 32.** Heating microscopy curves of samples with container, dross 64, and 5 wt% (a) or 10 wt% (b) CRT glass
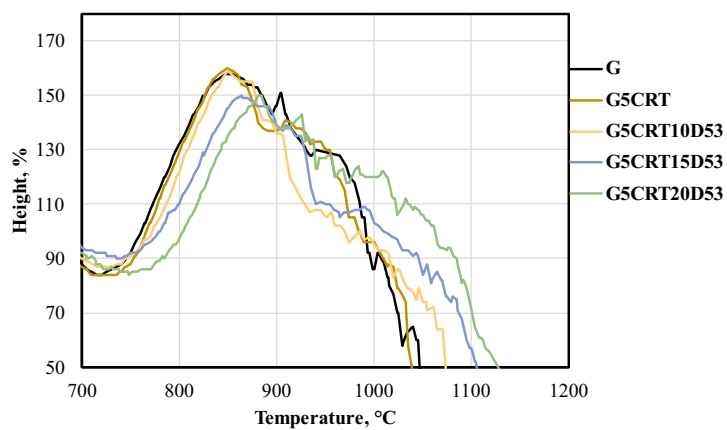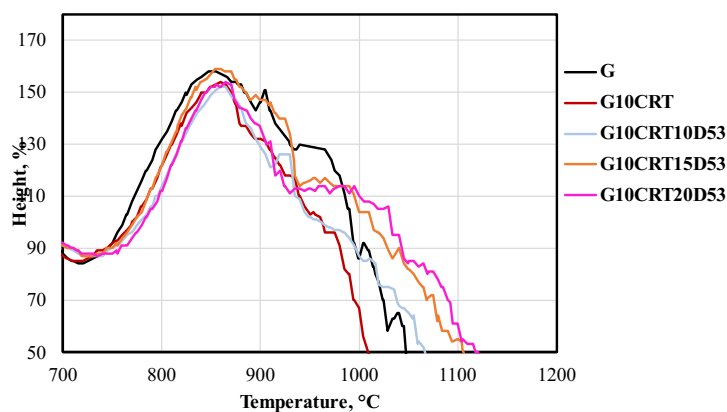
a



b

**Figure 33.** Heating microscopy curves of samples with container, dross X, and 5 wt% (a) or 10 wt% (b) CRT glass



a

b

**Figure 34.** Heating microscopy curves of samples with container, dross 53, and 5 wt% (a) or 10 wt% (b) CRT glass

### 3.2.3. Chemical composition of the foam glass

The following composition analysis will take into consideration the description of other oxides that can be found besides silicon oxide which is the basic component of the glasses (Figure 35). The oxides are ranged in a descending order of quantities. Figures B3 to B12 in the Annex B present a separated oxide composition graph for each sample.

Dross-free samples contain sodium oxide as a major component followed by calcium oxide, magnesium oxide, aluminium oxide, and minor components like iron, barium, and potassium oxides. Trace elements exist but in order of a few ppm.

A sample with container glass and aluminium dross type 64 shows the highest amount of aluminium oxide, followed by sodium, calcium, and magnesium oxides. A small amount of potassium and iron oxides can be seen with the existence of other trace elements (Figure B13, Annex B). Adding 5 wt% CRT glass to the dross caused an increase in the amount of barium oxide. Increasing the amount of CRT to 10 wt%, the amount of sodium and calcium increased to the detriment of aluminium oxide. Other oxides kept the same amount except for barium oxide which decreased noticeably.

By changing the dross type to dross X, the sample with container glass and dross has a composition equally shared between aluminium, calcium, and sodium oxides with minor oxides like $MgO$, $Fe_2O$, $K_2O$, and $TiO_2$. Same like dross type 64, adding 5 wt% only increased the amount of barium oxide. Eventually, the amount of trace elements (Pb, Se, Sb, Sn, Cr, P, and Zn) increases, it can be seen in the Figure B3, Annex B. For example, the lead amount increased from 16 to 181 ppm with 5 wt% CRT and to 308 ppm with adding 10 wt% CRT.

70

Adding 10 wt% CRT glass increased the amount of aluminium oxide and the amount of trace elements. In comparison with the previous dross, the barium oxide content appears to be higher. Shifting to aluminium dross type 53, the sample with dross and container glass shows different behaviour compared to the other dross types where the aluminium oxide is lesser and almost equal to the amount of sodium oxide followed by calcium oxide. Adding 5 wt% CRT only increased the amount of barium and potassium oxides. Increasing the CRT content to 10 wt% only raised the amount of aluminium oxide and trace elements (which can't be distinguished in the figure).

The unchanged amount of magnesium oxide in all the samples proves that magnesium oxide plays the role of a former in the glass structure. Magnesium usually decreases the viscosity of the glass by creating more non-bridging oxygen. But acting as a former may help to stabilize the structure of the glass.

The strong Si-O bonds present at low temperatures are responsible for the high viscosity of vitreous silica. These bonds only break at relatively high temperatures, which results in a slow reduction of viscosity. In addition, the viscosity of vitreous silica can be significantly reduced by trace amounts of impurities such as $Al_2O_3$, alkalis, and OH groups. Through the loosening up of the network, they create non-bridging oxygens that lower viscosity [96]. The introduction of $Al_2O_3$ causes a decrease in the number of non-bridging oxygens, resulting in higher viscosities at all temperature intervals. $Al_2O_3$ valence compensation can only take place if enough alkali ions exist. In the absence of alkali ions, the additional $Al^{3+}$ ions move into the coordination of 6 and this alters the behaviour in that the viscosity falls [96].

Based on the type of network modifiers, if they have a high field strength, they can bridge over the non-bridging oxygens, which means viscosity is not reduced as much. Low temperatures are particularly suited to the latter phenomenon, while high temperatures are more suited to the coordination of the network modifiers with high field strengths. Through this, the remaining network can be further relaxed, resulting in a decrease in viscosity. Network modifiers, therefore, have a temperature-dependent effect [96].

As we discuss binary alkali silicate systems, we will begin with $Na_2O$-$SiO_2$, which decreases the viscosity with increasing $Na_2O$ content by creating more non-bridging oxygens. In the case of introducing CaO into a pure $SiO_2$ melt, it substantially reduces viscosity because the number of nonbridging oxygens arises. This behaviour is quite different at low temperatures (400-600 °C), where the tendency for coordination is not sufficient to loosen the structure. Consequently, the structure becomes stronger, and the viscosity increases as the nonbridging oxygens are

bridged over. MgO also increases the viscosity by gradual substitution of CaO by MgO in soda-lime glasses.

In a soda-lime glass with PbO or an oxide of a transition element (ZnO), the polarizability of the cation can further affect the viscosity. The greater the added amount of lead, the lower the viscosity will become. Thus, PbO has an extremely strong viscosity-lowering effect across a wide range of temperatures. ZnO and PbO weakness the network, while due to their size, their migration is limited [96]. The $Ba^{2+}$ ions act as a modifier in the glass network, causing an unhinged packing of the glass network.
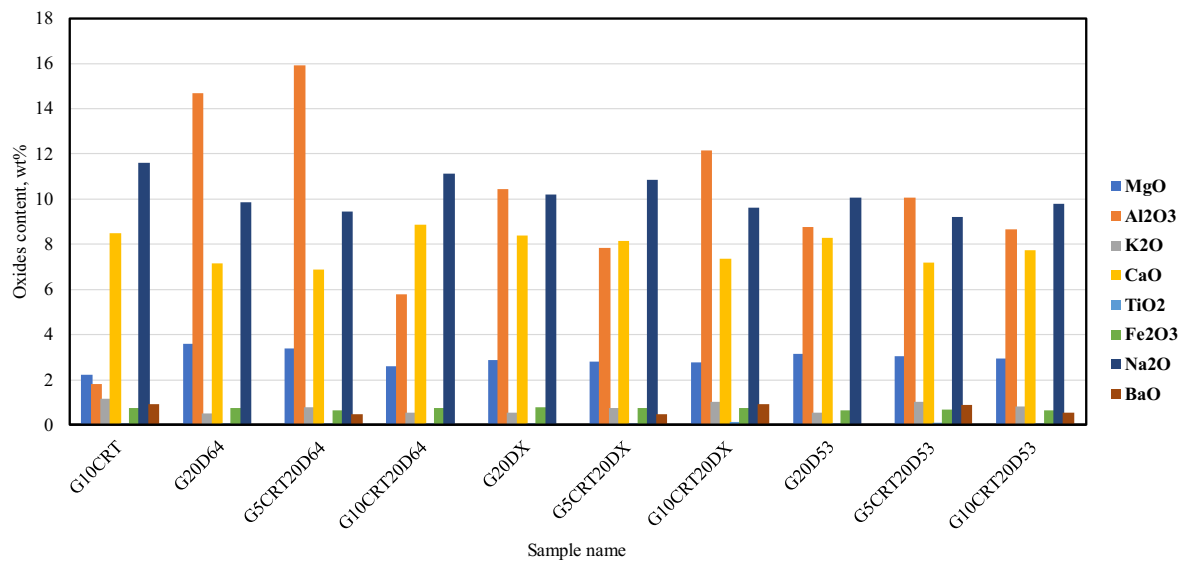


**Figure 35.** Chemical composition of the foam glasses

### 3.2.4. Macro- and microstructural characterization

<u>Macroscopic analysis</u>

To understand the effect of each composition, a detailed study of the macro- and the microstructure is needed. Figure 36 presents photos of the foam glasses with different compositions, where we can see the shape, distribution, and size of the cells. Figure 37 presents 2D and 3D CT scan of the sample which will help understand the structure changes with the composition.

In container glass foams, the cells are small and mostly homogenous in a hexagonal shape like a honeycomb structure. The average cell volume is about 4 $mm^3$. This cellular structure is the result of a highly viscous environment. Usually during the glass melting process, high gas content occurs if the melt were not refined. Adding 5 wt% CRT glass results only in a slight increase in the cell size. The volume of cells ranges from 1 $mm^3$ to 10 $mm^3$. There is a progressive increase in the volume of the cells in the foam structure as it expands. As the CRT glass content increases to 10 wt%, the cells increase in size and become oval with

heterogeneous sizes. The cell volume ranges from 5 mm$^3$ to 25mm$^3$ with the existence of intercell in the walls in the order of 1 mm$^3$. This increase may be due to the presence of high content of Na$_2$O, CaO, and BaO responsible for creating non-bridging oxygens and consequently decreased the viscosity. Lower viscosity will allow the creation of bigger bubbles.

By adding aluminium dross type 64, the cell size changed dramatically. Samples consisting of container glass and aluminium dross (G10D64, G15D64, and G20D64) show irregular cell shapes and larger-sized cells that can reach the 126 mm$^3$ cell volume (sample G10D64). The cell size increased with increasing the amount of the dross. Adding 5 wt% CRT glass didn't significantly change the microstructure of the foams. Based on the statistical analysis of cell size and frequency shown in Table 10, these observations can be confirmed. The sample with container glass has a maximum and a minimum cell size of 3.126 mm and 0.161 mm, closer to the minimum and maximum cell size detected in the sample with 5 wt% CRT glass content (Max=3.180 mm and Min= 0.141 mm). The sample with higher CRT glass content (10 wt%) shows a higher maximum cell size (Max=5.496 mm). By adding dross, the maximum cell size increase to reach 7.543 mm while the minimum cell size decreases to 0.03 mm.

The standard deviation reflects the dispersion within the cell size indicating the homogeneity of the structure where a deviation close to 0 denotes more homogenous cell sizes while a deviation close to 1 indicates a heterogeneous structure. foam glass made by container glass shows the lowest standard deviation (0.285) which means foam glass made by container glass exhibits the most homogenous structure. Adding 5 wt% CRT glass will increase the standard deviation to 0.528 so the cell distribution tends to be heterogeneous. Increasing the CRT glass content or adding aluminium dross will further increase the heterogeneity of the foam glass (0.747). The mode indicates the cell size which occurs most often in the data set. Except for container glass samples, other samples have a small common cell size (0.2 to 0.3 mm), which indicates that increasing dross and CRT glass content will increase both the cell size and the number of small pores within the walls.

The higher the dross content in the sample, the wider the spherical pores appear in the center. This was due to the boosted effect of the foaming process leading to cell growth and coalescence. The main oxides present in G10CRT20D64 are Na$_2$O and CaO which create a low viscosity environment. Aluminium oxides in dross tend to increase the viscosity to provide a more stable structure. This allows the fusion of the gas bubbles and the growth of big cells. Moreover, the high AlN content (10.6) boosted the foaming process.

Considering the foam glasses prepared with the aluminium dross X, samples with 10 to 15 wt% dross (G10DX and G15DX) have small, arranged, homogeneous cells indicating a high viscosity growth environment. Samples with 20 wt% dross exhibit large heterogeneous cell size (G20DX). The amount of $Na_2O$ is equal to the $Al_2O_3$ content, so the effect of those ions on the viscosity will be nullified but the effect of the alkali ions is boosted due the presence of CaO which will decrease the viscosity of the melt causing this heterogenous structure. Adding 5 wt% CRT glass gives more stability to the structure and the cells are more homogenous (G5CRT10DX) with slightly bigger cells in foam glass with 15 and 20 wt % dross due to the presence of high aluminium oxide content acting as foaming stabilizer by increasing the viscosity. Samples with 10 wt% CRT have the same morphology as samples with only dross and container glass. The only difference is in the G10CRT20DX sample, where the cells become wider. It is explained by the high content of $Na_2O$, BaO and CaO (18 wt%) compared to the aluminium oxide content (12 wt%), which will cause the destruction of the bridging oxygen in the glass structure and lowering the viscosity.

In comparison to the previous two dross types, samples with aluminium dross 53 have a homogenous cell structure except for samples with high amount of dross (20 wt%) and CRT glass (10 wt%). Samples with container glass and dross type 53 have small round cells indicating the high viscosity growth environment. Foam glass with 5 wt% CRT to 10 wt% dross kept their homogenous structure due to the slightly higher $Al_2O_3$. As the amount of dross increases to 20 wt%, the cell size becomes larger, and the cell structure becomes more heterogeneous. As the matrix viscosity increases in the presence of $Na_2O$ and CaO, the viscous forces created are exerted on the bubble, promoting bubble breakup.

| CRT Dross | 0 wt% | 5 wt% | 10 wt% |
|---|---|---|---|
| 0D |  |  |  |
| | G | 5CRT | 10CRT |

| | | | |
|---|---|---|---|
| 10D64 |  |  |  |
| | G10D64 | G5CRT10D64 | G10CRT10D64 |
| 15D64 |  |  |  |
| | G15D64 | G5CRT15D64 | G10CRT15D64 |
| 20D64 |  |  |  |
| | G20D64 | G5CRT20D64 | G10CRT20D64 |
| 10DX |  |  |  |
| | G10DX | G5CRT10DX | G10CRT10DX |
| 15DX |  |  |  |
| | G15DX | G5CRT15DX | G10CRT15DX |

| 20DX | | | |
|---|---|---|---|
| | G20DX | G5CRT20DX | G10CRT20DX |
| 10D53 | | | |
| | G10D53 | G5CRT10D53 | G10CRT10D53 |
| 15D53 | | | |
| | G15D53 | G5CRT15D53 | G10CRT15D53 |
| 20D53 | | | |
| | G20D53 | G5CRT20D53 | G10CRT20D53 |

**Figure 36.** Macrographs of the foam glasses (scale=5mm)
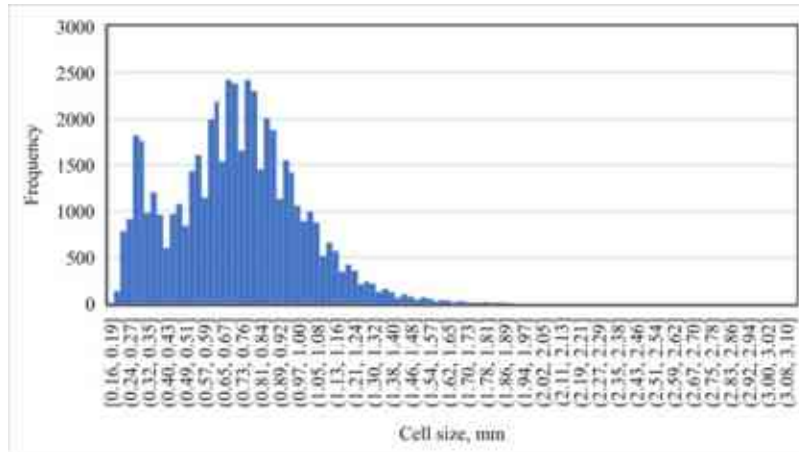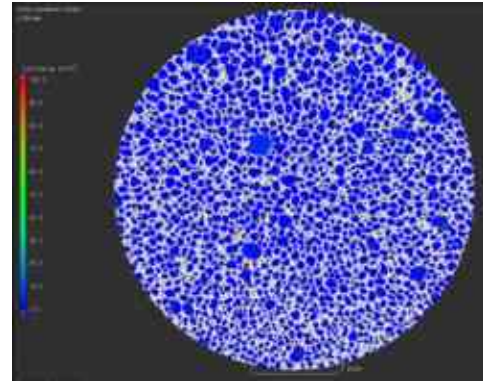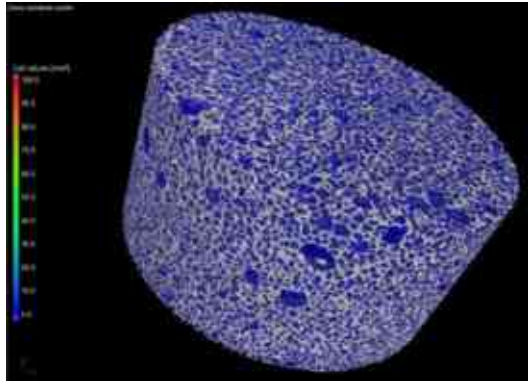
Container glass sample (**G**)
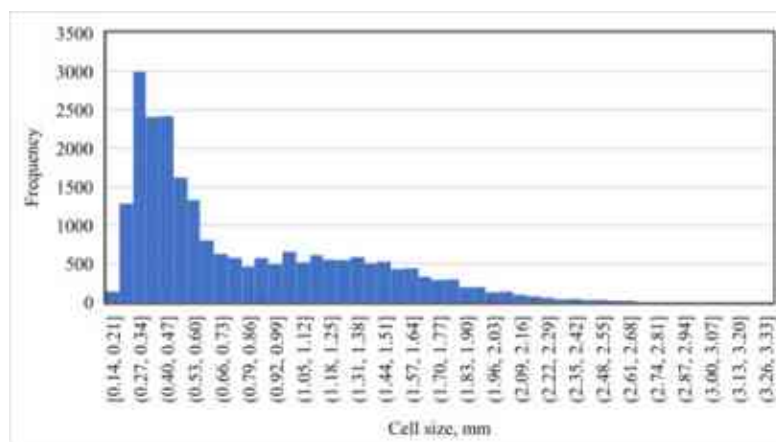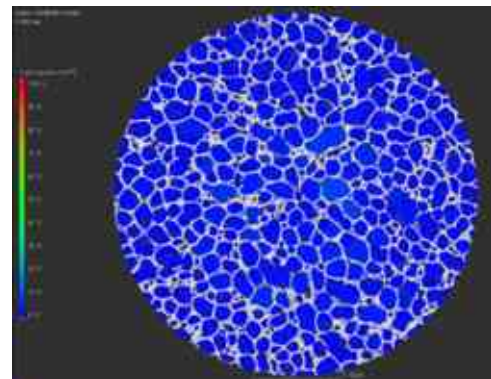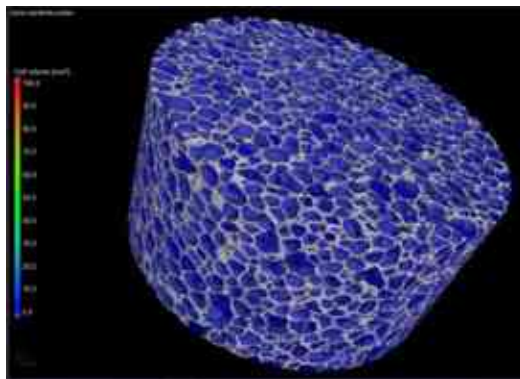






Container glass and 5 wt% CRT glass sample (**G5CRT**)
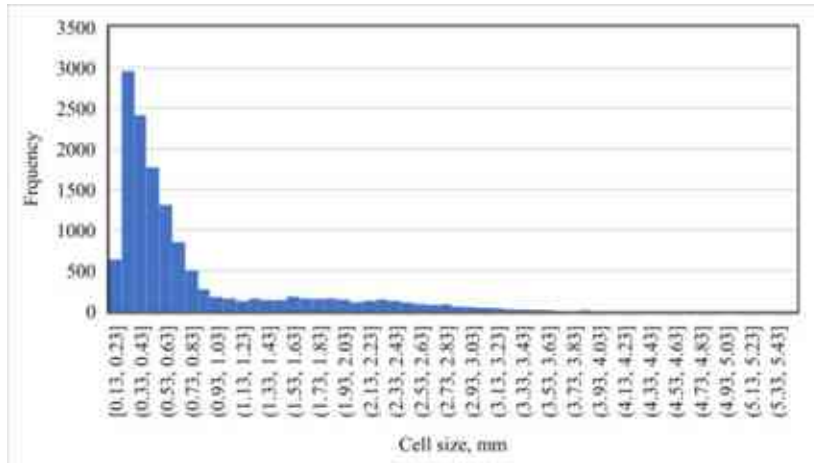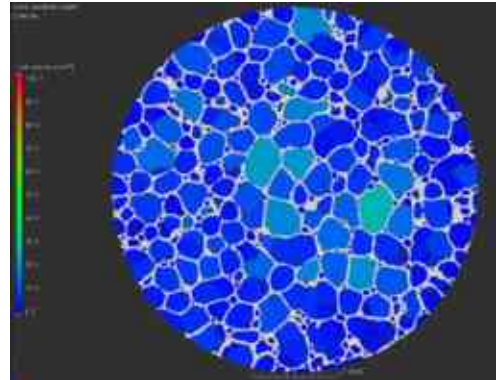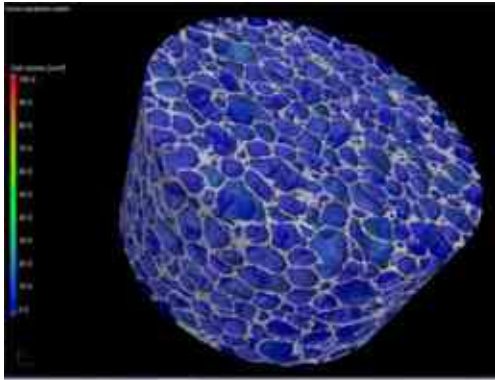
Container glass and 10 wt% CRT glass sample (**G10 CRT**)
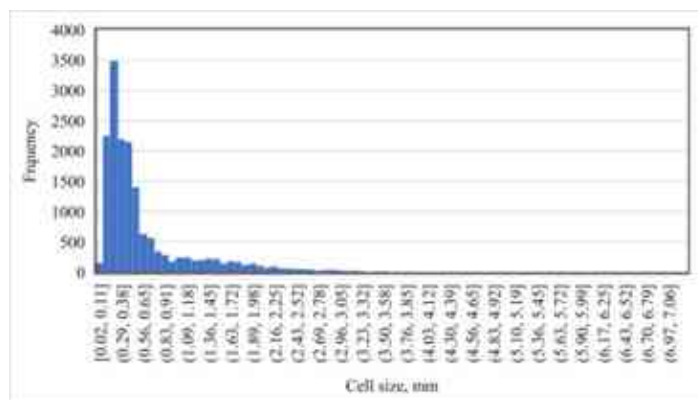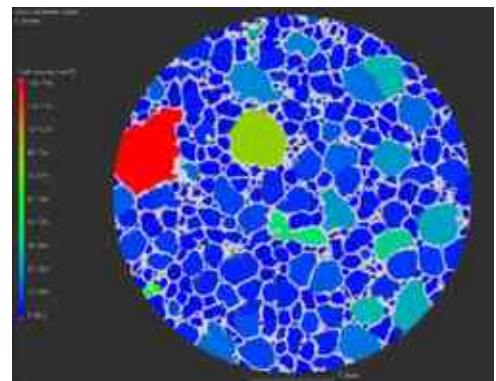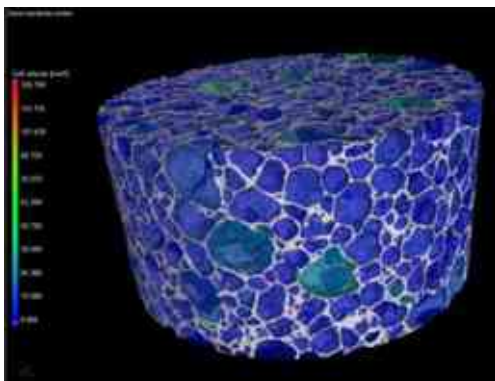






Container glass with 10 wt% dross sample (**G10D64**)
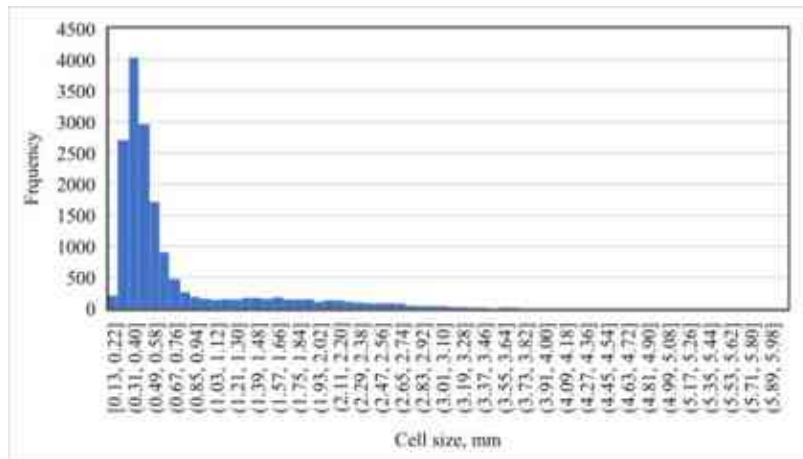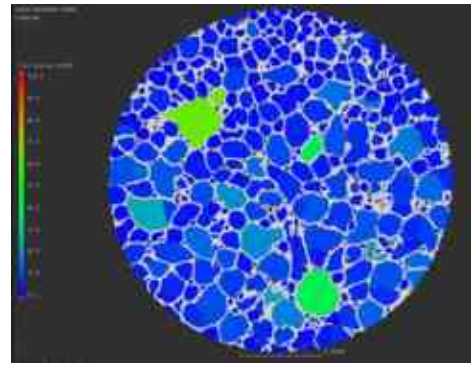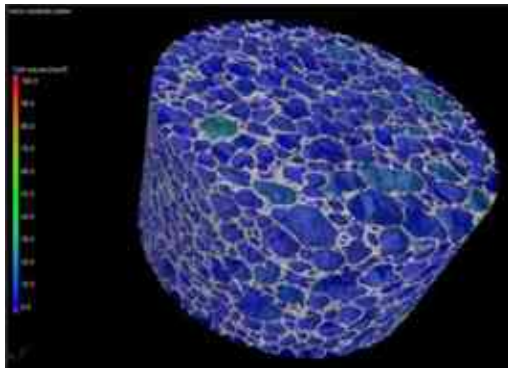
Container glass, 5 wt% CRT and 10 wt% dross sample (**G5CRT10D64**)
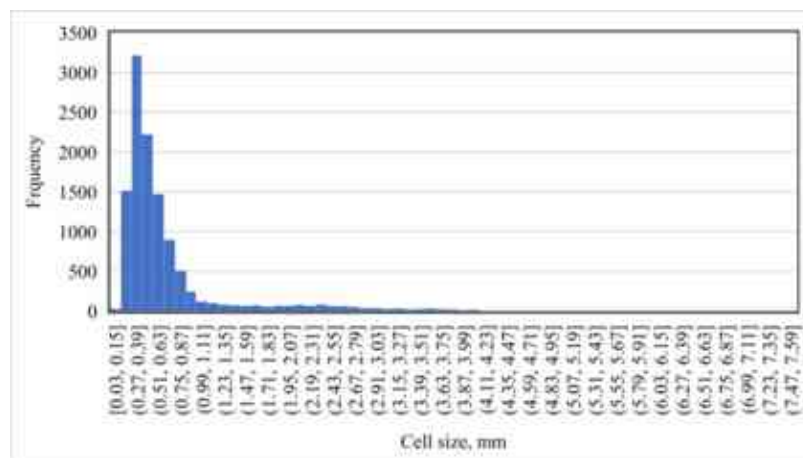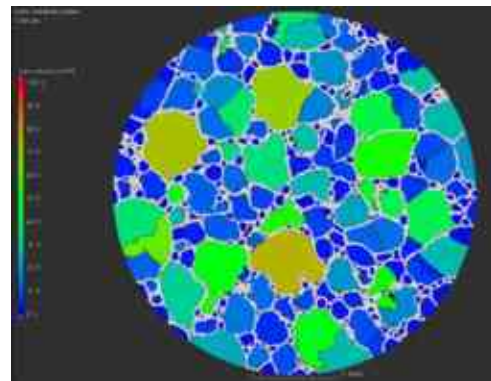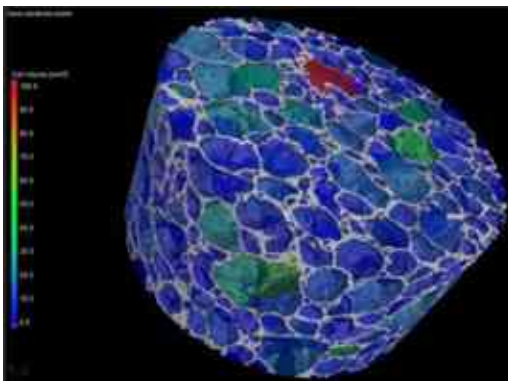


Container glass, 10 wt% CRT and 10 wt% dross sample (**G10CRT10D64**)

**Figure 37.** CT scans of the samples

**Table 10.** Statistical parameters of the cell size distribution determined from the 2D CT scan

|  | G | G10D64 | G5CRT | G5CRT10D64 | G10CRT | G10CRT10D64 |
|---|---|---|---|---|---|---|
| Average (mm) | 0.719 | 0.622 | 0.793 | 0.692 | 0.758 | 0.681 |
| Median (mm) | 0.716 | 0.384 | 0.565 | 0.433 | 0.475 | 0.443 |
| Mode (mm) | 0.736 | 0.264 | 0.303 | 0.312 | 0.273 | 0.272 |
| Maximum (mm) | 3.126 | 7.227 | 3.180 | 6.059 | 5.496 | 7.543 |
| Minimum (mm) | 0.161 | 0.024 | 0.141 | 0.131 | 0.131 | 0.030 |
| Standard deviation | 0.285 | 0.649 | 0.528 | 0.657 | 0.714 | 0.747 |

Microscopic analysis

For a full description of the cellular system, a scanning electron microscopy analysis was carried out. Herein, geometry, cell size, orientation, and type of connectivity are the key features for the characterization of foam glass (Figure 38).

The pores can be divided into nanopores (sub-nanopore: 0.1 to 1 nm, inter-nanopore: 1 to 10 nm, and super-nanopores: 10 to 100 nm), micropores (sub-micropore: 0.1 to 1 μm, inter-micropore: 1 and 10 μm, and super-micropore: 10 to100 μm), and millipores (sub-millipore: 0.1 and 1 mm, inter-millipore: 1 to10 mm, and super-millipore: 10 to 100 mm) [101].

Foam glass made with container glass has mostly sub-millipores that are shaped more likely tetrahedrahexagons than round. The walls of the cells are thin with oval super-micropores. Those pores are surrounded by thinner walls containing submicropores. With 5 wt% CRT glass added in, oval sub-millipores appear surrounded by a high number of round super-micropores. The millipores were deeper than in the container glass foam which may indicate open porosity. Adding 10 wt% of CRT glass results in slightly larger inter-millipores with neat and organized arrangements where the walls contain a smaller amount of super-nanopores compared to the other samples.

Adding 10 wt% aluminium dross type 64 will change the foam glass structure. Samples with container glass and dross show mostly inter-millipores and the walls are made of inter-micropores linked together. The concave part of the pore displays a needle structure that may indicate the existence of a crystallized phase. Micrographs of samples with 5 wt% CRT glass and dross have big and irregular inter-millipores while the walls are an agglomeration of inter- to super-micropores. Samples with the same amount of dross but rather higher amount of CRT glass content have the same cell structure as samples with 5 wt% dross but with slightly thicker walls despite the presence of the same inter- to super-micropores.

CRT act as stabilizer for foam structure possibly due to the existance of lead, present in glass as bivalent $Pb^{2+}$, which usually lowers the melting temperature. As AlN present in dross tends to boost the foam causing at certain point cells fusion, other compounds act as counter effect to increase the viscosity such as aluminium oxides which will decelerate the foaming process.
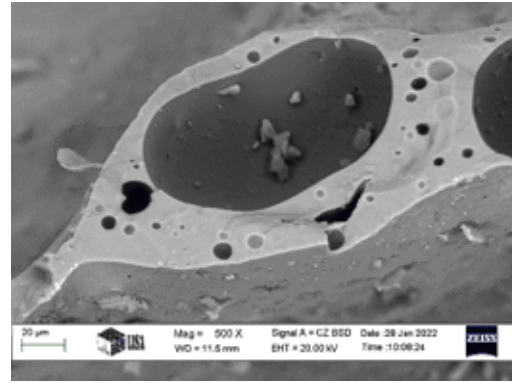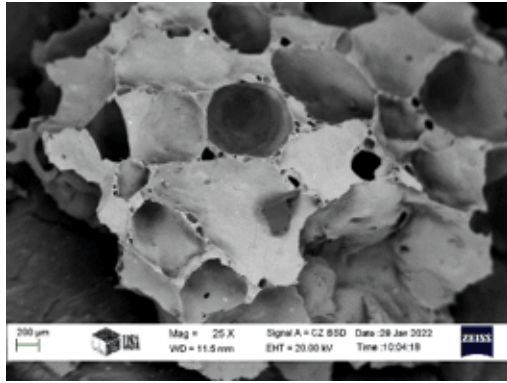


G
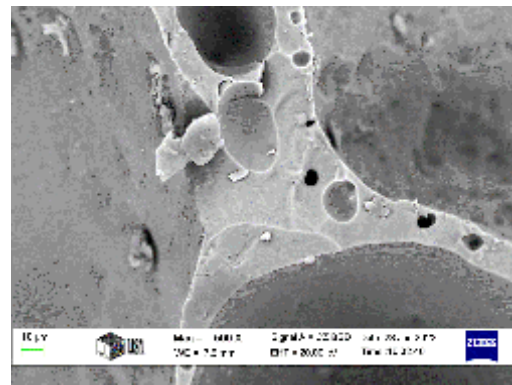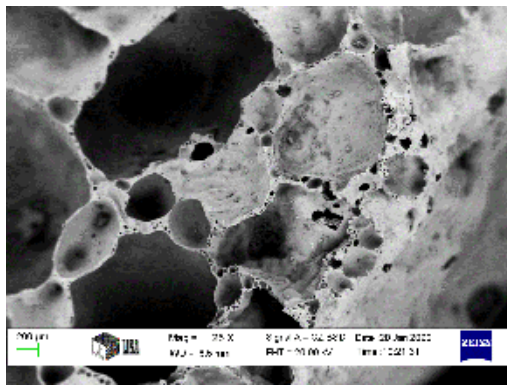


G5CRT
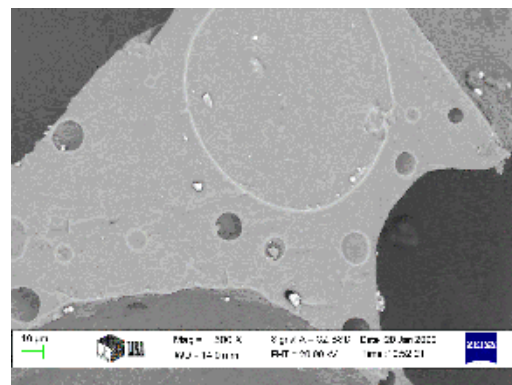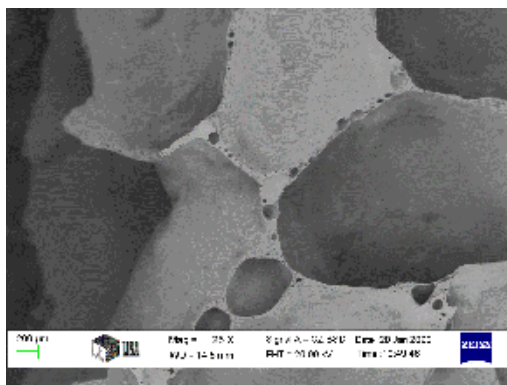


G10 CRT
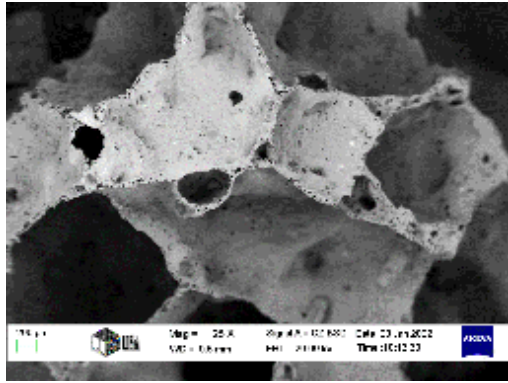
G10D64
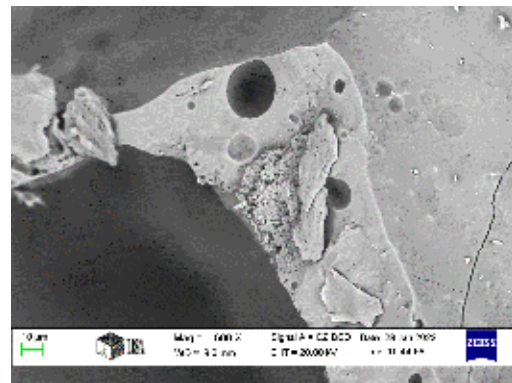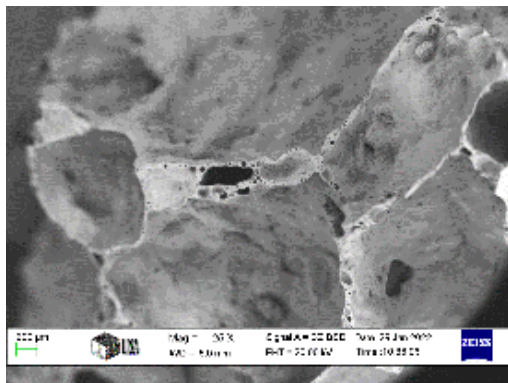


G5CRT10D64
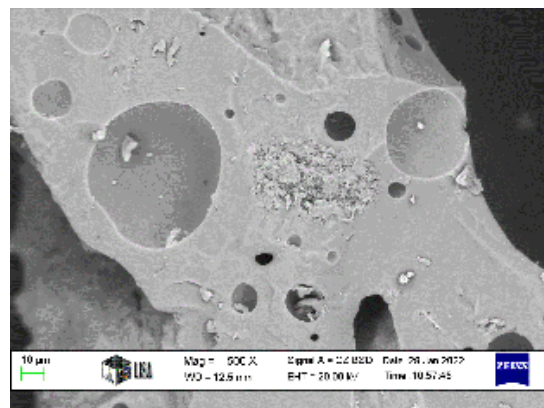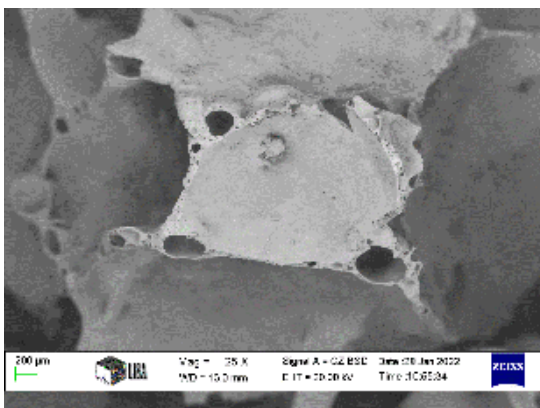


G10CRT10D64

**Figure 38.** Micrographs of the foam glasses

### 3.2.5. Volume expansion and density

<u>Volume expansion</u>

The change in volume after sintering can be calculated by comparing the expanded volume of the foamed sample with the original volume of the pressed sample. The volume expansion results are shown in Figure 39. All samples exhibited a high volume expansion.

Volume expansion is more specific than the foaming height as it take into consideration not only the height but also the expanded diameter of the sample. The maximum volume expansion

is detected in samples with dross types 64 and X (7.8) due to the presence of AlN (10.65 wt% and 19.64 wt% respectively) which will boost the foaming process. In the other hand, samples with dross 53 have the minimum expansion (7 to 6) due to the low content of AlN in the dross (1.5 wt%), thus the foaming process was hindered. When CRT glass content is increased, foam growth is restricted during sintering, resulting in a more homogeneous pore distribution. Having stable foam structure is more important than having higher volume expansion. If the glass foams are insufficiently heated or the viscosity is high, gas bubbles will not be generated. At the same time, if the viscosity is low or the foaming process is extremely intense the pores outer shell collapse, and bubble fusion take place. Thus, a moderate amount of AlN in the dross and a suitable viscosity for bubble growth are the keys to create stable foam structure.
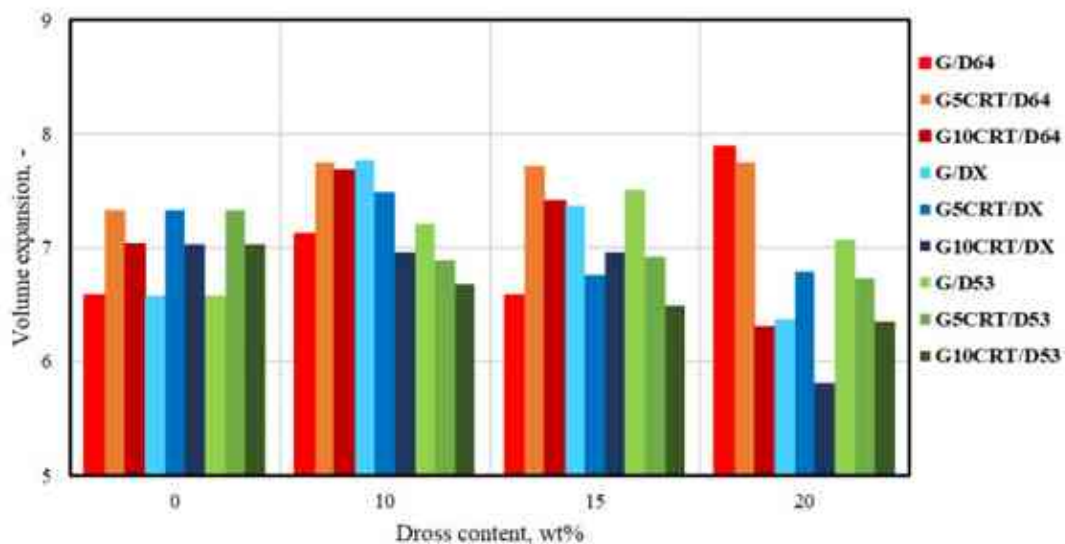


**Figure 39**. Volume expansion of the foam glasses

Density

As the density of the foam glasses in powder form is close to each other, the density of the foam glasses is slightly different (Table B1 in the Annex B). The density of the foam glass depends on the foam structure (the size and shape of the cells). Commercial foam glasses have a density range between 0.13 - 0.3 g/cm$^3$. The density of the foam glasses in this study varies from 0.15 to 0.21 g/cm$^3$ (Figure 40). Samples with container glass and dross have slightly lower or equal density to that of the container glass and the lowest densities compared to the other mixtures. It is due to their closed foam structure. Adding 5 wt% CRT glass to dross increased the density except for samples with 20 wt% dross type 64, due to the large amount of cell generated. Adding 10 wt% CRT and dross (64, X or 53) gives the highest densities.
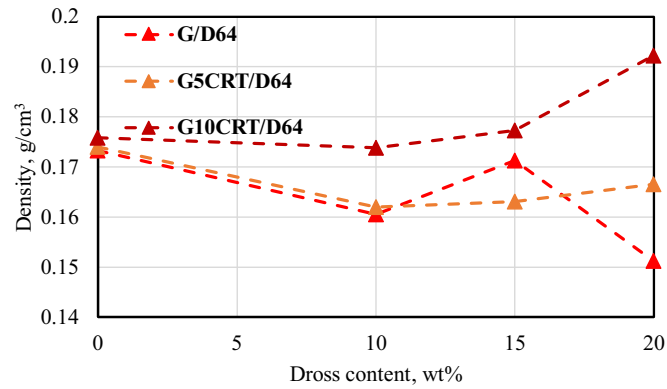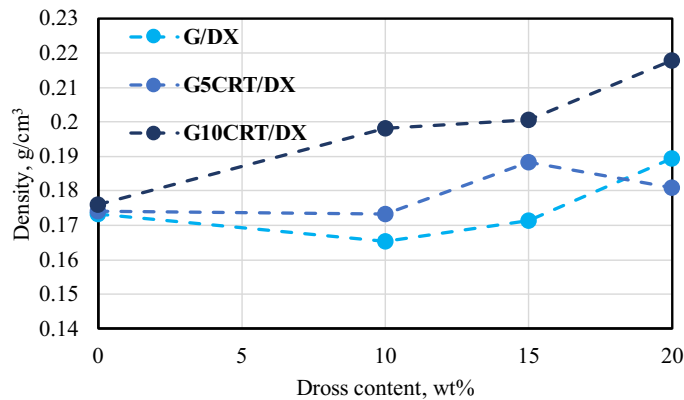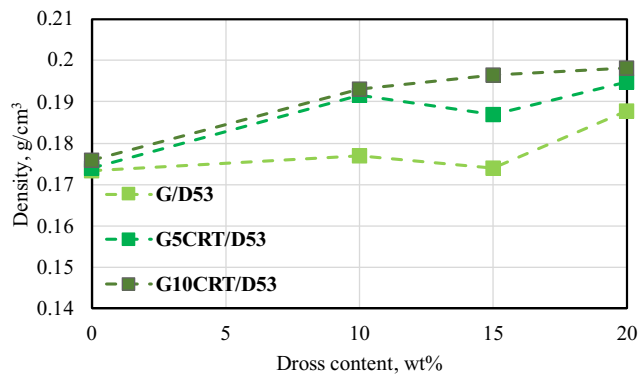
**Figure 40.** Density of samples with container glass, CRT glass, and dross 64 (a) or dross X (b) or dross 53 (c)

When $Al_2O_3$ is introduced into silicate glasses, the network former is replaced. This is because the $Al^{3+}$ cation has the coordination number 4 in such glasses and is thus a network former. The replacement of $SiO_2$ with $Al_2O_3$ will not affect the volume. Since the molar weight of aluminium oxide is greater than that of $Si_2O$, the density increases. The ratio of $Al_2O_3/Na_2O$

can determine the density behavior [96]. At first, the densities decrease as the $Al_2O_3/Na_2O$ ratio increases until it reaches 1.2, when it begins to rise due to the formation of $AlO_6$.

The table below (Table 11) presents the ratio of $Al_2O_3/Na_2O$ calculated from the foam glass composition. Let's take dross free sample as a reference where aluminium oxide content is less than in the other samples containing dross. The other two dross types (X and 53) stick to this rule, samples with coefficient higher than 1.2 have the highest density compared to sample with $Al_2O_3/Na_2O$ ratio less than 1.2 [100] [96]. Dross type 64 samples don't follow this rule. Despite the low amount of $Al_2O_3$ in the sample G10CRT20D64 (5.5 wt%), the density is high. It is may due to the presence of high amount of CaO (8 wt%) which tend to increase the density. This rule is mostly applied in dense glass while foam glass has other parameters that affect the density such as the porosity and the cell size and distribution.

**Table 11.** $Al_2O_3/Na_2O$ ratio in the foam glasses

| Sample code | $Al_2O_3/Na_2O$ |
|---|---|
| G10CRT | 0.15 |
| G20D64 | 1.49 |
| G5CRT20D64 | 1.68 |
| G10CRT20D64 | 0.52 |
| G20DX | 1.02 |
| G5CRT20DX | 0.72 |
| G10CRT20DX | 1.26 |
| G20D53 | 0.87 |
| G5CRT20D53 | 1.09 |
| G10CRT20D53 | 0.89 |

Figure 41 presents the volume expansion versus the apparent density. The apparent density is highly negatively correlated to the volume expansion. The density of samples with 10 wt% CRT glass increases as the amount of dross content increases which will decrease the expansion process of the sample. In CRT-free foam glasses, samples with 15 wt% dross have the lowest density and the higher volume expansion. A sample with only 10 wt% CRT glass content exhibits a low viscosity due to the high amount of CaO and $Na_2O$ (20 wt%), the viscosity will increase gradually by increasing the amount of $Al_2O_3$ (by adding aluminium dross) to create a denser foam structure with less expansion.
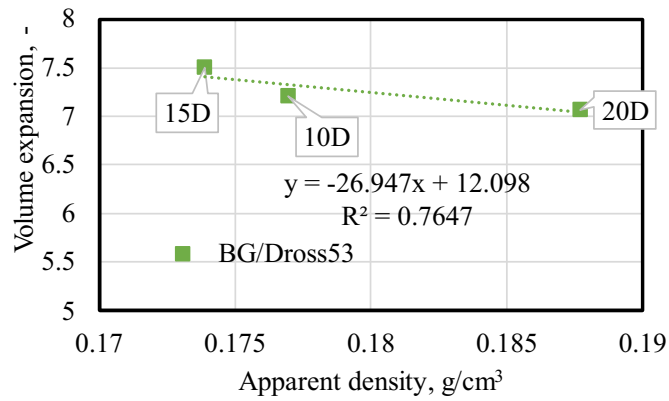
a
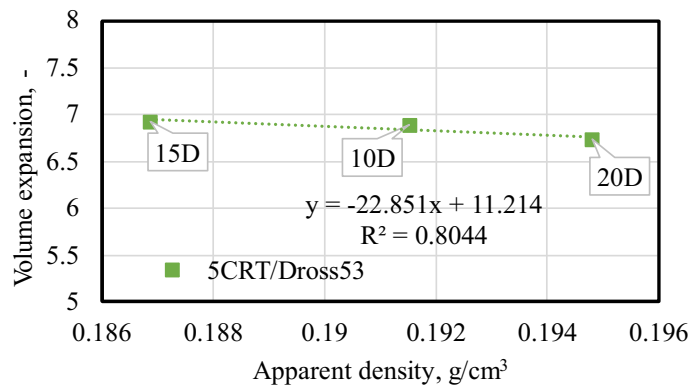


b
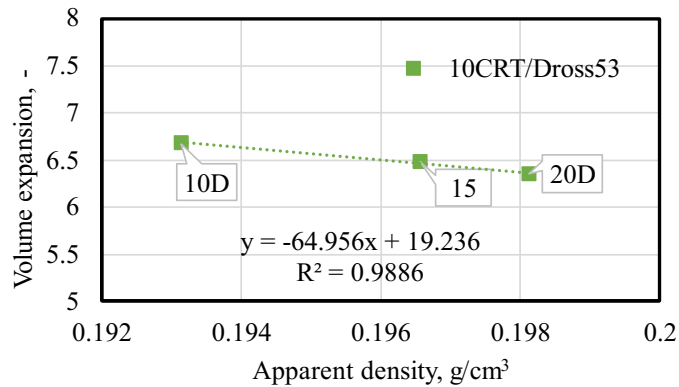


c

**Figure 41.** Volume expansion versus apparent density of CRT glass-free samples (a), container glass with 5 wt% CRT glass and dross 53 samples (b), and container glass with 10 wt% CRT glass and dross 53 samples (c)

### 3.2.6. Porosity and water absorption

Depending on the application field, foam glass can be either water resistant and still absorb mist and humidity or high absorption material used for drainage (sport grounds: tennnis or football fields).

It is also possible to classify pores according to their accessibility to their surroundings. Pores that are open to the exterior surface are known as open pores. When a pore is open on one side, it is called a blind pore, and if it is open on both sides, it is called a through pore. Closed pores can be the product of two phenomena. The first is caused by excessive heating, which results in the collapse of parts near the pores' outer shell. The second reason is due to the insufficient evolution of gaseous substances [102].

In this study, open and closed porosities were calculated (Equations 12, 13, 14). A good example of closed pores is observed in dross free samples, where pure container glass have the lowest absorption (15 %) (Figure 42) . Adding 5 or 10 wt% CRT glass to it slightly increases the water absorption to 30 wt%. If we compare the latest cell microstructure, we can see ressemblance to the microstructure of foam glass made with container and CRT glass. This is probably due to the limited amount of the gaseous substances generated during foaming. It can be seen with samples containing 10 wt% CRT  and dross. Open porosity usually lead to high water absorption that can be over 300 %. This tendency is observed in samples with 5 wt% CRT and dross. Adding 10 wt% CRT participate in stabilizing the pore structure and limiting the foaming process.

Samples with 10 wt% CRT and the different type of aluminum dross have the lowest water absorption (Figure 42). Water absorption can be lineraly correlated to the closed porosity and dross content. As the dross content increases, the generation of closed pores decreases causing higher absorption of water (Figure 43).
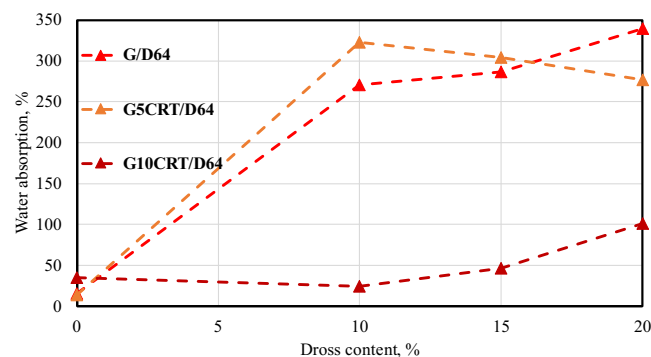


a
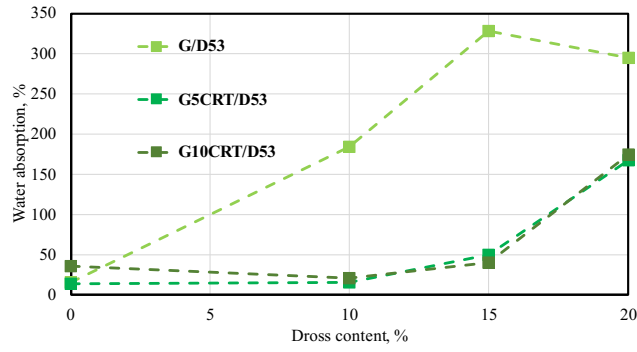
b
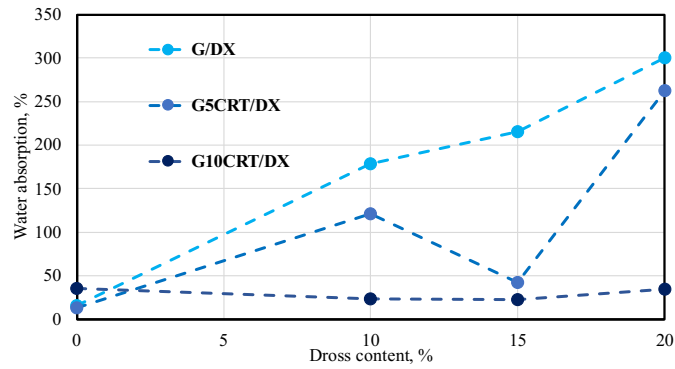


c

**Figure 42.** Water absorption of samples with container glass, CRT glass, and dross 64 (a) or dross X (b) or dross 53 (c)
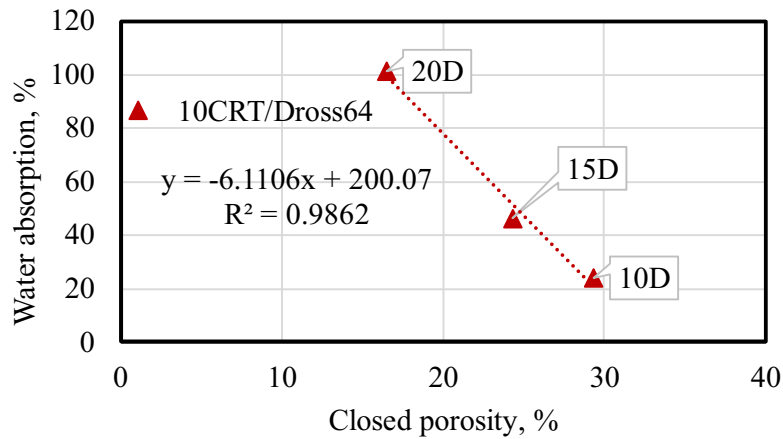


**Figure 43.** Water absorption versus closed porosity of the foam glass

### 3.2.7. Thermal conductivity

Thermal conductivity of commercial foam glass ranges from 0.035 to 0.08 W/m·K [5] [6] [7]. In this study, the thermal conductivity of the samples ranges between 0.038 W/m·K and

0.055W/m·K (Figure 44) which makes them a good thermal insulating material. Samples with open pores and higher water absorption have lower thermal conductivity compared to samples with closed cells. Foam glasses containing CRT glass have higher thermal conductivity than sample with only container glass. Cell size, wall thickness and homogeneity affect directly the thermal conductivity. Thermal conductivity of the G10CRT/DX increases when 10 wt% dross is added due to the formation of smaller cells while decreases with 15 wt% dross due to the formation of wider cells (G10CRT10DX, G10CRT15DX). The cells in G10CRT20DX are wider compared to the samples with less dross content and have thicker walls too which increases the thermal conductivity.
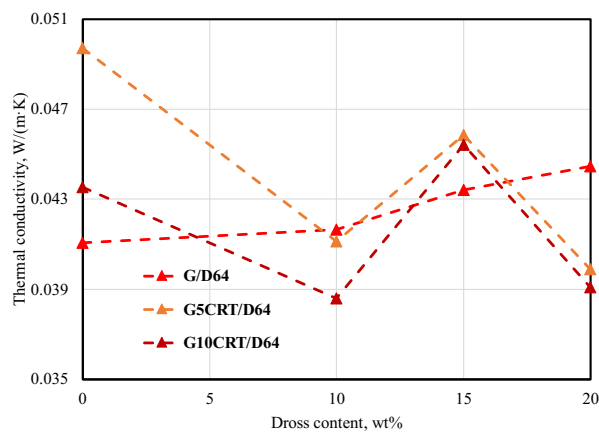


a
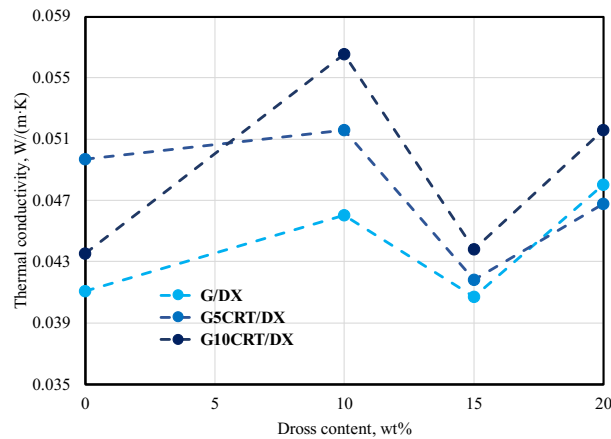


b
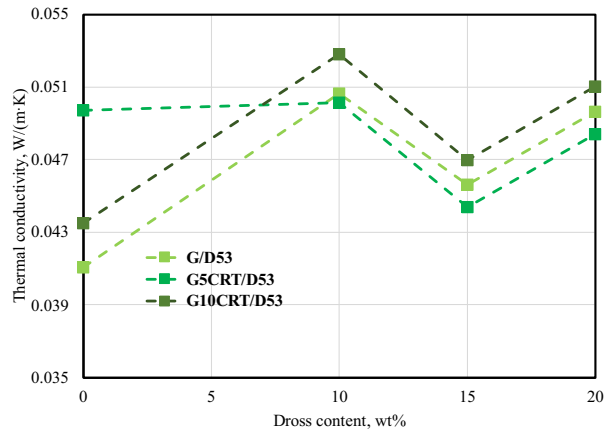
c

**Figure 44.** Thermal conductivity of samples with container glass, CRT glass, and dross 64 (a) or dross X (b) or dross 53 (c)

### 3.2.8. Compressive strength and mineral phases

Samples with dross 64 have the lowest compressive strength among the other samples with different dross (Figure 45). The compressive strength decreased with increasing the amount of the dross. The crystalline phases present are spinel, cristobalite, quartz, sillimanite, wollastonite, corundum, and magnetite. Samples with dross 53 show higher compressive strength with their well-packed structure that can divide and distribute the applied force between the cell walls (Figure 45-c). Dross 53 contains fewer crystal phases compared to dross 64 which contains mostly cristobalite, wollastonite, corundum, and magnetite. If the hardness of the total phases will be considered (Mohs hardness-Table 12), samples with dross 53 and X have the highest hardness (6-7) followed by dross 64 (6 to 6.5) and dross-free samples G10CRT which can't be true as the compressive strength of the sample G10CRT is higher than the compressive strength of the samples with dross type 64 and 10 wt% CRT. In conclusion, taking into account the hardness to interpret the results doesn't apply in the case of foam glass.

The samples with dross X and 5 wt% CRT glass have a decreasing tendency in function of the increasing dross content. Samples with 10 wt% CRT glass have a maximum at 15 wt% dross content (Figure 45-b). The crystalline phases present are spinel, cristobalite, wollastonite, corundum, diopside, and magnetite.

The weakness of samples containing dross 64 compared to the other two types of dross may be explained by the high amount of crystal phases present. In fact, dislocation propagates through the well-displayed plans of the crystal. By introducing amorphous phases to crystalline materials, grain boundaries and phase boundaries can be impeded from moving. The

90

compressive strength of foam glass is highly correlated with its porosity independently of its dross content (Figure 46). As the porosity increases, the compressive strength decreases. Porosity weakens the load bearing of the foam regardless of the type of porosity (open and closed pores).
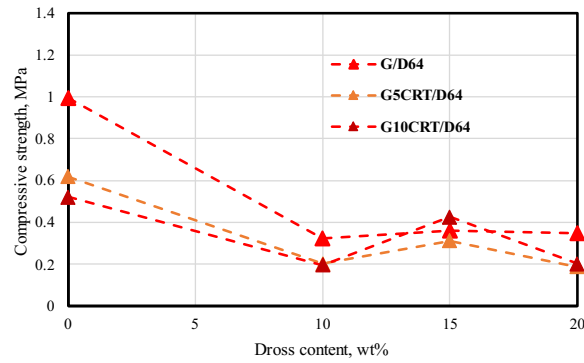


a
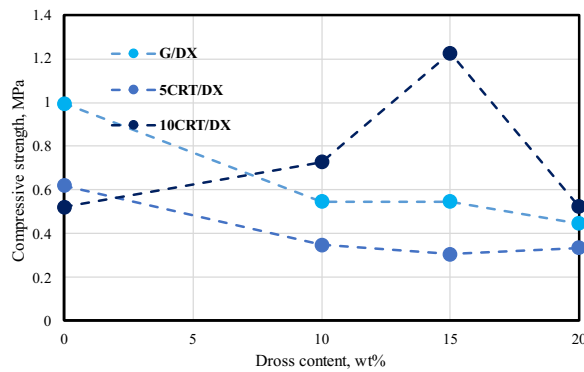


b
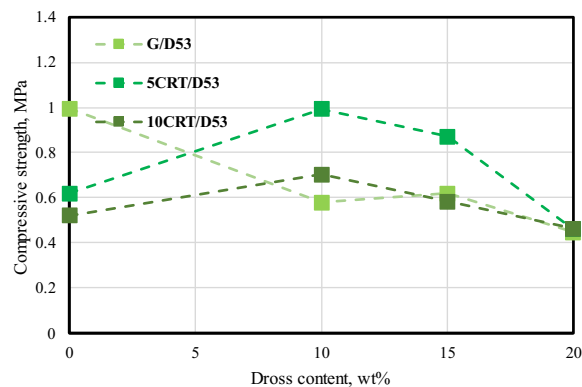


c

**Figure 45.** Compressive strength of samples with container glass, CRT glass, and dross 64 (a) or dross X (b) or dross 53 (c)

**Table 12.** Phases presented in the foamed samples and their corresponding Mohs hardness

| G20D64 | G10CRT | G10CRT20D64 | G20DX | G10CRT20DX | G20D53 | G10CRT20D53 | **Mohs hardness** [103] |
|---|---|---|---|---|---|---|---|
| Spinel | - | Spine | Spinel | Spinel | Spinel | Spinel | 7.5-8 |
| Cristobalite | Cristobalite | Cristobalite | Cristobalite | Cristobalite | Cristobalite | Cristobalite | 6-7 |
| Quartz | Quartz | Quartz | - | - | - | - | 7 |
| Sillimanite | - | Sillimanite | - | - | - | - | 5.5-7 |
| Wollastonite | Wollastonite | Wollastonite | Wollastonite | Wollastonite | Wollastonite | Wollastonite | 4.5-5 |
| - | Portlandite | - | - | - | - | - | 2 |
| - | Enstatite | | | | | | 5-6 |
| - | - | Corundom | - | Corundom | Corundom | Corundom | 9 |
| - | - | Brucite | Brucite | - | - | - | 2.5 |
| - | - | - | Diopside | Diopside | Diopside | | 5-6 |
| Magnetite | Magnetite | Magnetite | Magnetite | Magnetite | Magnetite | Magnetite | 5.5-6 |
| 6-6.5 | 5-5.5 | 6-6.5 | 5-6 | 6-7 | 6-7 | 6.5-7 | Average hardness |



$y = -0.0289x + 3.0287$
$R^2 = 0.9028$
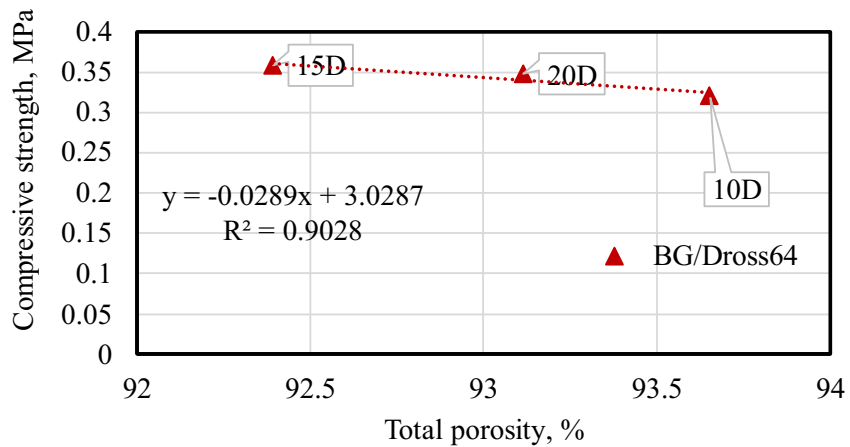
a
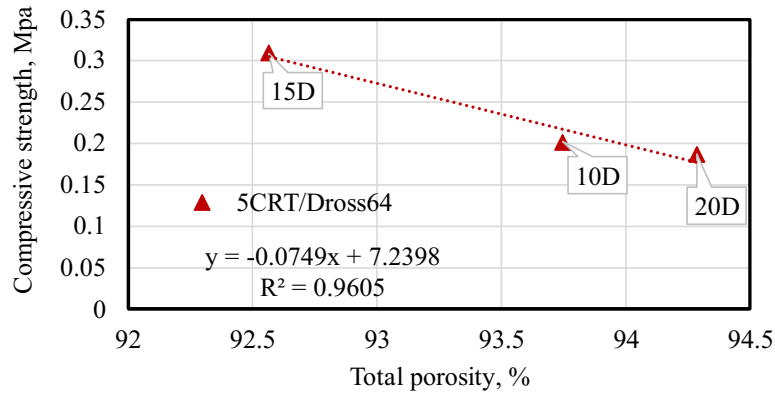
b

**Figure 46.** Compressive strength versus the total porosity of the foam glass made with container glass and dross 64 (a) and container and CRT glasses and dross 64 (b)

### 3.2.9. Leaching test results

To determine whether hazardous waste complies with specific acceptable values, the samples with the highest waste material content were selected to undergo the leaching test. During the basic characterization test, the key variable is the leaching behaviour of the hazardous elements measured. The produced elute is then characterized chemically by determining the elemental content and evaluation of components that can be leached. The results were compared to the limit values for the classification of waste materials "the establishing criteria and procedures for the acceptance of waste at landfills (2003/33/EC)" (Table B2 in Annex B).

Regardless of the variation of the sample's composition, the hazardous elements concentrations (Figure 47) are less than the safe limit (Table B2, Annex B). The samples are classified as non-hazardous materials except for sample G10CRT20D64-$H_2O$ where the maximum allowable amount of Sb should be 0.7 ppm but, in the sample, it exceeds to 0.8. Concerning the Pb-concentrations in the eluate, all samples recorded Pb-concentrations lower than the safe limit (≤10 ppm), fulfilling Pb-immobilization of 95 to 99 %.

To interpret the localisation of lead in the foam glass system we need to go through all the previous data. Three hypotheses can be declared as follows:

- Lead was vaporized during sintering.
- Lead can be integrated in the amorphous glass silicate phase and could be leached easily.
- Lead can bond into the small fraction of the crystalline phase.

The suggestion of vaporization can't be true as lead evaporates at temperature of 1740°C. The second thought is that lead can be integrated in the amorphous glass silicate which will facilitate

the total leaching process of the lead. It can't be the case as only minor part is leached. The last perception is that the lead is entrapped in one of the crystal phases. Lead may incorporate into crystal phase containing iron without being detected with the XRD due to its minor amount. Lead is very likely incorporated in the magnetite [104].
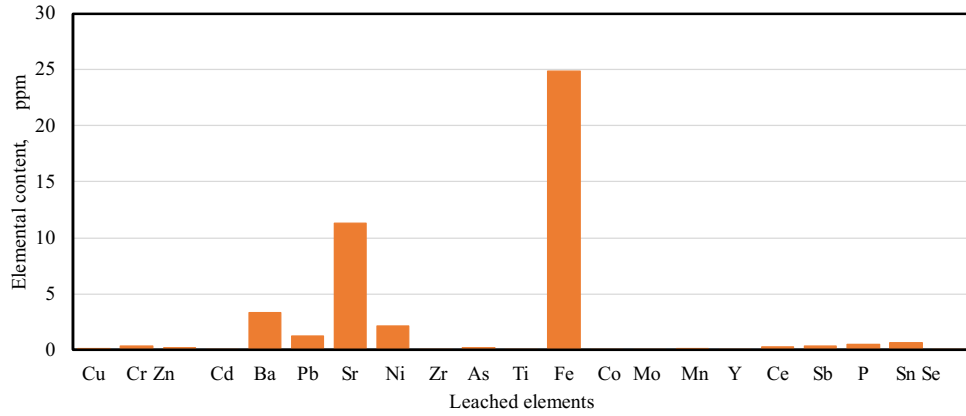


G10CRT
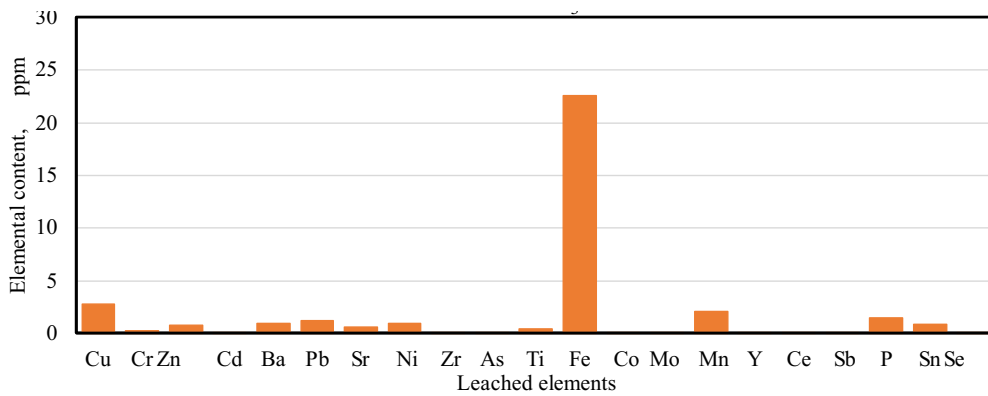


G20D64
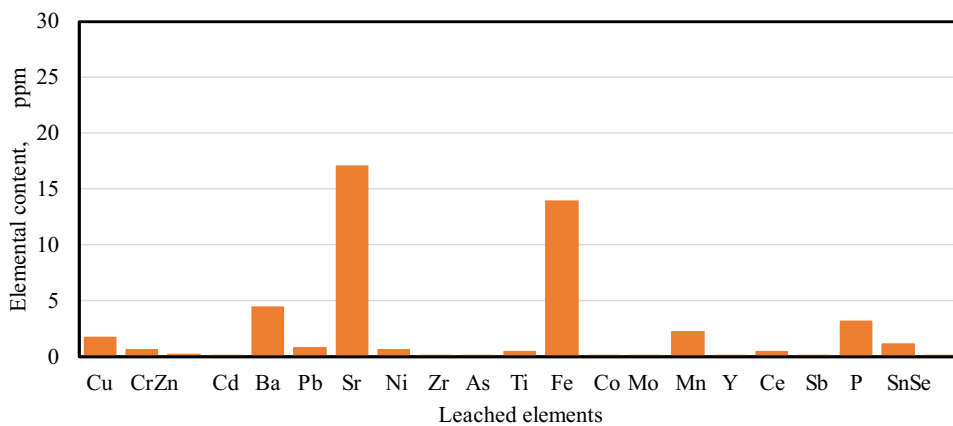


G5CRT20D64
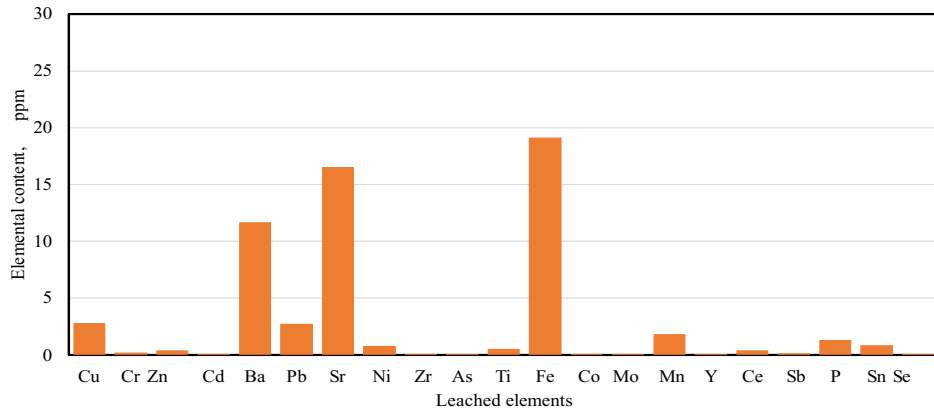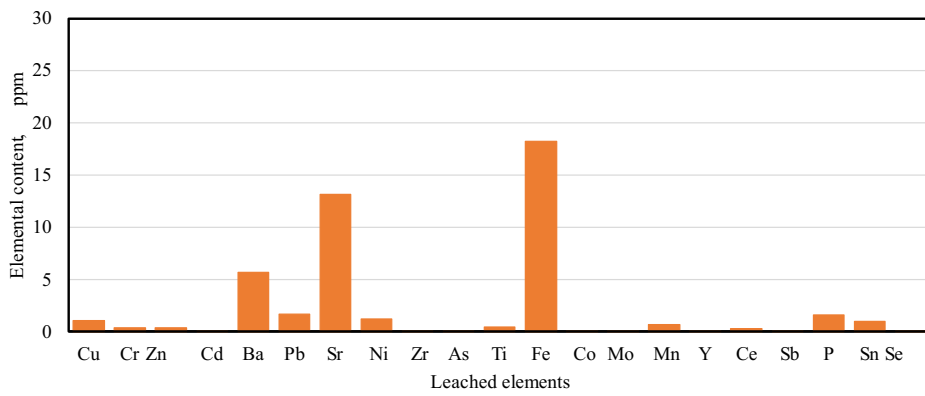
G10CRT20D64



G20DX
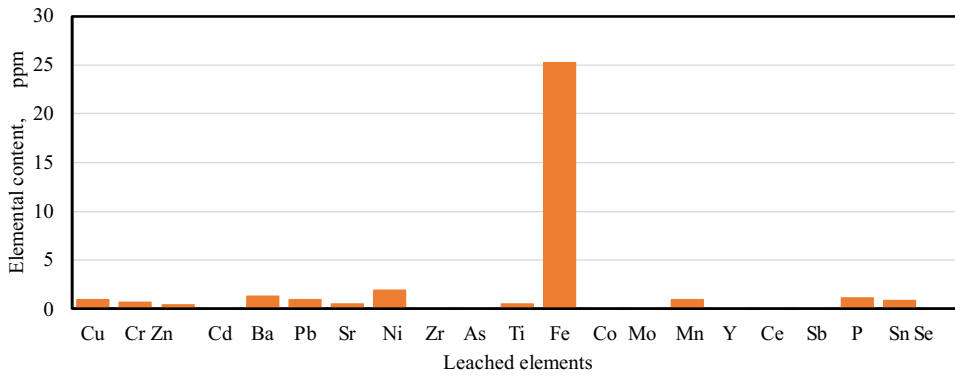


G5CRT20DX
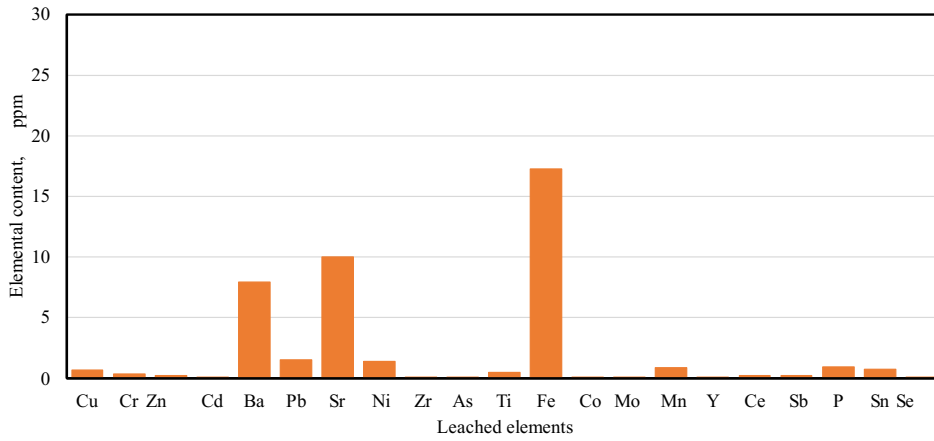
G10CRT20DX
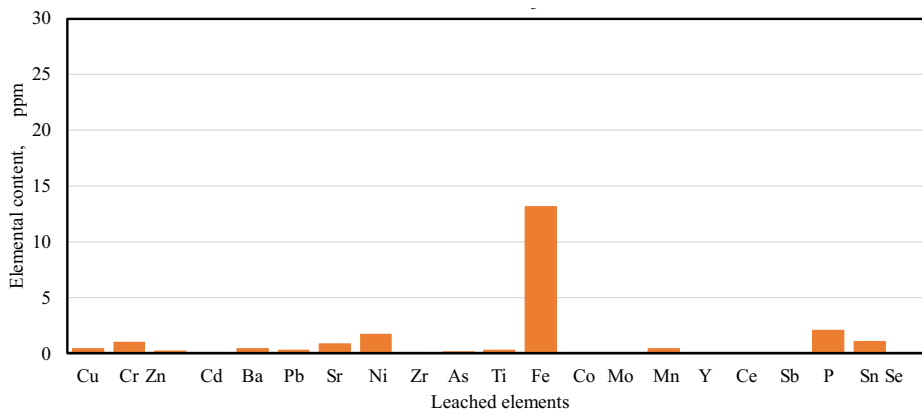


G20D53
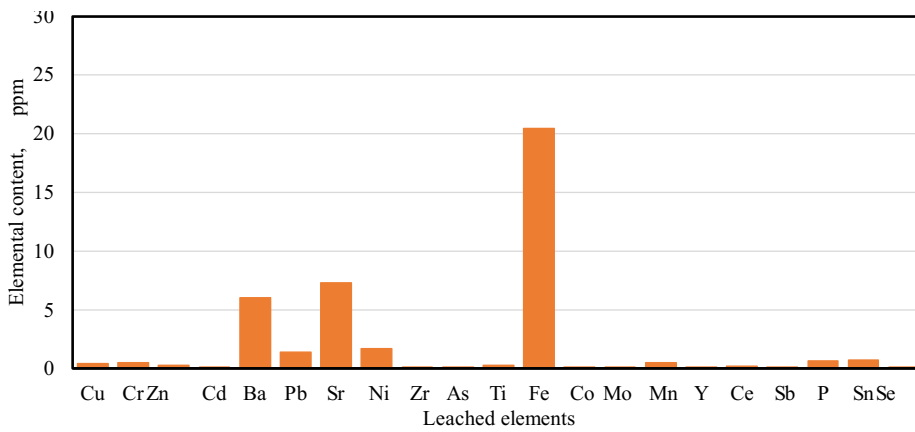


G5CRT20D53
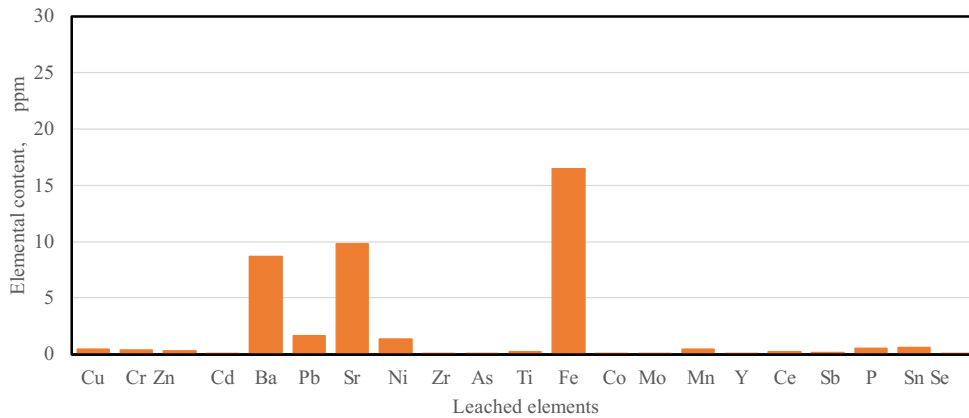
G10CRT20D53

**Figure 47.** The leaching behaviour in nitric acid (HNO₃) of the samples

### 3.2.10. Aging test results

A system's energy efficiency can be directly affected by the weathering resistance of its insulation materials. In order to guarantee long-term durability, it is imperative to investigate the weathering resistance of the foam glass. The final objective is to demonstrate that the product can continue to perform its safety function for its intended lifetime.

The thermal conductivity and the mass loss rate through time provide information regarding the degree of damage to the material under severe environmental conditions. Thus, it is necessary to determine the thermal conductivity and the mass loss rate.

The procedure consists of placing 10 g glass in an autoclave with 50 ml distilled water under a specific thermal cycle: temperature rise from room temperature to 100°C in 20 to 30 min, temperature plateau is kept at 100 °C for 10 min then the temperature increases in the container from 100 °C to 121 °C within 20 min to 22 min. Temperature plateau is set to be constant for 30 min at 121 °C.

This thermal cycle is equivalent to 36 months in real-time. From each mixture, three samples have been chosen to undergo the test. Two thermal cycles were applied on the same samples and for each cycle thermal conductivity and weight of the samples were recorded. The weight of the samples didn't change significantly in both cycles. There was no alteration in the inside and in the outer surface of the foam glass. The average thermal conductivity does not show any considerably change after the first and the second cycle, where it didn't exceed 0.06W/m·K This proves that the material properties can last at least 8 years (Figure 48).

To determine whether the resulting leachate solution is alkaline or acid a titration was needed. 0.05 ml of methyl red indicator solution was added to the eluate and titrated with a hydrochloric

acid solution (0,02mol/l.) until the colour is matching the reference liquid colour. The eluate of samples with 5 and 10 wt% CRT glass have an acidic content where the pHs were 6 and 5, respectively. The leachate of the foam glass made entirely by container glass and samples made with container glass and dross have an alkaline pH. It is may due to the presence of alkali compounds in the aluminium dross such as halite and some fluorite.
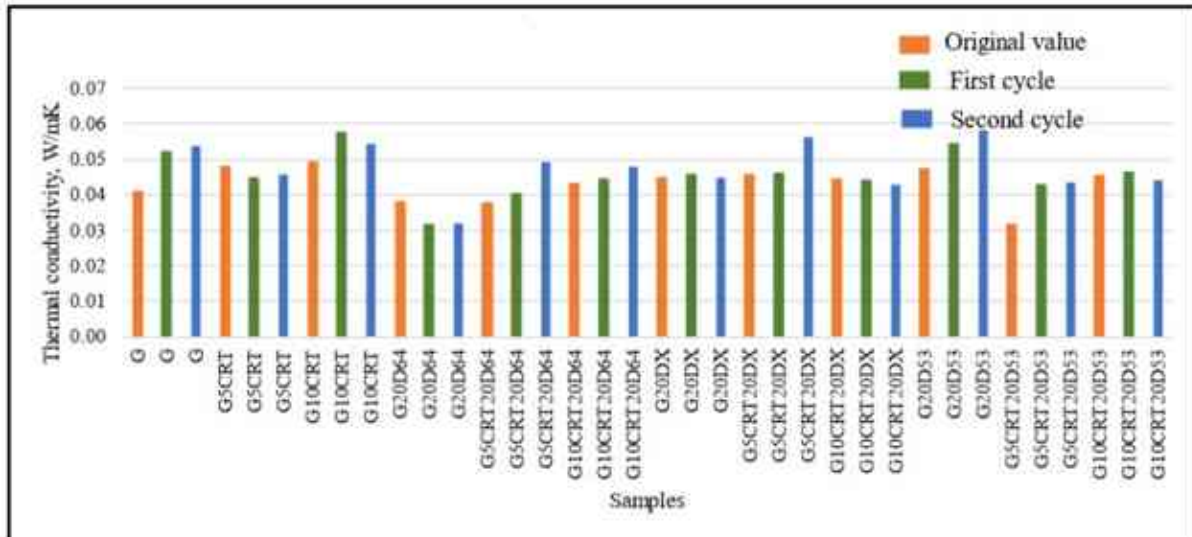


**Figure 48.** Thermal conductivity deterioration by the aging process

A more vigorous cycle was applied on two samples of G20D53. One sample was immersed in water and autoclaved at 200°C for 24 h, and the second one was placed in nitric acid in the autoclave at 200°C for 24 h. There was no weight loss, the structure of the foam and the cells were still intact, and no alteration occurred. The sample with water shows high white efflorescence due to the dissolved salts while samples in nitric acid show both efflorescence and oxidation (Figure 49). The thermal conductivity increased to reach 0.048 W/m·K in the sample immersed in water and further increased to reach 0.05 W/m·K in the sample placed in acid (Figure 50). This proves that even in very harsh conditions, the thermal conductivity didn't exceed the limit of commercial foam glass (0.035 to 0.08 W/m·K).

|     (A)     |     (B)     |

**Figure 49.** G20D53 sample in water - efflorescence (total dissolved salt) (A), Sample in acid - efflorescence (total dissolved salt) + oxidation (B)
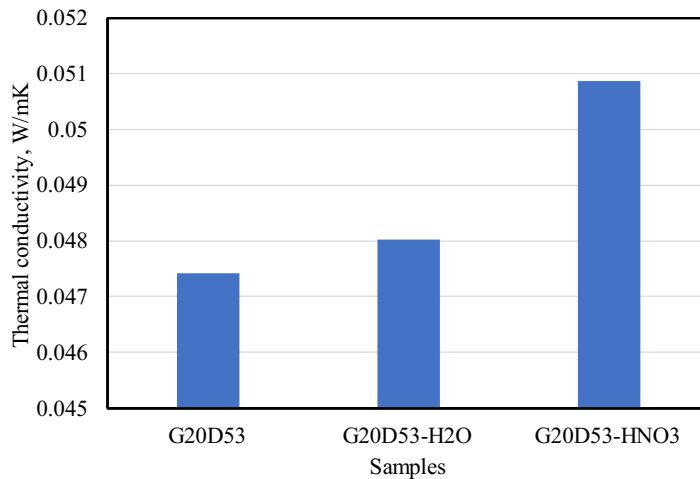


**Figure 50.** Thermal conductivity deterioration of the foam glass G20D53 under severe conditions

Based on the previous data, a forecast curve of the foam glass lifespan was made. In the worst-case scenario, the thermal conductivity will be around 0.07 W/m·K (Figure 51). If we have a good case, the thermal conductivity will be constant at around 0.05 W/m·K. To conform to this prediction, model a set of samples is placed on the rooftop of the university of Freiberg where the temperature and weight loss are measured once per 2 months. The data will be collected and compared to the accelerated model every 6 months (Figure 52).
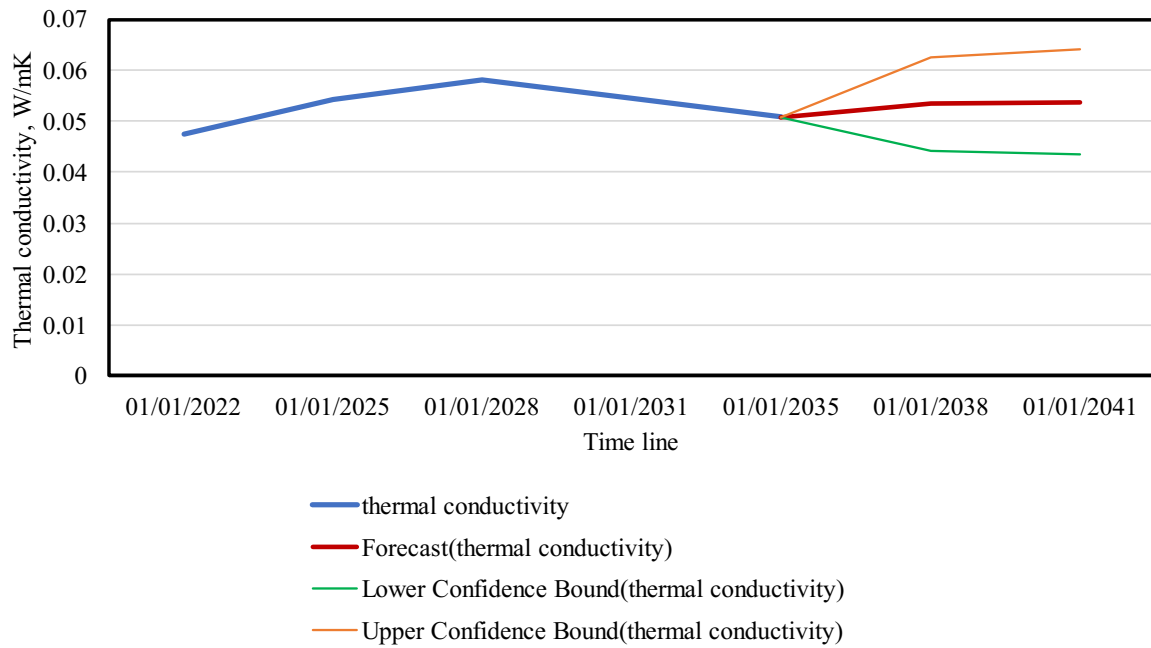
**Figure 51.** Thermal conductivity deterioration forecast



**Figure 52.** Weathering test set-up

## 3.3. Potential application field

Understanding waste types, quantities, and characteristics are essential to improving waste management strategies and green processing. Hazardous waste includes items harmful to humans and the environment like CRT glass and aluminium dross. Materials requiring special handling and sealing have high disposal costs. The most effective way is to incorporate them into functional materials like foam glass and end up with a win-win situation where no handling and sealing will be needed, the depletion of primary source materials will be reduced, and finally, the production price will be decreased to produce affordable materials.

In this work, foam glass was produced using up to 30 wt% dross and 10 wt% CRT. Moderating the amount of those waste materials gives foam glass different characteristics. As a result of these properties, foam glass can be associated with specific applications:

Foam glass made with container glass and aluminium dross 64 (10,15 and 20 wt%) has up to 90 % open pores. Their densities range from 0.16 to 0.18 g/cm$^3$ and their compressive strength reaches 0.3 to 0.6 g/cm$^3$, making them a candidate product for drainage. The same rules are applied to other samples made with dross types X and 53 where the open porosity ranges from 85% to 91%. This foam glass has excellent chemical stability against acids which will help with liquid waste disposal.

Closed-porosity foam glass is usually used as an insulation material. It is observed in dross-free samples, where pure container glass has the lowest absorption (15%). Samples with 5 and 10 wt% CRT glass content slightly increase the water absorption to 30 wt% with low thermal conductivity 0.04 W/mK, low density 0.17 g/cm$^3$, and high strength (0.99 to 0.5 MPa).

Samples with 30 wt% have excellent pressure resistance and can withstand high loads up to 11 MPa. Despite their high density (2.5 g/cm$^3$), the combination of the high strength and the low thermal conductivity (0.07 W/mK) makes foam glass an ideal material for underground pipeline insulation. This work can be a learning source for students.

## 3.4. Conclusions

Foam glass was made based on recycled container glass material, cathode ray tube (CRT) glass, and treated secondary aluminium dross. Three types of aluminium dross were used. The physical and chemical characteristics were examined with a special focus on the effect of the foam glass composition on the microstructure, density, water absorption, thermal conductivity, and compressive strength. The chemical stability and durability of the final product were studied. Accordingly, the following are the main observations and conclusions from this study. Aluminium dross composition depends on the initial scrap used. The dross used in the first research part contains aluminium nitride which acts as a foaming agent and decomposes to release gaseous products ($NH_3$, $N_2$, and NO) [97]. To compare the effect of aluminium dross, three types with different compositions were used in this study. One dross type with high AlN and salt content (dross X), the second dross is low on AlN and salts (dross 64), and the third dross 53 contains low amount of AlN (1.5%).

**The effect of adding aluminium dross and CRT glass on the**

<u>Foaming process</u>

Dross 53 has the lowest foaming height while dross X and 64 have the highest foaming height. This confirms the effect of the AlN as a foaming agent. Samples with dross X contain a high amount of salts (23.48 wt%) which helps to lower the foaming temperature compared to the other two dross types, it is the fluxing effect of alkali oxides.

<u>Viscosity</u>

Not only the foaming agent is important to obtain a stable foam structure but also the oxides present. Oxides can change the physical and chemical properties of the foam glass by modifying the viscosity during foaming. High viscosity can limit gas bubbles growth while low viscosity can't retain gas bubbles. The solution is to find the equilibrium between the amount of bridging and non-bridging oxygen. $Al_2O_3$ present in aluminium dross causes a decrease in the non-bridging oxygens, resulting in higher viscosities while $Na_2O$ and CaO content create non-bridging oxygens. MgO has more of a neutral effect as remains unchanged in all the samples which prove that magnesium plays the role of a former in the glass structure. PbO and ZnO present in CRT glass has an extremely strong viscosity-lowering effect which will weaken the network. The $Ba^{2+}$ ions act as a modifier in the glass network, causing an unhinged packing of the glass network. While oxides in glass decrease the viscosity during foaming, oxides in the aluminium dross increase the viscosity to stabilize the foam structure.

<u>Microstructure</u>

In container glass foams, the cells are small and homogenous in a hexagonal shape like a honeycomb structure. Adding CRT glass will give the same morphology as the pure container glass foam but with a slightly higher cell size. This increase may be due to the high content of $Na_2O$, CaO, and BaO, where the total amount is around 21 wt%, responsible for creating non-bridging oxygen and consequently decreasing the viscosity. Lower viscosity will allow the creation of bigger bubbles. Adding aluminium dross type 64 and type X increases the cell size. Aluminium oxides in dross tend to increase the viscosity to provide a more stable structure. This allows the fusion of the gas bubbles and the growth of big cells. Moreover, the high AlN content boosted the foaming process. In comparison to the previous two dross types, samples with aluminium dross 53 have a more stable cell structure close to that of the container glass.

Density and volume expansion

The apparent density is highly negatively correlated with the volume expansion. The density of samples with 10 wt% CRT glass increases as the amount of dross content increases which will decrease the expansion process of the sample. A sample with only 10 wt% CRT glass content exhibits a low viscosity due to the high amount of CaO and $Na_2O$ (20 wt%). This viscosity will increase gradually by increasing the amount of $Al_2O_3$ to create a denser foam structure with less expansion. Samples without CRT glass or with 5 wt% CRT glass have a similar amount of the network former and modifier. Therefore, the foam density didn't show a significant change by increasing aluminium dross.

Water absorption

In this study, open and closed porosities were observed. A good example of closed pores is found in dross-free samples, where pure container glass has the lowest absorption (15%). Water absorption can be linearly correlated with the closed porosity and dross content. As the dross content increases, the generation of closed pores decreases causing higher water absorption.

Thermal conductivity

The thermal conductivity of commercial foam glass ranges from 0.035 to 0.08 W/m·K. The thermal conductivity of the samples ranges between 0.038 W/m·K and 0.055 W/m·K which makes them a good thermal insulating material.

Compressive strength

As seen with dross type 64, a high crystal content could weaken the foam glass' load-bearing capacity. Dislocation propagates through the well-displayed plans of the crystal. By introducing amorphous phases to crystalline materials, grain boundaries and phase boundaries can be impeded from moving. The compressive strength of foam glass is highly correlated with its porosity independently of the dross content. As the porosity increases, the compressive

strength decreases. Porosity weakens the load bearing of the foam regardless of the type of porosity (open and closed pores).

**The chemical stability of the foam glass**

Regardless of the variation in the sample composition, the hazardous element concentrations are less than the safe limit. The samples are classified as non-hazardous materials. Concerning the Pb-concentrations in the eluate, all samples recorded Pb-concentrations lower than the safe limit (≤10 ppm), fulfilling Pb-immobilization of 80%. Lead may incorporate into a crystal phase containing iron without being detected with XRD due to its minor amount. Lead is very likely incorporated into magnetite [104] .

**The chemical durability of the foam glass**

The procedure to test the durability of the foam glass is conducted according to the hydrolytic resistance of glass grains at 121 °C – (ISO 720:2020 Test methods and classification). It consists of placing 10 g glass in an autoclave with 50 ml distilled water under a specific thermal cycle: temperature rise from room temperature to 100°C in 20 to 30 min, temperature plateau is kept at 100 °C for 10 min then the temperature increases in the container from 100 °C to 121 °C within 20 min to 22 min.  Temperature plateau is set to be constant for 30 min at 121 °C. This thermal cycle is equivalent to 36 months in real-time. The structure of the foam and the cells were still intact, and no alteration occurred. This proves that the final product can withstand up to 8 years without weight loss or changes in thermal conductivity (specific testing condition).

# Summary

Foam glass was successfully produced using nearly 100% waste materials: container glass material, cathode ray tube (CRT) glass (5 and 10 wt%) with two particle sizes 63 and 32 μm, secondary aluminum dross (10, 20, and 30 wt%), and silicon carbide (2 wt%). The produced foam glass has optimal properties that can compete with commercial foam glass. The main drawn conclusions are:

- The resultant foam glass is a lightweight material with a density of 0.15 to 0.19 $g/cm^3$. Added aluminium dross enhanced the foaming ability of the glass powder due to AlN content and decreased the foaming temperature allowing saving energy. Lead content in CRT glass helped to further decrease the foaming temperature. The countereffect of the aluminium oxides versus calcium and sodium oxides contributes to stabilizing the foaming structure.

- The produced foam glass exhibits a low thermal conductivity (0.038 W/m·K-0.05 W/m·K) due to the heterogeneity distribution of the cells resulting in attenuating the heat convection. It makes them an effective thermal insulating material. Foam glasses with high absorption (open porosity) and low absorption (closed porosity) were produced. Foam glass with closed porosity can be used as an insulation material in housing and building while samples with open porosity can be used in filtration.

- As some of the used raw materials are hazardous (CRT glass and aluminium dross), the toxicity test under standard conditions shows up to 99% immobilization of the hazardous elements which ensures the safety use of the product under European regulations.

- The aging test proves that the final product can withstand up to 8 years without weight loss or changes in thermal conductivity (specific testing conditions).

# Claims /New scientific results

**Claim on foam glass production based on secondary raw materials**

**1.** Based on the experimental results, I established that foam glass could be successfully produced by using secondary raw materials in the following ranges: 68-98 wt% waste container glass, 5-10 wt% cathode ray tube glass, 10-30 wt% aluminium dross), and 2 wt% silicon carbide as foaming agent. The resultant foam glass is a porous, lightweight material having 0.15 to 0.19 g/cm$^3$ density, low thermal conductivity (0.038 W/m·K-0.05 W/m·K), suitable compressive strength (up to 0.9 MPa), and appropriate chemical stability (up to 99% immobilisation of the hazardous elements).

**Claims on the effect of raw materials on the foaming mechanism**

The phase analysis revealed (Table C1) that due to the different composition of the initial aluminium alloys, the treated drosses had similar phases but in different ratios. From the aspect of foaming mechanism, the most important constituents were the AlN and the salt phases.

**Table C1.** Mineral composition (wt%) of the aluminium drosses (XRD analysis)

| Phase name and formula | Dross type | | |
|---|---|---|---|
| | **64** | **X** | **53** |
| Spinel ($MgAl_2O_4$) | 22.54 | 23.49 | 54.76 |
| Wurtzite (AlN) | 10.65 | 19.64 | 1.5 |
| Corundom ($Al_2O_3$) | 6.77 | 14.18 | 12.6 |
| Nordstrandite ($Al(OH)_3$) | 18.01 | 11.82 | 17.03 |
| Bayerite ($\beta$-$Al(OH)_3$ | 39.25 | - | 8.98 |
| Calcite ($Ca(CO_3)$) | - | - | 2.62 |
| Calcite Magnesium ($(CaMg)(CO_3)$ | - | 7.39 | - |
| Halite (NaCl) | 8.71 | 13.58 | 1.79 |
| Fluorite ($CaF_2$) | | 9.9 | 0.56 |
| Sylvite (KCl) | - | - | 0.17 |
| Salts together | 8.71 | 23.48 | 2.52 |

Heating microscopy was used to characterize the foaming behaviour of the materials. In this method the foaming temperature was defined as the temperature where the sample reached the maximum height.

**2.1.** I established that aluminium drosses having more than 10 wt% aluminium nitride (AlN) content (lines dross X, dross 64 on Figure C1) possess a self-foaming mechanism due to the decomposition of AlN in which gaseous products are released. The decomposition takes place at a temperature between 800-920°C and drives the expansion of the foam. In the lack of AlN

(line dross 53 on Figure C1), the foaming process is less intensive as only the decomposition of SiC assists it.
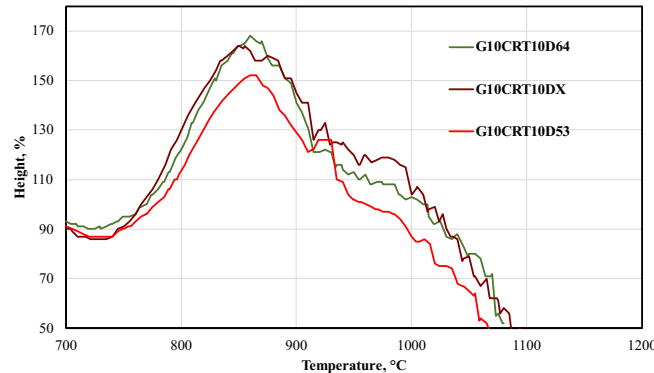


**Figure C1.** Effect of the aluminium dross types (X, 64, 53) on the foaming behaviour

**2.2.** I established that there is no significant difference between mixtures with 63 µm particle size of the CRT glass and those with 32 µm particle size (Figure C2-line CRT63 and -line CRT32). Combining the two-particle sizes of the CRT may decrease the foaming height from 145% to 120%. By using two different particle sizes, the voids between particles may be filled, thereby reducing the amount of oxygen in the sample and limiting the oxidation reaction during foaming (Figure C2-line CRT32-63).
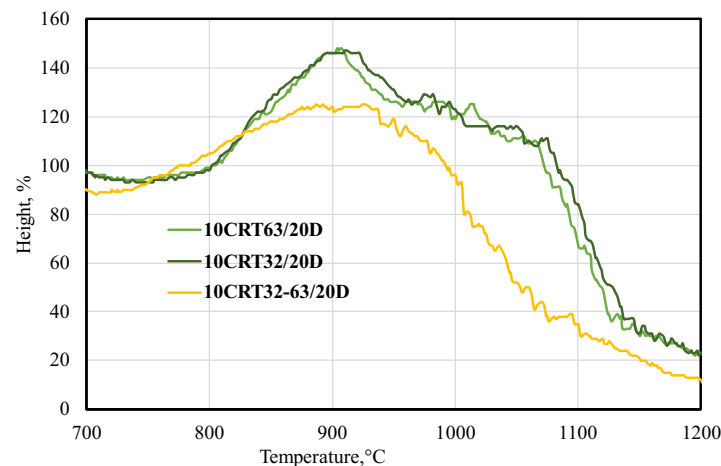


**Figure C2.** Effect of CRT glass particle size on the foaming process

**2.3.** I established that the salt content (NaCl, KCl, $CaF_2$) also affects the foaming behaviour as salts lower the foaming temperature due to the fluxing effect of alkalis. In sample G10CRT20DX with the highest salt content (23 wt%), there is a 20°C reduction in the foaming temperature compared with the sample (G10CRT20D53) having 2.52 wt% salt content (Table C2).

**Table C2.** Effect of salt content on the foaming temperature

| Sample name | Salt content (wt%) | Foaming temperature (°C) |
|---|---|---|
| G10CRT20D64 | 8.71 | 859 |
| G10CRT20DX | 23.48 | 845 |
| G10CRT20D53 | 2.52 | 865 |

**2.4.** CRT glass has almost the same composition as container glass except the hazardous element. Lead is the most abundant hazardous element beside barium (2342 ppm). I established that the lead content of CRT glass lowers the melting temperature of the glass due to the existence of lead presented in CRT glass as bivalent $Pb^{2+}$. The polarizability of this cation can further decrease the viscosity across a wide range of temperatures by creating non bridging oxygens. It can be seen in Figure C3 where CRT-free sample (G15D64) has higher foaming temperature (869 °C) than the sample G10CRT15D64 having 10 wt% CRT glass (855°C).
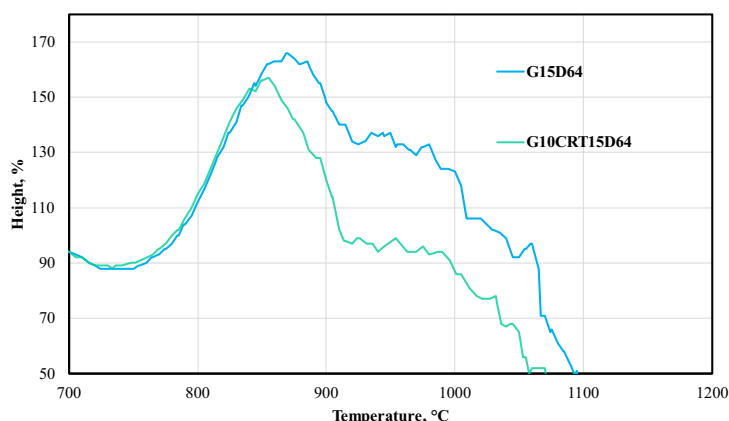


**Figure C3.** Effect of lead in CRT glass on the foaming behaviour

**Claims on the effect of the raw materials on the viscosity of glass mixtures and volume expansion**

The viscosity is one of the most important properties of the glass, as it determines the behaviour of the glass during the melting. It can be directly measured or calculated from the oxide composition of the glass. The components of a glass are classified as network formulating, modifying or intermediate. The stability thus the viscosity of the glass network is based on the ratio of bridging and non-bridging oxygens. Besides the foaming agent, the viscosity of the

glass affects the expansion process of the foam. One way to characterize the viscosity is through determining the final composition of the foam glass (Figure C4).

**3.1**. I established that dross-free samples contain sodium oxide as a major component followed by calcium oxide, magnesium oxide, aluminium oxide. Usually, high concentration of $Na_2O$ and CaO ($Na_2O$+CaO= 20 wt%) creates more non-bridging oxygens resulting in decreasing the viscosity and allowing gas bubble formation. Further decrease in the viscosity may provoke gas escaping and destruction of the bubbles. The high amount of $Al_2O_3$ in aluminium dross 64 (16 wt%-Figure C4) causes a decrease in the number of non-bridging oxygens, resulting in higher viscosities. If the amount aluminium, calcium, and sodium oxides are similar, it can create an equilibrium effect on the viscosity to create a more stable foam structure.

**3.2**. Due to its PbO content, adding CRT glass has an extremely strong viscosity-lowering effect by acting as a modifier. Lead weaknesses the network by creating non-bridging oxygen while due to its size, its migration is limited.
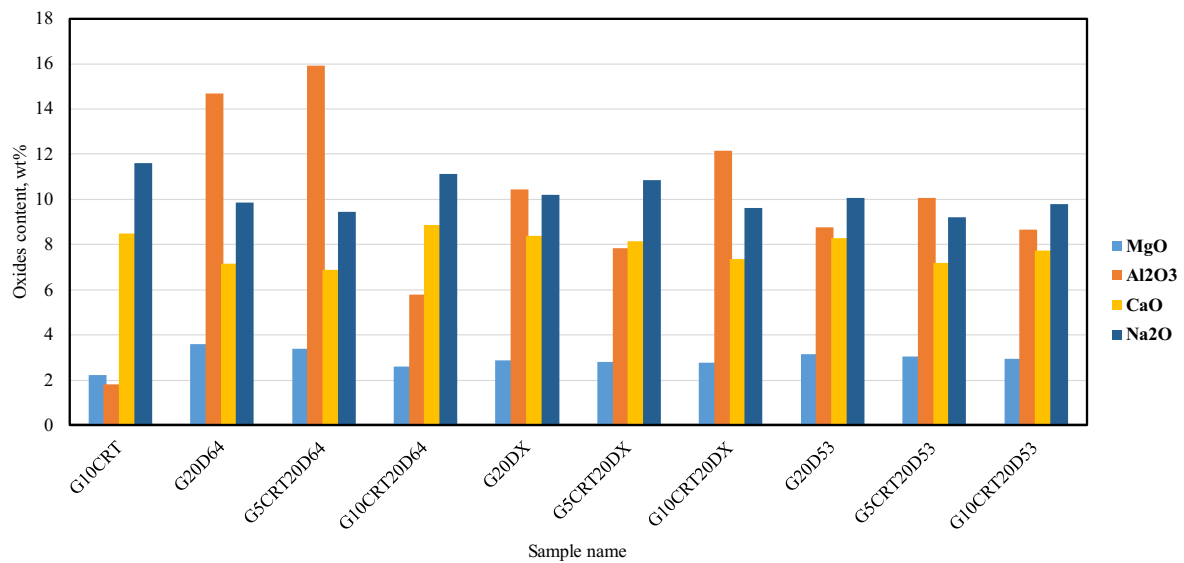


**Figure C4.** MgO, $A_2O_3$, CaO, and $Na_2O$ content in foam glasses

**3.3.** I established that the maximum volume expansion is detected in samples with dross types 64 and X (volume expansion coefficient=7.8) due to their high AlN content (10.65 wt% and 19.64 wt%, respectively) which will boost the foaming process.

**3.4.** Due to the low AlN content (1.5 wt%) in dross 53, samples with dross 53 have the minimum expansion (7 to 6), which hinders the foaming. Besides, when CRT glass content is increased, foam growth is restricted during sintering, resulting in a more homogeneous pore distribution. It is related to the high viscosity generated due to the high alkali content especially with 10 wt% CRT glass leading to bubble collapse during foaming.

**3.5.** If the glass foams are insufficiently heated or the viscosity is high, gas bubbles will not be generated. On the contrary, the outer shell of the pores collapses if the viscosity is low or the foaming process is too intense, resulting in bubble fusion. The key to prevent bubbles from limited growth or overgrowth is controlling the aluminium nitride content and alkali oxides to create a suitable viscosity for bubbles generation.

**Claims on cell size characterization**

Foam glass's cell structure will determine its physical properties, mainly density, thermal conductivity, and compressive strength. Herein, cell size, geometry, orientation, distribution, and type of connectivity are the key features for the characterization of foam glass. A full description of the cellular system is essential to explain not only the properties of the foams but also the viscosity environment at the exact foaming temperature. From the CT data of the cell sizes detected, I calculated the average, maximum, and minimum cell sizes. I used statistical data analysis of the cell size and distribution generated by the CT scan and linked it to the oxide's component of the foam glass to understand the effect of $Al_2O_3$, CaO, $Na_2O$, BaO, and Pb on the glass structure.

**4.1.** I determined that the mode indicated the most frequent cell size, and the standard deviation (SD) reflected the degree of dispersion of the cell sizes. An SD value close to 0 or to 1 indicates a homogenous or a heterogeneous cell structure, respectively. This can be seen in Figure C5 where foam glass with container glass has a homogenous structure with a standard deviation of 0.28 while sample G10CRT10D64 has a heterogenous cell distribution which can be seen in the macrograph and in the standard deviation value (0.714).



Sample G with SD=0.28          Sample G10CRT10D64 with SD=0.714

**Figure C5.** Macrograph of the sample made with container glass and the sample made with 10 wt% CRT and 10 wt% dross 64

**4.2.** I established that samples with only container glass and samples with 5 wt% CRT glass had almost the same homogenous cell structure with a maximum and a minimum cell size around 3.1 mm and 0.1 mm, respectively (Table C3). It is due to the high viscosity environment

which gives limited access for bubbles to growth. Increasing the CRT glass to 10 wt%, the maximum cell size increased to 5.496 mm and the standard deviation (SD) increased to 0.714 so the cell distribution tends to be heterogeneous. This increase may be due to the presence of high content of $Na_2O$, CaO, and BaO responsible for creating non-bridging oxygens and consequently decreasing the viscosity. Lower viscosity will allow the creation of bigger bubbles and heterogeneous structure (Figure C6).
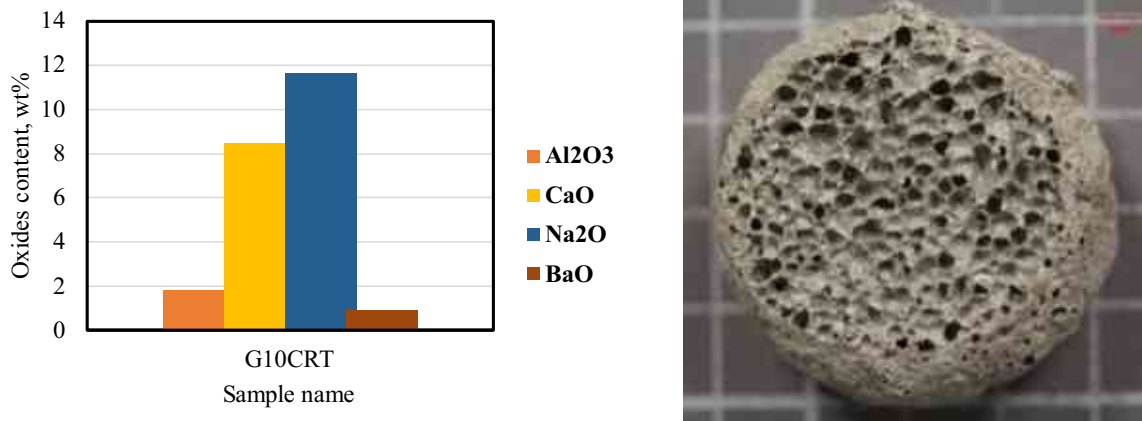


**Figure C6.** Main oxide composition and macrograph of the sample G10CRT

**Table C3.** Statistical parameters of the cell size distribution determined from the 2D CT scan

|  | G | G5CRT | G10CRT |
|---|---|---|---|
| Average (mm) | 0.719 | 0.793 | 0.758 |
| Median (mm) | 0.716 | 0.565 | 0.475 |
| Mode (mm) | 0.736 | 0.303 | 0.273 |
| Maximum (mm) | 3.126 | 3.180 | 5.496 |
| Minimum (mm) | 0.161 | 0.141 | 0.131 |
| Standard deviation, SD | 0.285 | 0.528 | 0.714 |

**Claims on the effect of dross composition on the cell sizes**

Aluminium dross composition varies depending on the initial source. Besides aluminium nitrides, the main dross oxides that can affect the properties of foam glass are $Al_2O_3$, CaO, $Na_2O$, and MgO. Since MgO content didn't seem to change in the samples (an average of 3.5 wt%), it is considered a component of the network formation and excluded in this study.

**5.1.** I established that adding aluminium dross to container glass increased the maximum cell size from 3.1 mm to 7 mm in samples with 10 wt% dross. The higher the dross content in the sample, the wider spherical pores appear in the center due to the boosted effect of the foaming

process generated by the high AlN content (10.6 wt%) leading to cell growth and coalescence. The most frequent cell size in container glass sample reported to be 0.7 mm while the most frequent cell size in samples with dross or dross and CRT is around 0.2 mm to confirm that adding aluminium dross increases both cell size and the number of small pores within the walls, resulting in an enhanced heterogeneity in the structure of the foam glass (indicated by SD=0.747) (Table C4). Samples with high amount of $Al_2O_3$ (16 wt%) (Figure C7) have rounder and smaller cells indicating high viscosity environment compared to the sample containing higher alkaline oxides (CaO+$Na_2O$=20 wt%) with bigger agglomeration of cells (Figure C8). Both samples contain the same amount of dross but different amount of CRT glass. In this case, increasing CRT glass content created a less viscous environment which cause the bubble to collide and agglomerates to create bigger cells.
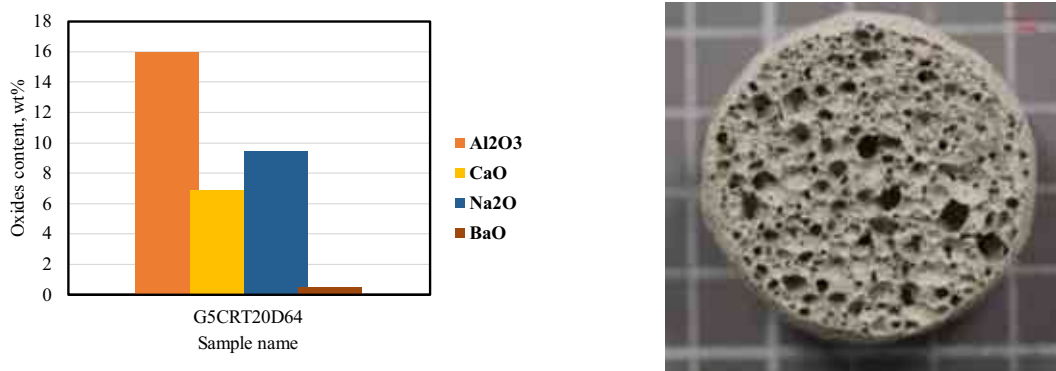


**Figure C7.** Main oxide composition and macrograph of the sample G5CRT20D64
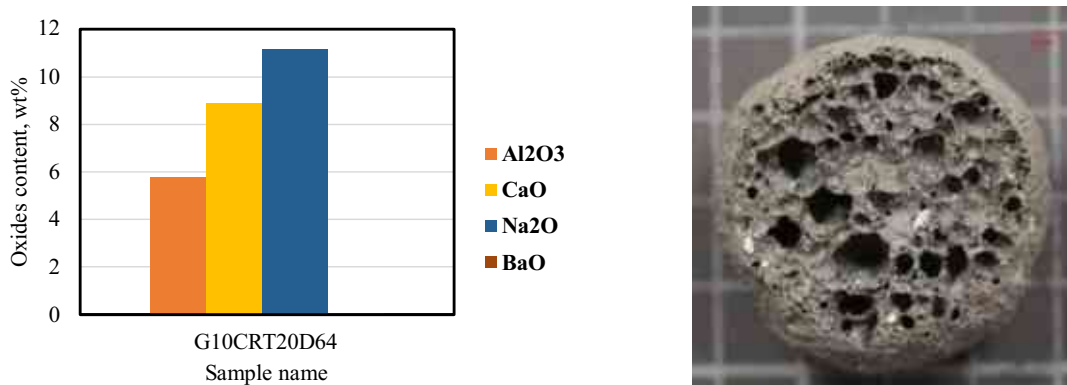


**Figure C8.** Main oxide composition and macrograph of the sample G10CRT20D64

**5.2.** I established that samples with container glass and 20 wt% dross X exhibit large heterogeneous cell sizes suggesting a low-viscosity environment (Figure C9). Since the amount of $Na_2O$ equals $Al_2O_3$, the effect of those ions on the viscosity will be nullified. However, the effect of the alkali ions will be boosted since the presence of CaO will decrease the viscosity of the melt. Sample G10CRT20DX has wider cells (Figure C10). It is explained by the high

content of $Na_2O$, BaO, and CaO (18 wt%) compared to $Al_2O_3$ content (12 wt%), which results in the destruction of the bridging oxygens in the glass structure and lowering the viscosity.

**Table C4.** Statistical parameters of the cell size distribution determined from the 2D CT scan

|  | G10D64 | G5CRT10D64 | G10CRT10D64 |
|---|---|---|---|
| Average (mm) | 0.622 | 0.692 | 0.681 |
| Median (mm) | 0.384 | 0.433 | 0.443 |
| Mode (mm) | 0.264 | 0.312 | 0.272 |
| Maximum (mm) | 7.227 | 6.059 | 7.543 |
| Minimum (mm) | 0.024 | 0.131 | 0.030 |
| Standard deviation | 0.649 | 0.657 | 0.747 |
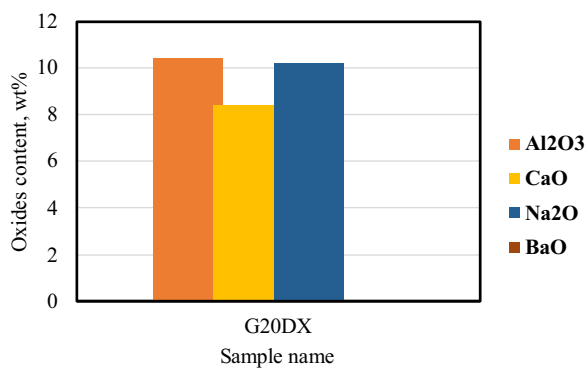


**Figure C9.** Main oxide composition and macrograph of the sample G20DX
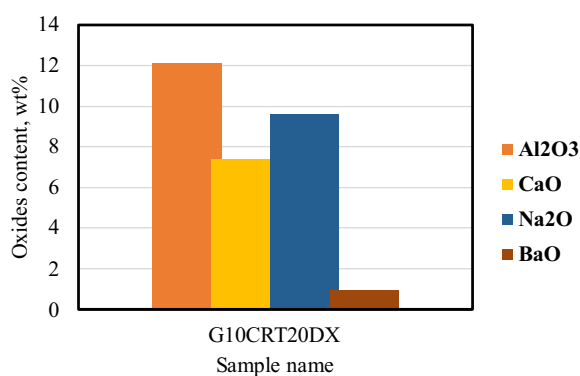


**Figure C10.** Main oxide composition and macrograph of the sample G10CRT20DX

**5.3.** I established that adding aluminium dross 53 will create a homogeneous cell structure compared to the previous two types of dross. It may be explained by the limited effect of the AlN rather than by the effect of the alkali ions (Figure C11). In the counterpart, samples with 20 wt% dross and 10 wt% CRT glass, shows an increase in the cell size, and the structure

becomes more heterogeneous (G10CRT20D53) (Figure C12). It is due to high content of $Na_2O$ and CaO content (19 wt%) which decreases the viscosity, the viscous forces created are exerted on the bubble, causing it to break. Even with the low AlN content (1.5 wt%), a high amount of dross X combined with 10 wt% CRT glass content may boost the foaming process due to the alkali content which decreased the viscosity allowing for bubble formation to create big cells.



**Figure C11.** Macrograph of the sample G5CRT10D53
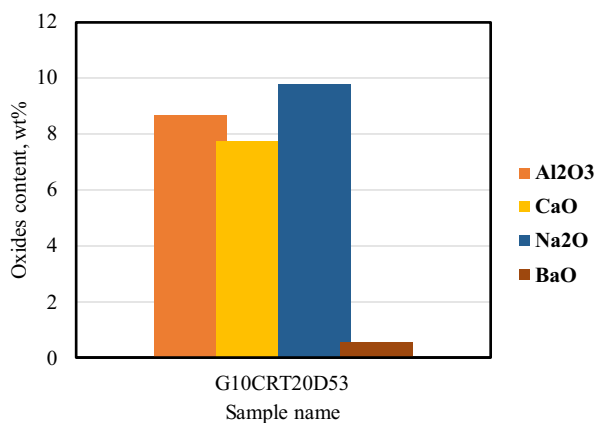


**Figure C12.** Main oxide composition and macrograph of the sample G10CRT20D53

**Claims on the type and shape of the pores**

I established that adding CRT and dross will not only change the cell size but also cell shapes, connectivity and the intercell in the walls.

**6.1.** Foam glass made with container glass has mostly sub-millipores (0.1 and 1 mm) that are more tetrahedra hexagons than round. The walls of the cells contain oval super-micropores (10 to 100 μm). Those oval super-micropores have walls containing sub-micropores (0.1 to 1 μm). This can indicate a high viscosity growth environment.

**6.2.** Sample with 5 wt% CRT has oval sub-millipores that appear surrounded by a high number of round super-micropores. The millipores were deeper than in the container glass foam which may indicate open porosity. Adding 10 wt% of CRT glass results in slightly larger inter-millipores (1 to 10 mm) where their walls contain a smaller amount of super-nanopores (10 to 100 nm) compared to the other samples.

**6.3.** A sample containing container glass and dross 64 shows mostly inter-millipores, as well as -inter-micropores linked together. The walls of the inter-micropores are formed by alignment of nanopores. The concave part of the pore displays a needle structure that may indicate the existence of a crystallized phase. The CT scan results proves that adding aluminium dross will generate higher nanopores which can be seen in the micrographs (Figure C13).

**6.4.** AlN in dross boost the foaming process to generate more irregular pores while other compounds will act as counteracting effects to increase the viscosity, such as aluminium oxides, which will slow down the foaming process and generate rounder smaller cells.



|  |  |
|---|---|
| G | 5CRT |
| 10CRT | G10D64 |
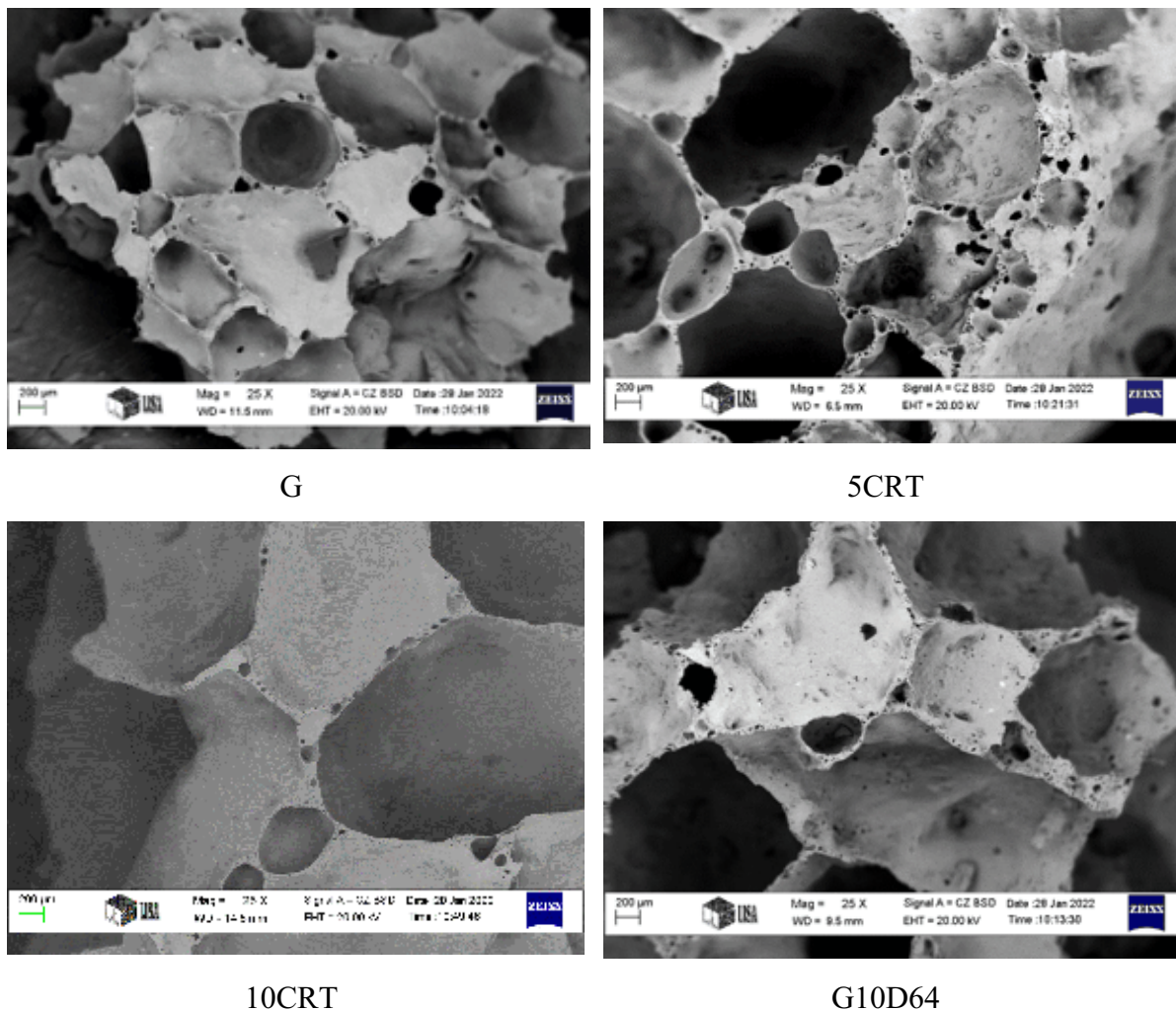
**Figure C13.** Micrographs of the foam glasses

**Relationship between the $Al_2O_3$/$Na_2O$ ratio, the density and the amount of raw materials**

I established that the density of foam glass depends on the cell structure (the size and shape of the cells) and the amount of dross and CRT glass added. Secondly, I excluded the mixtures with 30 wt% dross content due to the high density generated (0.9 $g/cm^3$) and focused on using 10 to 20 wt% dross and study the effect of using drosses with different composition.

**7.1.** Firstly, I revealed that the average cell size is highly ($R^2 = 0.9095$) negatively correlated to the density of the foam glass (Figure C14).

$$y = -0.4741x + 1.286$$

As the aluminium dross content increases the average cell size of the foam decreases and the density increases. It is due to the indirect effect of the dross oxides on the viscosity and thus the foaming process.
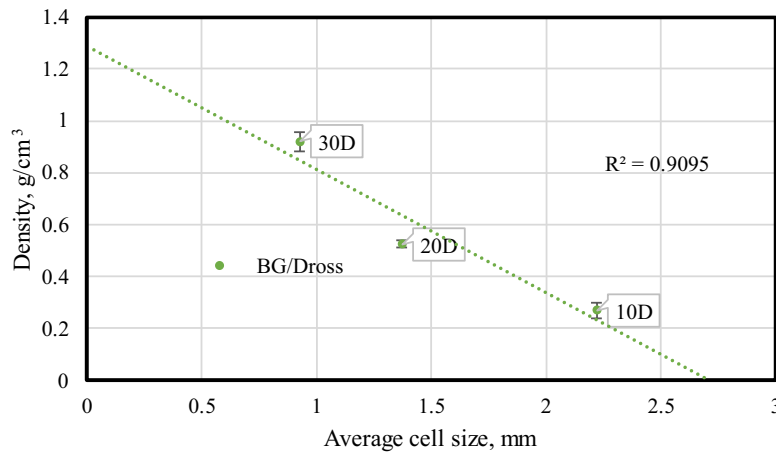


**Figure C14.** Density versus average cell size of foam glass made with container glass and dross

**7.2.** I established that the ratio of $Al_2O_3/Na_2O$ used to determine the density behaviour in soda lime silicate glass can be applied to foam glass with dross X and 53 where the density will decrease as the $Al_2O_3/Na_2O$ ratio increases to 1.2, then starts to increase again.

**7.3.** Despite the low amount of $Al_2O_3$ in the sample G10CRT20D64 (5.5 wt%) allowing the alkali oxides to act and create lower viscosity and bigger cell sizes, the density is high. It may be related to the presence of a high amount of CaO (8 wt%) which tends to increase the density.

**7.4.** Not only the $Al_2O_3$ and $Na_2O$ content will affect the density but also the volume expansion, porosity and the cell size. As it can be seen in Figure C15, the apparent density is highly ($R^2 = 0.9886$) negatively correlated with the volume expansion as follows:

$$y = -64.956x + 19.236$$

The density of samples increases as the amount of dross content increases which will decrease the expansion process of the sample.
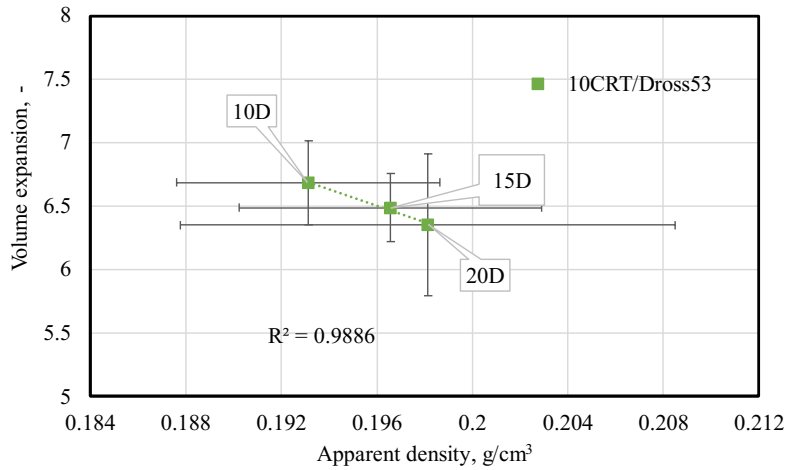
**Figure C15.** Volume expansion versus apparent density of samples with container glass, 10 wt% CRT, and Dross 53 (10CRT/Dross 53)

**Effect of pore types and cell structure on the water absorption**

There are two types of foam glass: water-resistant and still absorbing mist and humidity, and high-absorption material used for drainage. It depends on the type of pores formed. Pores that are open to the outside are known as open pores. It is generated in high viscosity environment where the separating walls are not completely formed. On the other hand, closed pores can be the product of two phenomena. The first is caused by intensive heating, which results in the collapse of parts near the pores' outer shell. The second reason is due to the insufficient evolution of gaseous substances. I established that both high and low absorption foams can be generated depending on the initial composition.

**8.1.** Dross-free samples have the lowest absorption values (13 to 35 %), whereas container glass with 5 wt% CRT glass has the lowest absorption (13 %). It may be caused by the intensive heating, resulting in the outer shell collapsing, or due to the insufficient evolution of gaseous substances during foaming, which seems to be the cause as dross-free samples doesn't contain AlN, so the foaming process is limited.

**8.2.** Samples containing 10 wt% CRT and 10 wt% dross have the lowest water absorption (20 to 24 %) compared to the other samples with dross. Adding 10 wt% CRT contributes to stabilizing the pore structure and limiting the foaming process.

**8.3.** Water absorption can be linearly correlated ($R^2$=0.9862) with the closed porosity and dross content as follows:

$$y = -6.1106x + 200.07$$

As the dross content increases, the generation of closed pores decreases causing higher absorption of water (Figure C16).
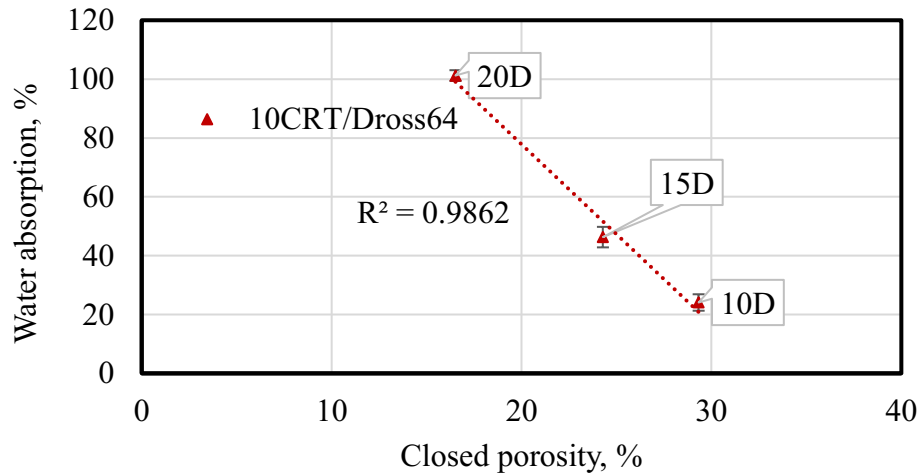


**Figure C16.** Water absorption versus closed porosity of the foam glass in 10CRT/Dross64 samples

**Claim on cell size, homogeneity, and thermal conductivity relationship**

The thermal conductivity of a material is the amount of heat transferred through its surface due to a temperature difference. Material with a lower thermal conductivity resists heat transfer better, so it is more effective as an insulation. If gases can be trapped, they make good insulation materials since they have poor thermal conduction properties which is the case of foam glass.

**9.1.** I established that the average cell size and wall thickness can directly affect the thermal conductivity of the foam glass. As the average cell size increases the thermal conductivity decreases ($R^2$=0.946):

$$y = -0.0135x + 0.0699$$
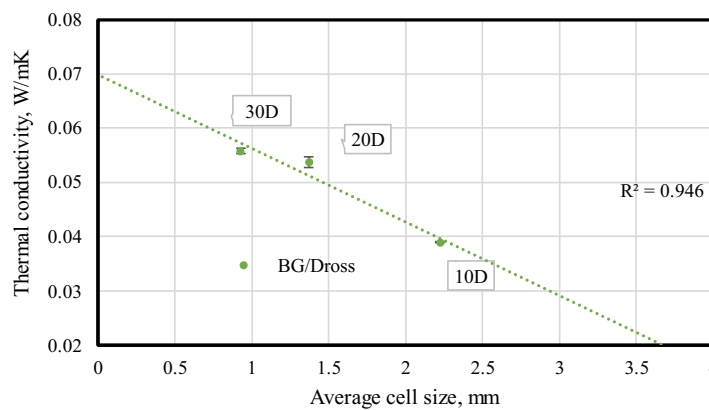


**Figure C17.** Thermal conductivity versus the average cell size

**9.2.** I established that the homogeneity of cell's structure affects directly the thermal conductivity. As the standard deviation indicates the homogeneity of the foam glass structure, a heterogeneous cell size distribution will give better thermal insulation. G10CRTD64 foam glass has a heterogeneous cell structure (SD=0.7) and is the least thermally conductive. Herein, the heat flow propagates usually through solids, so the flow will only propagate through the walls. If the walls are thin and contain high number of pores, the heat flow will be attenuated (Figure C18).



**Figure C18.** Thermal conductivity versus standard deviation of the cell size

**Effect of foam structure phases on the compressive strength**

Foam glass is typically used in road, harbour, bridge, ramp, and culvert foundation work because it reduces loads on the soil as well as horizontal loads on structures. This led to the necessity to investigate the foam glass compressive strength.

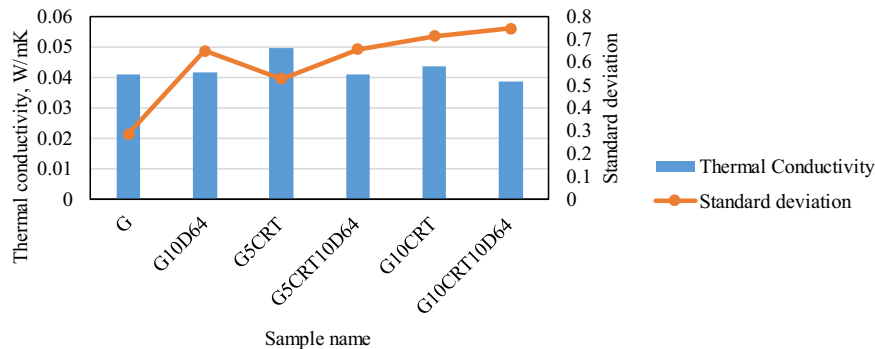**10.1.** I established that the compressive strength is related to the structure of the foams rather than the crystals content. Samples with dross 64 have the weakest compressive strength which decreases with increasing the amount of dross. As cell size increases the ability to withstand load will further be weak. On the other hand, samples with dross 53 have high compressive strength, due to their well-packed structure that can divide and distribute the applied force between the cell walls. The low compressive strength of samples containing dross 64 compared to the other two types of dross may be explained by the high amount of crystal phases present. Dislocation usually, propagates through the crystal plan. By introducing amorphous phases to crystalline materials, grain boundaries, and phase boundaries can be impeded from moving.

**10.2** The hardness of the total phases (Table C5) will determine the hardness of the foam. Samples containing dross 53 and X will have the highest hardness (6-7), followed by dross 64 (6 to 6.5) and dross-free samples G10CRT (5-5.5). Neither can be true since the sample G10CRT has a higher compression strength than the samples with dross 64 and 10 wt% CRT glass. For foam glass, the hardness of the phases doesn't apply.

**Table C5.** Effect of hardness and number of mineral phases on the compressive strength

| Sample | Mohs hardness | Compressive strength (MPa) | Number of phases |
|---|---|---|---|
| G10CRT20D53 | 6.5-7 | 0.5 | 5 |
| G10CRT20DX | 6-7 | 0.5 | 6 |
| G10CRT20D64 | 6-6.5 | 0.2 | 8 |
| G10CRT | 5-5.5 | 0.5 | 6 |

**10.3.** I revealed that the compressive strength of foam glass was highly correlated ($R^2$=0.9605) with its porosity independently of its dross content (Figure C19) according to the following equation:

$$y = -0.0749x + 7.2398$$

As porosity increases, the compressive strength decreases. Porosity weakens the load-bearing capacity of the foam regardless of the type of porosity (open or closed pores).
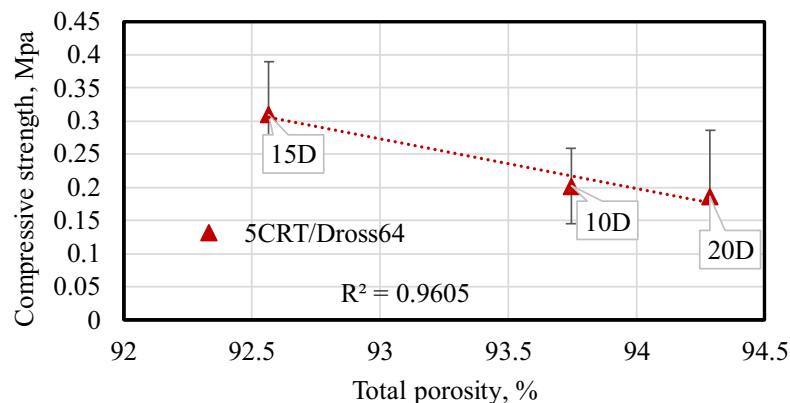


**Figure C19.** Compressive strength versus the total porosity of the foam glass made with container glass and dross 64 (5CRT/Dross64)

**Claims on the leaching characteristics**

To determine whether hazardous waste complies with specific acceptable values, the samples with the highest waste material content were selected to undergo the leaching test. The leaching behaviour of the hazardous elements was observed.

**11.1.** I established that the leaching rate of the hazardous elements is extremely low with immobilisation up to 99 %. For example, the lead concentration in the eluates was below the safe limit (≤10 ppm) for all samples (Table C6), resulting in a Pb immobilization of up to 99%

(minimum immobilization = 95%). This indicate that the lead is trapped in a crystal phase rather than the glassy phase.

Because of its small amount, lead can become trapped in iron-containing crystal phases without being detected by the XRD. The crystal phase is probably magnetite [104], as it is observed in the XRD results.

**Table C6.** Lead content in foam glass and in leachate

| Sample code | Lead in foam glass (ppm) | Lead leached (ppm) | Lead immobilisation (%) |
|---|---|---|---|
| G20D64 | 33 | 1.16 | 99.61 |
| G5CRT20D64 | 139 | 0.77 | 98.92 |
| G10CRT | 315.7 | 1.20 | 96.19 |
| G10CRT20D64 | 18.17 | 0.01 | 99.99 |
| G20DX | 16.08 | 1.66 | 99.73 |
| G5CRT20DX | 181.3 | 0.96 | 98.25 |
| G10CRT20DX | 307.9 | 1.53 | 95.30 |
| G20D53 | 7.6 | 0.25 | 99.99 |
| G5CRT20D53 | 293 | 1.38 | 95.94 |
| G10CRT20D53 | 190.9 | 1.69 | 96.77 |

**Chemical durability and aging observation and prediction**

As there was no specific test to determine the durability of the foam glass, I used the standard for the hydrolytic resistance of glass grains (ISO 720:2020) which seems the harshest test. I applied a specific thermal cycle to accelerate the weathering test (1 cycle = 36 months in real-time). Dross-free samples and samples with the highest dross content (20 wt%) and 5 to 10 wt% CRT were selected to undergo this test.

**12.1.** The weight and thermal conductivity of the samples didn't change. There was no alteration on the inside or outside surface of the foam glass and the average thermal conductivity didn't exceed 0.06 W/mK. This proves that the product can withstand up to 8 years before its properties start to degrade.

**12.2.** Using the accelerated weathering data, I established to build a forecast of the thermal conductivity estimation of 20 years from now. The prediction was done using the forecast function in Excel by using linear regression where in the worst case, the thermal conductivity may reach 0.07 W/mK which considered still in the range of insulation material (Figure 20).
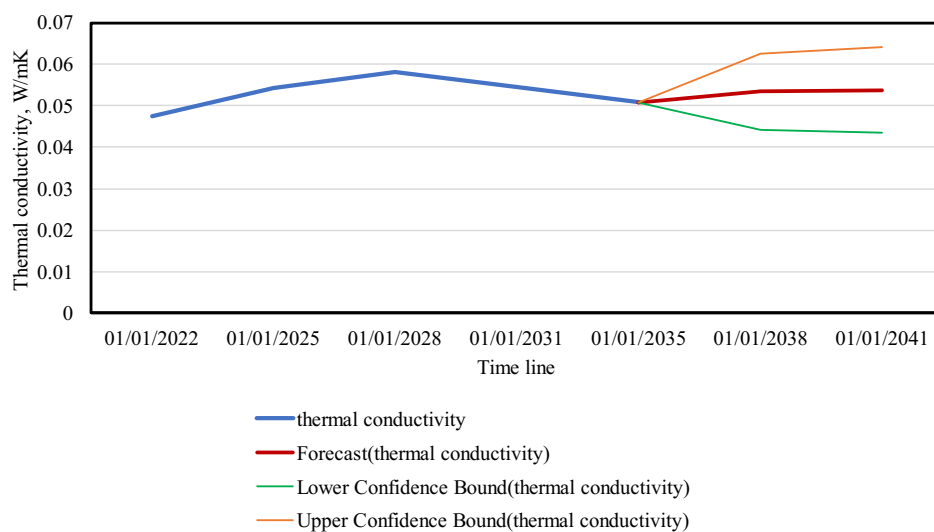
**Figure C20.** Thermal conductivity deterioration forecast

**12.3.** I applied a more vigorous cycle to two samples of G20D53 using nitric acid at a high temperature (200 °C). There was no weight loss (5 g), the structure was preserved, and no alteration occurred. The sample with water shows high white efflorescence due to the dissolved salts while samples in nitric acid show both efflorescence and oxidation. The thermal conductivity increased to reach 0.048 W/m·K in the sample immersed in water and further increased to reach 0.05 W/m·K in the sample placed in acid (Figure C21 and C22).

The foam glass has excellent chemical stability against acids which will help with liquid waste disposal.



**(A)**                                    **(B)**

**Figure C21.** G20D53 sample in water - efflorescence (total dissolved salt) (A), Sample in acid - efflorescence (total dissolved salt) + oxidation (B)
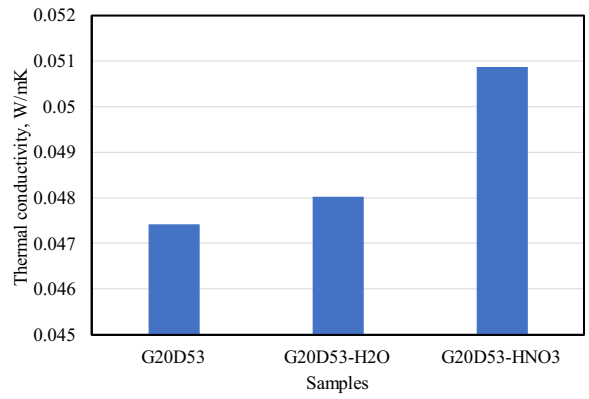
**Figure C22.** Thermal conductivity deterioration of the foam glass G20D53 under severe conditions

# List of publications

**Journal article**

M. Sassi and A. Simon, "Waste-to-Reuse Foam Glasses Produced from Soda-Lime-Silicate Glass, Cathode Ray Tube Glass, and Aluminium Dross," *Inorganics,* vol. 10, no. 1, p. 1, 2021.

**Conference Proceeding**

1- Y. Illés, M. Sassi, H. Zakiyya and T. Kékesi, "Fluoride Salts from Secondary Aluminium Dross The Fundamental Kinetic Characteristics of Aqueous Dissolution of Chloride and," in International Multidisciplinary Scientific Conference, Miskolc, 2019.

2- M. Sassi, J.-E. F. M. Ibrahim and A. Simon, "Characterization of foam glass produced from waste CRT glass and aluminium dross," in Journal of Physics Conference Series, Miskolc, 2020

**Oral Presentations**

1. M. Sassi, Foam glass made by container glass, cathode ray tube glass and aluminium dross ISCAME international conference, Debrecen, Hungary, 2019

2. M. Sassi, Foam glass production based on container glass cathode ray tube glass and aluminium dross, Conference EC-Siliconf 1 International Conference, Lillafüred, Hungary, 2019

3. M. Sassi, Characterization of foam glass produced from waste materials, Conference EC-Siliconf 2, international conference, lillafüred, Hungary, 2021

4. M. Sassi, Different methods of the production of foam glass, 2nd ICG-CGCRI Tutorial-completion certificate (silver medal), India, 2021

5. M. Sassi, Glass foam synthesis and properties, the Ceramics and Silicates Conference, Miskolc, Hungary, 2021

**Poster Presentation**

1. M. Sassi, The chemical durability and stability of foam glass made from soda lime-silicate glass, cathode ray tube glass, and aluminium dross, The 26th International Congress on Glass, Berlin, Germany, 2022

# Curriculum Vitae

## Education

**2018 – 2022 PhD in material sciences,** Institute of Ceramics, and polymers UNIVERSITY OF MISKOLC

**2016 – 2018 Master's degree in petroleum engineering** UNIVERSITY OF MISKOLC

**2012 – 2015 Geoscience Engineering Diploma** UNIVERSITY OF TUNIS EL MANAR

**2009 – 2012 Preparatory studies in geology and biology of soukra** (ISEP BG), TUNISIA

## Work Experience

**Since 09/2022 Researcher in R-Zement**, Karlsruhe Institute of Technology, Germany

**02/2022 to 08/2022 Guest researcher** Institut für Glas und Glastechnologie, TU Bergakademie Freiberg, Germany

**2017 - 2018 Internship, TDE SERVICES** Budapest, Hungary

# Acknowledgement

# Bibliography

[1]   P. C. Román, J. V. Calvo, A. L. Gil, J. König and M. Á. Rodríguez-Perez, "Modelling of the mechanisms of heat transfer in recycled glass foams," *Construction and Building Materials,* vol. 274, p. 122000, 2021.

[2]   D. Bozsaky, "The historical development of thermal insulation materials," *Periodica Polytechnica Architecture,* vol. 41, no. 2, p. 49–56., 7 April 2017.

[3]   "Brewsterbros," [Online]. Available: https://www.brewsterbros.com/. [Accessed 15 July 2022].

[4]   "The world counts," [Online]. Available: https://www.theworldcounts.com/challenges/planet-earth/waste/hazardous-waste-statistics. [Accessed 15 July 2022].

[5]   N. Karandashova, B. Goltsman and E. Yatsenko, "Analysis of Influence of Foaming Mixture Components on Structure and Properties of Foam Glass," in *IOP Conf. Series: Materials Science and Engineering*, Novocherkassk, 2017.

[6]   H. Wang, Z. Chen, R. Ji, L. Liu and X. Wang, "Integrated utilization of high alumina fly ash for synthesis of foam glass ceramic," *Ceramics International,* vol. 44, no. 12, pp. 13681-13688, 2018.

[7]   C. Xi, F. Zheng, X. Jiahe, W. Yang, Y. Peng, Y. Li, P. Li and Q. Zhen, "Preparation of glass-ceramic foams using extracted titanium tailing and glass waste as raw materials," *Construction and Building Materials,* vol. 190, p. 896–909, 2018.

[8]   Y. Attila, M. Guden and A. Tasdemirci, "Foam glass processing using a polishing glass powder residue," *Elsevier Ceramics International,* vol. 39, pp. 5869-5877, 2013.

[9]   M. Marinov, L. Lakov and Toncheva, "Granulated foam glass. Production, physical and mechanical properties," *SCIENTIFIC PROCEEDINGS XIII INTERNATIONAL CONGRESS "MACHINES. TECHNOLOGIES. MATERIALS,* vol. 10 , no. 12, pp. 42-44, 2016.

[10]  L. Hu, F. Bu, F. Guo and Z. Zhang, "Construction method of foam glass thermal insulation material in sloping roof," *IOP Conf. Series: Earth and Environmental Science,* vol. 61, p. 012122, 2017.

[11]  Foamit, "Foamit, Applications for Civil Engineering," 2019. [Online]. Available: http://www.foamit.fi/wp-content/uploads/2016/10/Foamedglass.pdf. [Accessed 15 februry 2019].

[12]  M. Pavlíková, A. Pivák, M. Záleská, A.-M. Lauermannová, F. Antončík, M. Lojka, O. Jankovský and Z. Pavlík, "Assessment of wood chips ash as efficient admixture in

foamed glass-MOC composites," *Journal of Materials Research and Technology,* vol. 19, pp. 2287-2300, 2022.

[13] W. S. Mustafa, B. Nagy and J. Szendefy, "Impact of compaction ratio, loading period and environmental condition on compressional behavior of foam glass aggregate," *Construction and Building Materials,* vol. 343, p. 128111, 2022.

[14] D. Baidzhanov, Z. S. Nuguzhinov, F. V. I and P. A. Kropachev, "Thermal insulation material based on local technogenic raw material," *Glass and Ceramics,* vol. 73, no. 11 – 12, pp. 427-430, 2016.

[15] R. Lebullenger and F. O. Mear, "Glass recycling," in *Springer Handbook of Glass*, Springer, 2019, pp. 1355-1377.

[16] C. Miao, L. Liang, F. Zhang, S. Chen, K. Shang, J. Jiang, Y. Zhang and J. Ouyang, "Review of the fabrication and application of porous materials from silicon-rich industrial solid waste," *International Journal of Minerals, Metallurgy and Materials,* vol. 29, no. 3, p. 424, 2022.

[17] Q. Ma, Q. Wang, L. Luo and F. Chaozhen, "Preparation of high strength and low-cost glass ceramic foams," *IOP,* vol. 52, no. 39, 2018.

[18] J. Zhang, X. Zhang, B. Liu, C. Ekberg, S. Zhao and S. Zhang, "Phase evolution and properties of glass ceramic foams prepared by bottom ash, fly ash and pickling sludge," *International Journal of Minerals, Metallurgy and Materials,* vol. 29, no. 3, p. 563, 2022.

[19] Q. Zipeng, G. Li, Y. Tian and M. a. P. S. Yuwei, "Numerical Simulation of Thermal Conductivity of Foam Glass Based on the Steady-State Method," *MDPI,* vol. 12, no. 1, p. 54, 2018.

[20] V. Cosmin and I. Lazău, "Glass foam from window panes and bottle glass wastes," *Central European Journal of Chemistry,* vol. 12, pp. 804-811, 2013.

[21] H. Shi, K.-q. Feng, H.-b. Wang, C.-h. Chen and H.-l. Zhou, "Influence of aluminium nitride as a foaming agent on the preparation of foam," *International Journal of Minerals, Metallurgy and Materials,* vol. 23, no. 5, p. 595, 2016.

[22] J. Li, X. Zhuang, E. Monfort, X. Querol, A. S. Llaudis, O. Font, N. Moreno, F. J. García Ten and I. Maria, "Utilization of coal fly ash from a Chinese power plant for manufacturing highly insulating foam glass: Implications of physical, mechanical properties and environmental features," *Elsevier, Construction and Building Materials,* vol. 175, p. 64–76, 2018.

[23] J. König, R. R. Petersen, Y. Yuea and D. Suvorova, "Gas-releasing reactions in foam-glass formation using carbon and MnxOy as the foaming agents," *Ceramics International,* vol. 43, no. 5, pp. 4638-4646, 2017.

[24] R. C. da Silvaa, E. T. Kubaski, E. T. Tenório-Neto, M. K. Lima-Tenório and S. M. Tebcherani, "Foam glass using sodium hydroxide as foaming agent: Study on the

reaction mechanism in soda-lime glass matrix," *Journal of Non-Crystalline Solids,* vol. 511, p. 177–182, 2019.

[25] R. Ji, Y. Zheng, Z. Zou, Z. Chen, S. Wei, X. Jin and M. Zhang, "Utilization of mineral wool waste and waste glass for synthesis of foam glass at low temperature," *Construction and Building Materials,* vol. 2015, p. 623–632, 2019.

[26] Z. Chen, H. Wang, R. Ji, L. Liu, C. Cheeseman and X. Wang, "Reuse of mineral wool waste and recycled glass in ceramic foams," *Ceramics International,* vol. 45, p. 15057–15064, 2019.

[27] C. Bai, H. Li, E. Bernardo and P. Colombo, "Waste-to-resource preparation of glass-containing foams from geopolymers," *Ceramics International,* vol. 45, pp. 7196-7202, 2019.

[28] C. Arriagada, I. Navarrete and M. Lopez, "Understanding the effect of porosity on the mechanical and thermal performance of glass foam lightweight aggregates and the influenceof production factors," *Construction and Building Materials,* vol. 228, p. 116746, 2019.

[29] J. König, V. Nemanic, M. Zumer, R. R. Petersen, M. B. Østergaard, Y. Yue and D. Suvorov, "Evaluation of the contributions to the effective thermal conductivity of an open-porous-type foamed glass," *Construction and Building Materials,* vol. 214, p. 337–343, 2019.

[30] A. Rincon, D. Desideri and E. Bernardo, "Functional glass-ceramic foams from 'inorganic gel casting' and sintering of glass/slag mixtures," *Journal of Cleaner Production,* vol. 187, pp. 250-256, 2018.

[31] G. Yuxi, Z. Yihe, H. Hongwei, M. Ke, H. Kunran, H. Pan, X. Wang, Z. Zhilei and M. Xianghai, "Novel glass ceramic foams materials based on red mud," *Ceramics International,* vol. 40, p. 6677–6683, 2014.

[32] L. Taoyong, L. Changwei, L. Jianlei, H. Lei, G. Hua, L. Cui, Z. Xin, T. Hui, Y. Qifeng and L. Anxian, "Phase evolution, pore morphology and microstructure of glass ceramic foams derived from tailings wastes," *Ceramics International,* vol. 44, p. 14393–14400, 2018.

[33] L. Taoyong, L. Changwei, L. Piao, L. Jianlei, L. Cui, H. Lei, X. Zhou, Y. Qifeng and L. Anxian, "Preparation and characterization of partially vitrified ceramic material," *Journal of Non-Crystalline Solids,* vol. 505, p. 92–101, 2019.

[34] D. Tulyaganov, H. Fernandes, S. Agathopoulos and J. Ferreira, "Preparation and characterization of high compressive strength foams from sheet glass," *Journal of Porous Material,* vol. 13, p. 33–139, 2006.

[35] L. Yang, Z. Shili, M. Shuhua, L. Chunli and W. Xiaohui, "Preparation of sintered foamed ceramics derived entirely from coal fly ash," *Construction and Building Materials,* vol. 163, p. 529–538, 2018.

[36] L. Taoyong, L. Piao, G. Xiaogang, Z. Jiashuo, H. Qianxing, L. Zhiwei, X. Zhou, Y. Qifeng, T. Yougen and L. Anxian, "Preparation, characterization and discussion of glass ceramic foammaterial: Analysis of glass phase, fractal dimension and self-foaming mechanism," *Materials Chemistry and Physics,* vol. 243, p. 122614, 2020.

[37] A. H. A., M. S. Mohammed, M. A. Arif and H. Shoukry, "Reuse of lead glass sludge in the fabrication of thermally insulating foamed glass with outstanding properties and high Pb-stabilization," *Environmental Science and Pollution Research,* vol. 29, p. 47209–47224, 2022.

[38] G. Khater, B. S. Nabawy, A. A. El-Kheshen, M. Abdel-Baki and M. Farag, "Utilizing of solid waste materials for producing porous and lightweight ceramics," *Materials Chemistry and Physics,* vol. 280, p. 125784, 2022.

[39] C. Zhai, Y. Yu, Y. Zhu, J. Zhang, Y. Zhong, J. Yeo and M. Wang, "The Impact of Foaming Effect on the Physical and Mechanical Properties of Foam Glasses with Molecular-Level Insights," *Molecules,* vol. 27, no. 3, p. 876, 2022.

[40] Y. Qi, X. Xiao, Y. Lu, J. Shu, J. Wang and M. Chen, "Cathode ray tubes glass recycling: A review," *Science of The Total Environment,* Vols. Volume 650, Part 2, pp. 2842-2849, 2019.

[41] G. Mucsi, B. CsYke, M. Kertész and L. Hoffmann, "Physical Characteristics and Technology of Glass Foam from Waste Cathode Ray Tube Glass," *Journal of Materials,* vol. 2013, p. 11, 2013.

[42] F. Méar, P. Yot, M. Cambon and M. Ribes, "The characterization of waste cathode-ray tube glass," *Waste Management,* vol. 26, no. 12, pp. 1468-1476, 2006.

[43] E. Bernardo, G. Scarinci, S. Hreglich and G. Zangiacomi, "Effect of time and furnace atmosphere on the sintering of glasses from dismantled cathode ray tubes," *Journal of the European Ceramic Society,* vol. 27, no. 2-3, p. 1637–1643, 2007.

[44] E. Restrepo, R. Widmer and M. Schluep, "Leaded glass from cathode ray tubes (CRTs): A Critical Review of Recycling and Disposal Options," United Nations University, Bonn, 2016.

[45] S. Pindar and N. Dhawan, "Characterization and recycling potential of the discarded cathode ray tube monitors," *Resources, Conservation and Recycling,* vol. 169, p. 105469, 2021.

[46] D. Jin, J. Wang, L. You, D. Ge, C. Liu, H. Liu and Z. You, "Waste cathode-ray-tube glass powder modified asphalt materials: Preparation and characterization," *Journal of Cleaner Production,* vol. 214, p. 127949, 2021.

[47] J. Iwaszko, M. Lubas, M. Sitarz, M. Zajemska and A. Nowak, "Production of vitrified material from hazardous asbestos-cement waste and CRT glass cullet," *Journal of Cleaner Production,* vol. 317, p. 128345, 2021.

[48] H. Zhao and C.-S. Poon, "Recycle of large amount cathode ray tube funnel glass sand to mortar with supplementary cementitious materials," *Construction and Building Materials,* vol. 308, p. 124953, 2021.

[49] T. Liu, S. Qin, D. Zou and W. Song, "Experimental investigation on the durability performances of concrete using cathode ray tube glass as fine aggregate under chloride ion penetration or sulfate attack,," vol. 163, pp. 634-642, 2018.

[50] H. Wei, A. Zhou, T. Liu, D. Zou and H. Jian, "Dynamic and environmental performance of eco-friendly ultra-high performance concrete containing waste cathode ray tube glass as a substitution of river sand,," *Resources, Conservation and Recycling,* vol. 162, p. 105021, 2020.

[51] W.-J. Long, Y.-c. Gu, D. Zheng and N. Han, "Utilization of graphene oxide for improving the environmental compatibility of cement-based materials containing waste cathode-ray tube glass," *Journal of Cleaner Production,* vol. 192, pp. 151-158, 2018.

[52] B. K. Brian Hilton, K. Winnebeck, C. Chandrasiri, E. Ariyachandra and S. Peethamparan, "The functional and environmental performance of mixed cathode ray tubes and recycled glass as partial replacement for cement in concrete,," *Resources, Conservation and Recycling,* vol. 151, p. 104451, 2019.

[53] W. Meng, X. Wang, W. Yuan, J. Wang and G. Songa, "The recycling of leaded glass in cathode ray tube (CRT)," *Procedia Environmental Sciences,* vol. 31, p. 954 – 960, 2016.

[54] J. König, A. Lopez-Gil, P. Cimavilla-Roman, M. A. Rodriguez-Perez, R. R. Petersen, M. B. Østergaard, N. Iversen, Y. Yue and ˇ. S. Matjaz, "Synthesis and properties of open- and closed-porous foamed glass with a low density," *Construction and Building Materials,* vol. 247, p. 118574, 2020.

[55] Ø. Martin B, R. R. Petersena, J. Königb and Y. Yue, "Effect of alkali phosphate content on foaming of CRT panel glass using Mn3O4 and carbon as foaming agents," *Elsevier, Journal of Non-Crystalline Solids,* vol. 482, pp. 217-222, 2018.

[56] M. B. Østergaard, M. Zhang, X. Shen, R. R. Petersen, J. Konig, P. D. Lee, Y. Yue and B. Cai, "High-speed synchrotron X-ray imaging of glass foaming and thermal conductivity simulation," *Acta Materialia,* vol. 189, pp. 85-92, 2020.

[57] B. Ø. Martin, R. P. Rasmus, J. König, M. Bockowski and Y. Yue, "Impact of gas composition on thermal conductivity of glass foams prepared," *Elsevier, Journal of Non-Crystalline Solids,* vol. 1, no. X 1, p. 100014, 2019.

[58] P. Tsakiridis, "Aluminium salt slag characterization and utilization – A review," *Journal of Hazardous Materials,* vol. 217–218, p. 1–10, 2012.

[59] P. Tsakiridis, P. Oustadakis and S. Agatzini-Leonardou, "Aluminium recovery during black dross hydrothermal treatment," *Journal of Environmental Chemical Engineering,* vol. 1, no. 1–2, pp. 23-32, 2013.

[60] A. Kudyba, S. Akhtar, I. Johansen and J. Safarian, "Aluminum recovery from white aluminum dross by a mechanically activated phase separation and remelting process," *The Journal of The Minerals, Metals & Materials Society (TMS),* vol. 73, no. 9, p. 2625–2634, 2021.

[61] Y. Li, Q. Ziyi, L. Chunlei, Q. Yi, W. Haibin, P. Li and W. Yi, "Hazardous characteristics and transformation mechanism in hydrometallurgical disposing strategy of secondary aluminum dross," *Journal of Environmental Chemical Engineering,* vol. 9, no. 6, p. 106470, 2021.

[62] A. Meshram, R. Jha and S. Varghese, "Towards recycling: Understanding the modern approach to recover waste aluminium dross," *Materials Today: Proceedings,* vol. 46 Part 3, pp. 1487-1491, 2021.

[63] K. V. Shailendra, K. D. Vijay and P. D. Shashi, "Utilization of aluminium dross for the development of valuable product – A review," *Materials Today: Proceedings,* Vols. Volume 43, Part 1, pp. 547-550, 2021.

[64] M. Mahinroosta and A. Allahverdi, "Hazardous aluminum dross characterization and recycling strategies: Acritical review," *Journal of Environmental Management,* vol. 223, pp. 452-468, 2018.

[65] P. Ramaswamy, P. Tilleti, S. Bhattacharjee, R. Pinto and S. A. Gomes, "Synthesis of value added refractories from aluminium dross and zirconia composites," *Materials Today: Proceedings,* vol. 22 part 4, p. 1264–1273, 2020.

[66] G. Qin, G. Qiang, L. Yongli, R. Baozeng, F. Mingbo, L. Huilin, T. Dengchao and D. Min, "Innovative technology for defluorination of secondary aluminum dross by alkali leaching," *Minerals Engineering,* vol. 172, p. 107134, 2021.

[67] A. Tripathy, S. Mahalik, C. .. Sarangi, B. Tripathy, K. Sanjay and I. Bhattacharya, "A pyro-hydrometallurgical process for the recovery of alumina from waste aluminium dross," *Minerals Engineering,* vol. 137, pp. 181-186, 2019.

[68] Z. Zhengping, L. Han, R. Li, L. Fengqin and Z. Hongliang, "A new approach to recover the valuable elements in black aluminum dross," *Resources, Conservation and Recycling,* vol. 174, p. 105768, 2021.

[69] H. Shen, B. Liu, Z. Shi, S. Zhao, J. Zhang and S. Zhang, "Reduction for heavy metals in pickling sludge with aluminum nitride in secondary aluminum dross by pyrometallurgy, followed by glass ceramics manufacture," *Journal of Hazardous Materials,* vol. 418, p. 126331, 2021.

[70] H. Lv, M. Xie, L. Shi, H. Zhao, Z. Wu, L. Li, R. Li and F. Liu, "A novel green process for the synthesis of high-whiteness and ultrafine aluminum hydroxide powder from secondary aluminum dross," *Ceramics International,* vol. 48, no. 1, pp. 953-962, 2022.

[71] H. Shen, B. Liu, C. Ekberg and S. Zhang, "Harmless disposal and resource utilization for secondary aluminium dross: A review," *Science of The Total Environment,* vol. 760, p. 143968, 2021.

[72] Q. Li, Q. Yang, G. Zhang and Q. Shi, "Investigations on the hydrolysis behavior of AlN in the leaching process of secondary aluminum dross,," *Hydrometallurgy,* vol. 182, pp. 121-127, 2018.

[73] M. Sassi and A. Simon, "Waste-to-Reuse Foam Glasses Produced from Soda-Lime-Silicate Glass, Cathode Ray Tube Glass, and Aluminium Dross," *Inorganics,* vol. 10, no. 1, p. 1, 2021.

[74] M. Sassi, J.-E. F. M. Ibrahim and A. Simon, "Characterization of foam glass produced from waste CRT glass and aluminium dross," in *Journal of Physics Conference Series*, Miskolc, 2020.

[75] A. A. El-Amir, M. A. Attia, M. Newishy, T. Fend and M. Emad, "Aluminium dross/soda lime glass waste-derived high-quality glass foam," *Journal of Materials Research and Technology,* vol. 15, pp. 4940-4948, 2021.

[76] N. Su, Z. Li, Y. Ding, H. Yang, J. Zhang and G. Fu, "Waste, Waste to Wealth Strategy: Preparation and Properties of Lightweight Al2O3-SiO2-Rich Castables Using Aluminum Dross," *Materials,* vol. 14, no. 24 , p. 7803, 2021.

[77] N. A. Roslan, S. Z. Abidina, O. U. Osazuwa, S. Y. Chin and Y. Taufiq-Yap, *International Journal of Hydrogen Energy,* vol. 46, no. 60, pp. 30959-30975, 2021.

[78] E. Elsarrag, A. Elhoweris and Y. Alhorr, "The production of hydrogen as an alternative energy carrier from aluminium waste," *Energy, Sustainability and Society,* vol. 7, p. 9, 2017.

[79] E. David and J. Kopac, "Hydrolysis of aluminum dross material to achieve zero hazardous waste," *Journal of Hazardous Materials,* vol. 209–210, pp. 501-509, 2012.

[80] P. Liu, L. Liu, Z. Zhou, Y. Li, H. Yuan, Huhetaoli and T. Lei, "Co-pyrolysis of pine sawdust with aluminum dross for immobilization of heavy metal and enhancing hydrogen generation," *Fuel,* vol. 305, p. 121597, 2021.

[81] A. Meshram, A. Jain, D. Gautam and K. K. Singh, "Synthesis and characterization of tamarugite from aluminium dross: Part I," *Journal of Environmental Management,* vol. 232, pp. 978-984, 2019.

[82] G. Scarinci, G. Brustain and E. Bernardo, "Glass Foams," in *Cellular Ceramics: Structure, Manufacturing, Properties and Applications*, M. Scheffler and P. Colombo, Eds., Freiburg, 2005, pp. 158-176.

[83] J. König, R. Rasmus and Y. Yuanzheng, "Fabrication of highly insulating foam glass made from CRT panel glass," *Ceramics International 41,* p. 9793–9800, 2015.

[84]  M. Davraz, ·. K. M., A. A. E., Ş. Kılınçarslan, Y. E. Delikanlı and M. Çabuk, "An investigation of foaming additives and usage rates in the production of ultra-light foam glass," *Journal of Thermal Analysis and Calorimetry,* vol. 147, p. 3567–3576, 2022.

[85]  Y. Liu, J. Xie, P. Hao, Y. Shi, Y. Xu and X. Ding, "Study on Factors Affecting Properties of Foam Glass Made from Waste Glass," *Journal of renewable materials,* vol. 9, no. 2, pp. 237-253, 2021.

[86]  O. Corning, "FOAMGLAS," 2020. [Online]. [Accessed 1 May 2022].

[87]  S. M. El-Haggar, "Sustainability of Municipal Solid Waste Management," in *Sustainable Industrial Design and Waste Management*, 2007, pp. 149-196.

[88]  S. S. Owoeye, G. O. Matthew, F. O. Ovienmhanda and S. O. Tunmilayo, "Preparation and characterization of foam glass from waste container glasses and water glass for application in thermal insulations," *Ceramics International,* vol. 46, no. 8, p. 11770–11775, 2020.

[89]  J. Zhang, B. Liu, S. Zhao, H. Shen, J. Liu and S. Zhang, "Preparation and characterization of glass ceramic foams based on municipal solid waste incineration ashes using secondary aluminum ash as foaming agent," *Construction and Building Materials,* vol. 262, p. 120781, 2020.

[90]  M. B. Østergaard, M. Zhang, X. Shen, R. R. Petersen, J. König, P. D. Lee, Y. Yue and B. Cai, "High-speed synchrotron X-ray imaging of glass foaming and thermal conductivity simulation," *Acta Materialia,* vol. 189, pp. 85-92, 2020.

[91]  y. I. Illés, M. Sassi, H. Zakiyya and T. Kékesi, "Fluoride Salts from Secondary Aluminium DrossThe Fundamental Kinetic Characteristics of Aqueous Dissolution of Chloride and," in *International Multidisciplinary Scientific Conference* , Miskolc, 2019.

[92]  "C-THERM TCi," [Online]. Available: https://ctherm.com/products/tci_thermal_conductivity/how_the_tci_works/mtps/.

[93]  "Glass Viscosity Calculation," [Online]. Available: https://glassproperties.com/viscosity/. [Accessed 1 November 2021].

[94]  I. Ben Kacem, L. Gautron, D. Coillot and D. R. Neuville, "Structure and properties of lead silicate glasses and melts," *Chemical Geology,* vol. 461, pp. 104-114, 2017.

[95]  E. M. M. Ewais, M. A. Attia, A. A. El-Amir, A. M. Elshenway and T. Fend, "Optimal conditions and significant factors for fabrication of soda lime glass foam from industrial waste using nano AlN,," *Journal of Alloys and Compounds,* vol. 747, pp. 408-415, 2018.

[96]  H. Scholze, Glass, Springer, 1991.

[97]  H. Shi, K.-q. Feng, H.-b. Wang, C.-h. Chen and H.-l. Zhou, "Influence of aluminium nitride as a foaming agent on the preparation of foam," *International Journal of Minerals, Metallurgy and Materials,* vol. 23, no. 5, p. 595, 2016.

[98] J. König, R. R. Petersen and Y. Yue, "Influence of the glass–calcium carbonate mixture's characteristics on the foaming process and the properties of the foam glass," *Journal of the European Ceramic Society,* p. 1591–1598, 2014.

[99] J. Cotton, "AZO Material," [Online]. Available: https://www.azom.com/article.aspx?ArticleID=1389.

[100] H. G. Pfaender, Schott guide to glass, London: Chapman and Hall, 1996.

[101] T. Mays, "A new classification of pore sizes," *Studies in Surface Science and Catalysis,* vol. 160, pp. 57-62, 2007.

[102] B. D. Zdravkov, J. J. Cermak, M. Sefara and J. Janku, "Pore classification in the characterization of porous materials: A perspective," *Central european journal of chemistry,* vol. 5, no. 2, p. 385–395, 2007.

[103] H. M. King, "Mohs Hardness Scale," [Online]. Available: https://geology.com/minerals/mohs-hardness-scale.shtml.

[104] C. Mavrogonatos, P. Voudouris, J. Berndt, S. Klemme, F. Zaccarini, P. Spry, V. Melfos, A. Tarantola, M. Keith, R. Klemd and K. Haase, "Trace Elements in Magnetite from the Pagoni Rachi Porphyry Prospect, NE Greece: Implications for Ore Genesis and Exploration," *Minerals,* vol. 725, p. 9, 2019.

[105] O. J. o. t. E. Communities, "COUNCIL DECISION: 19 December 2002, establishing criteria and procedures for the acceptance of waste at landfills pursuant to Article 16," 2003.

[106] D. Aurora López, T. Hanan, P. Carlos, A. Francisco José and A. L. Félix, "A hazardous waste from secondary aluminium metallurgy as a new raw material for calcium aluminate glasses," *Journal of Hazardous Materials ,* 2009.

[107] M. Mostafa and A. Ali, "Enhanced alumina recovery from secondary aluminum dross for high purity nanostructured alumina powder production: Kinetic study," *Journal of Environmental Management,* 2018.

[108] T. Kekesi, "Characterization and complete utilization of aluminium melting dross," 2018.

[109] M. Bensharada, R. Telford, B. Stern and V. Gaffney, "Loss on ignition vs. thermogravimetric analysis: a comparative study to determine organic matter and carbonate content in sediments," *J Paleolimnol ,* p. 191–197, 2022.

[110] "Impact of glass from cathode ray tubes (CRT) in achieving the WEEE recycling and recovery targets," WEEE Forum, 2018.
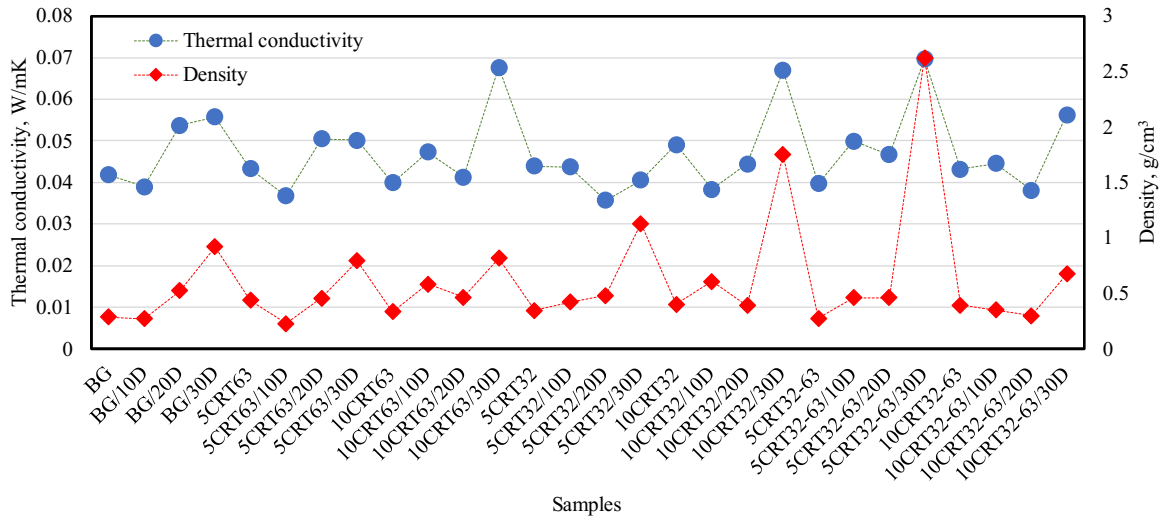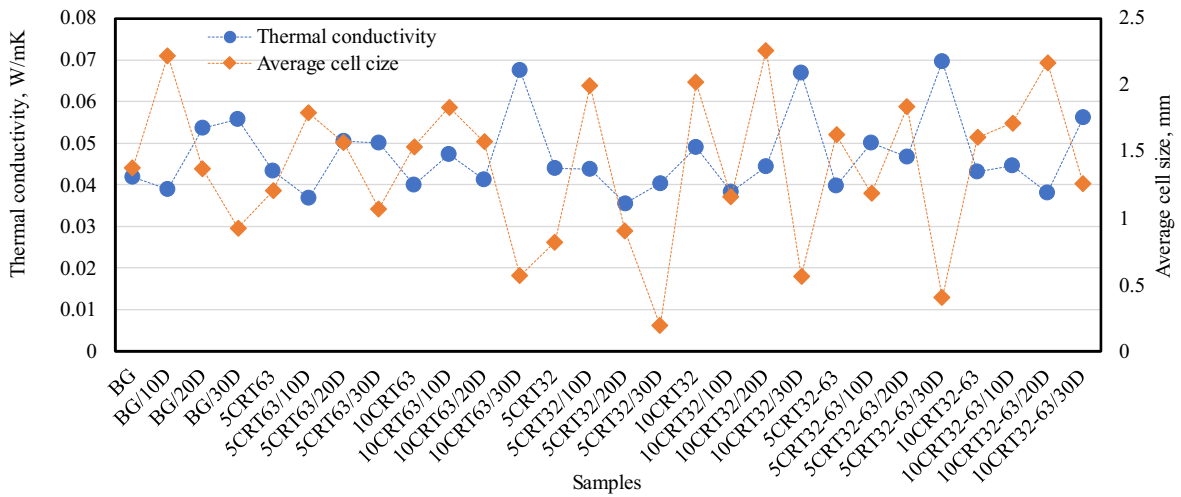
# Annex A
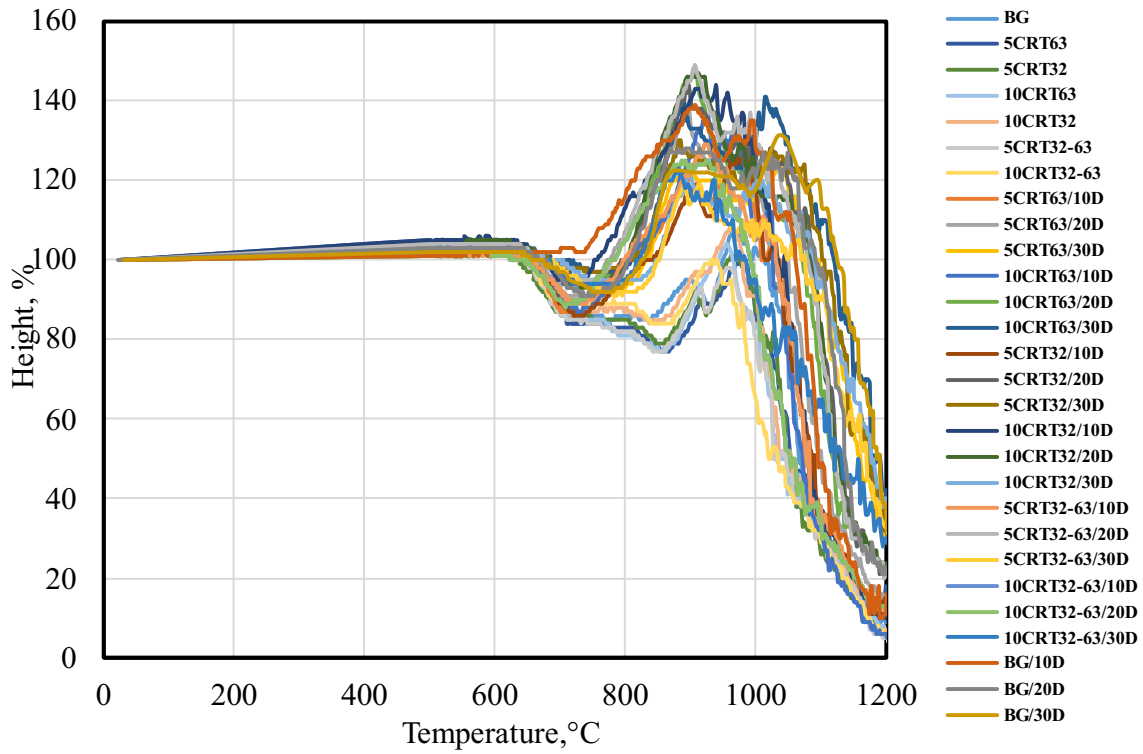


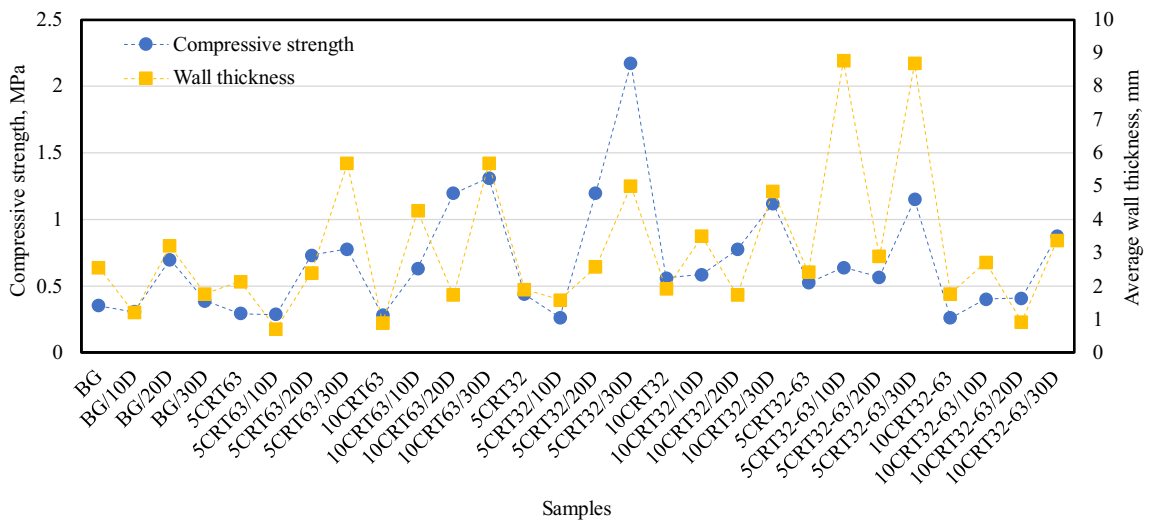**Figure A1.** Heating microscopy of the mixtures
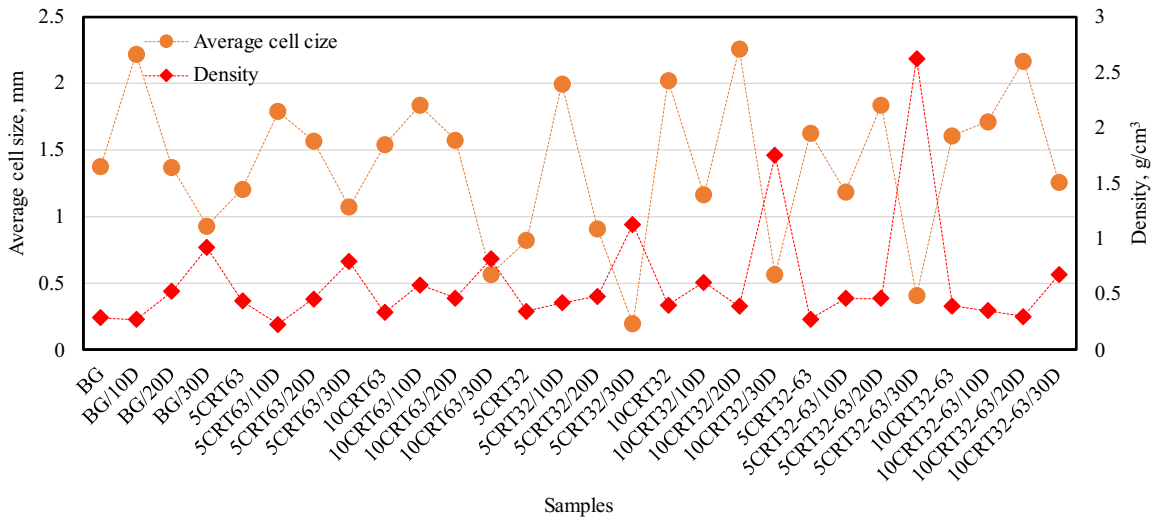


**Figure A2.** Average cell size versus Density of the foam glass

**Figure A3.** Thermal conductivity versus density of the foam glass
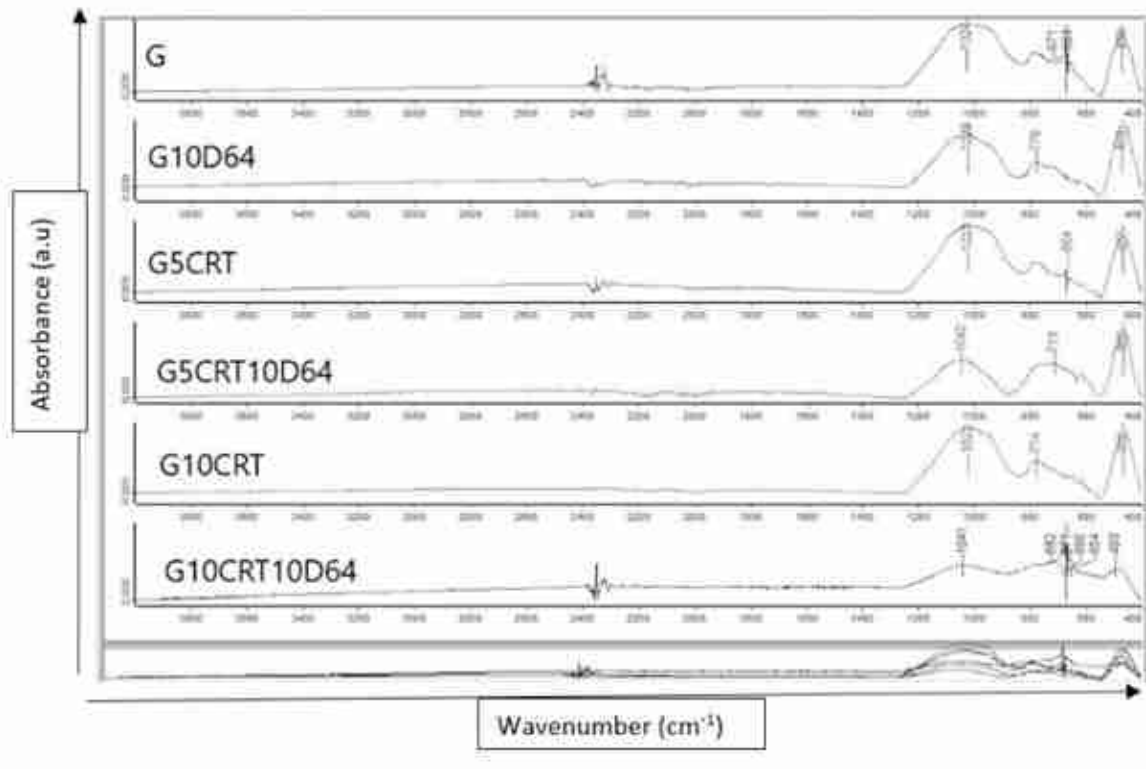


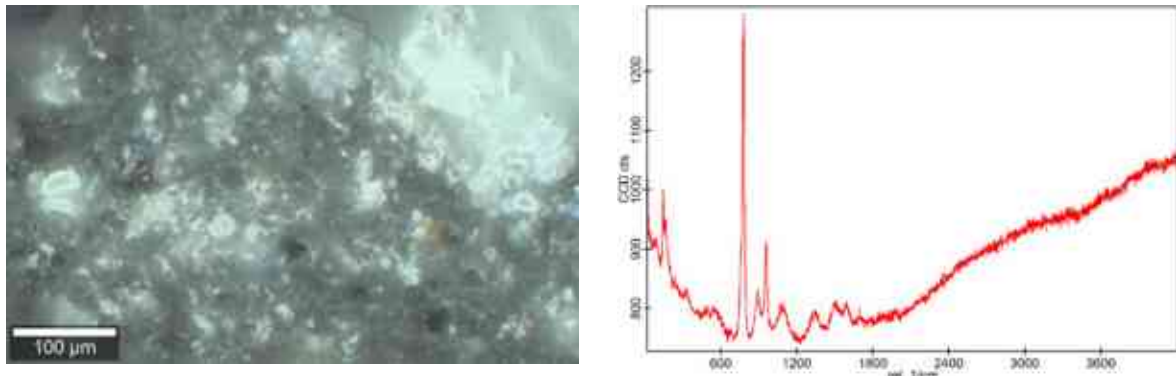**Figure A4.** Thermal conductivity versus average cell size of the foam glass



**Figure A5.** Compressive strength versus average wall thickness of the foam glass

# Annex B



**Figure B1.** Fourier transform-infrared (FTIR) spectra of foam glass



**Figure B2.** Raman spectra of sample with 20 wt dross type 64

**Table B1.** Apparent porosity, open and closed porosity of the samples

| Name | Absorption | Apparent ρ | ρ (g/cm³) | ρ_p (g/cm³) | Total φ | Closed φ | Open φ |
|---|---|---|---|---|---|---|---|
| G | 15.43 | 0.17 | 0.32 | 2.26 | 92.33 | 46.22 | 46.11 |
| G10D64 | 270.74 | 0.16 | 1.35 | 2.53 | 93.65 | 5.56 | 88.09 |
| G15D64 | 286.80 | 0.17 | 1.60 | 2.25 | 92.39 | 3.10 | 89.29 |
| G20D64 | 339.85 | 0.15 | 1.62 | 2.20 | 93.11 | 2.46 | 90.66 |
| G5CRT | 13.30 | 0.17 | 0.34 | 2.15 | 91.90 | 42.82 | 49.08 |
| G5CRT10D64 | 322.80 | 0.16 | 0.48 | 2.59 | 93.74 | 27.81 | 65.93 |
| G5CRT15D64 | 303.91 | 0.16 | 1.82 | 2.19 | 92.56 | 1.52 | 91.05 |
| G5CRT20D64 | 277.08 | 0.17 | 1.58 | 2.92 | 94.29 | 4.81 | 89.48 |
| G10CRT | 35.13 | 0.18 | 0.45 | 2.48 | 92.92 | 31.70 | 61.22 |
| G10CRT10D64 | 24.10 | 0.17 | 0.46 | 2.16 | 91.94 | 29.33 | 62.61 |
| G10CRT15D64 | 46.31 | 0.18 | 0.56 | 2.34 | 92.42 | 24.29 | 68.14 |
| G10CRT20D64 | 101.21 | 0.19 | 0.82 | 2.75 | 93.00 | 16.52 | 76.48 |
| G10DX | 178.66 | 0.17 | 1.18 | 2.42 | 93.16 | 7.20 | 85.97 |
| G15DX | 215.21 | 0.17 | 1.18 | 2.23 | 92.31 | 6.80 | 85.51 |
| G20DX | 300.62 | 0.19 | 1.22 | 2.48 | 92.35 | 7.87 | 84.47 |
| G5CRT10DX | 121.04 | 0.17 | 0.81 | 2.18 | 92.07 | 13.51 | 78.56 |
| G5CRT15DX | 42.72 | 0.19 | 0.65 | 2.61 | 92.78 | 21.67 | 71.12 |
| G5CRT20DX | 262.77 | 0.18 | 1.32 | 2.56 | 92.94 | 6.64 | 86.30 |
| G10CRT10DX | 23.82 | 0.20 | 0.40 | 2.55 | 92.22 | 41.30 | 50.92 |
| G10CRT15DX | 22.31 | 0.20 | 0.76 | 2.58 | 92.23 | 18.52 | 73.72 |
| G10CRT20DX | 34.84 | 0.22 | 1.20 | 2.12 | 89.74 | 7.95 | 81.79 |
| G10D53 | 184.37 | 0.18 | 1.65 | 2.30 | 92.31 | 3.04 | 89.27 |
| G15D53 | 328.16 | 0.17 | 0.48 | 2.48 | 92.99 | 28.94 | 64.05 |
| G20D53 | 294.70 | 0.19 | 2.14 | 2.29 | 91.80 | 0.57 | 91.23 |
| G5CRT10D53 | 15.62 | 0.19 | 0.31 | 2.48 | 92.27 | 54.05 | 38.22 |
| G5CRT15D53 | 49.20 | 0.19 | 0.45 | 2.56 | 92.70 | 34.23 | 58.48 |
| G5CRT20D53 | 167.29 | 0.19 | 0.54 | 2.50 | 92.21 | 28.55 | 63.66 |
| G10CRT10D53 | 20.34 | 0.19 | - | 2.60 | 92.57 | - | - |
| G10CRT15D53 | 39.94 | 0.20 | 0.86 | 2.49 | 92.09 | 14.84 | 77.25 |
| G10CRT20D53 | 174.72 | 0.20 | 1.61 | 3.27 | 93.95 | 6.29 | 87.66 |
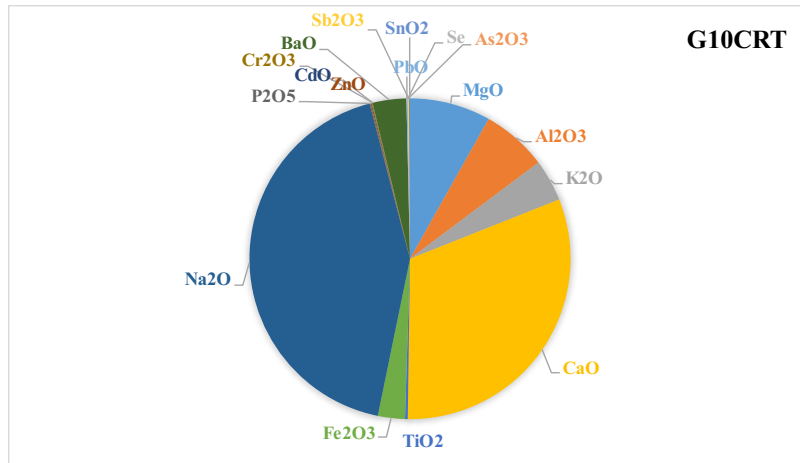
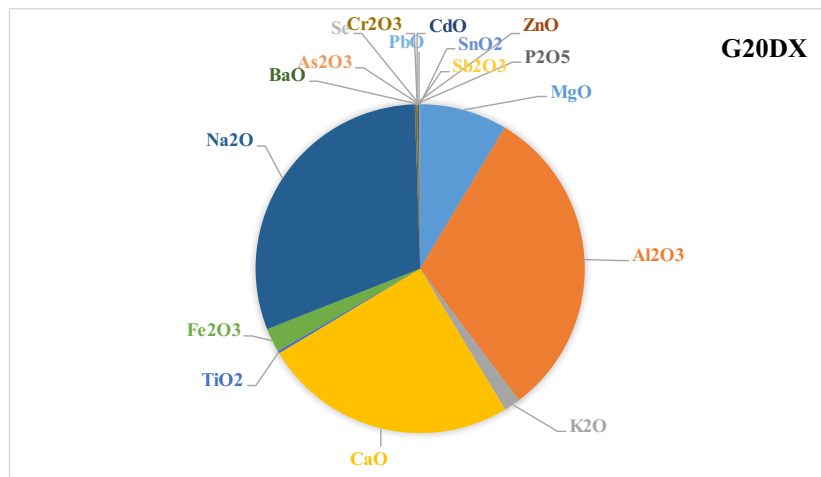**Figure B3.** Oxide content of foam glass made of container glass 10 wt CRT
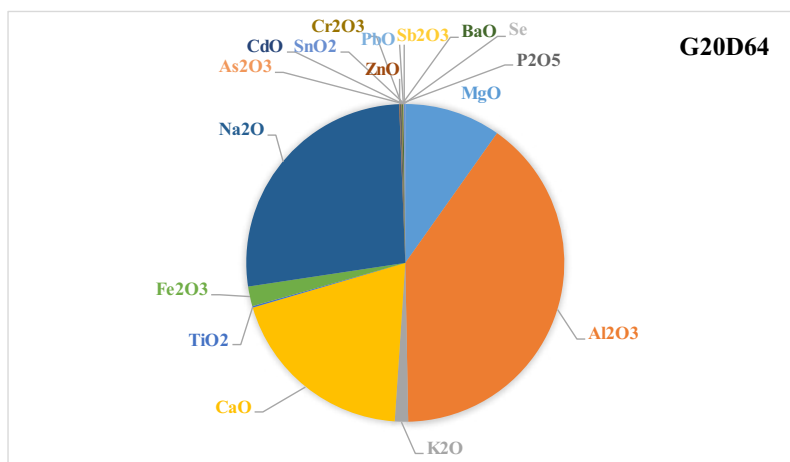


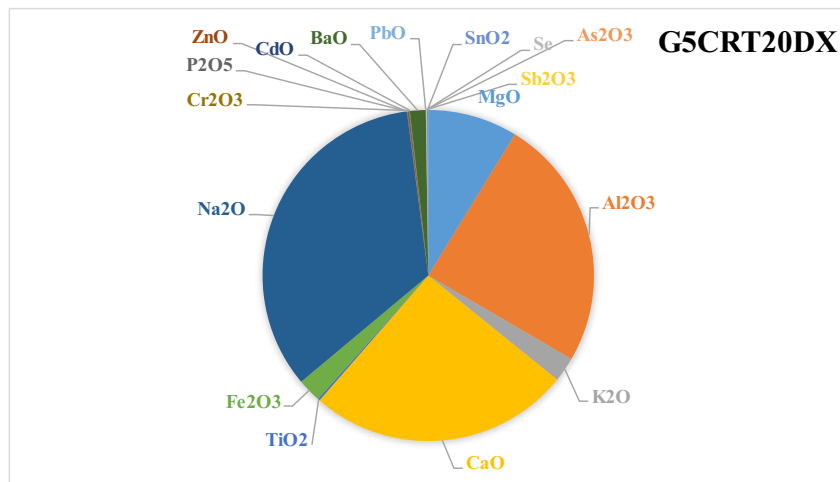**Figure B4.** Oxide content of foam glass made of container glass and 20 wt dross 64
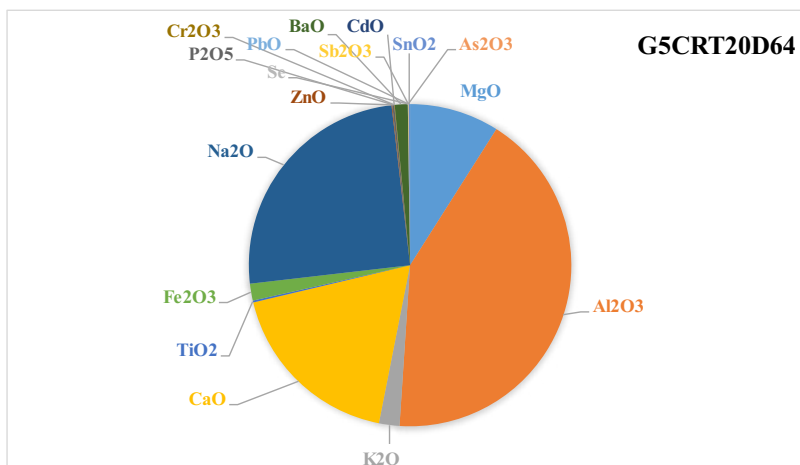


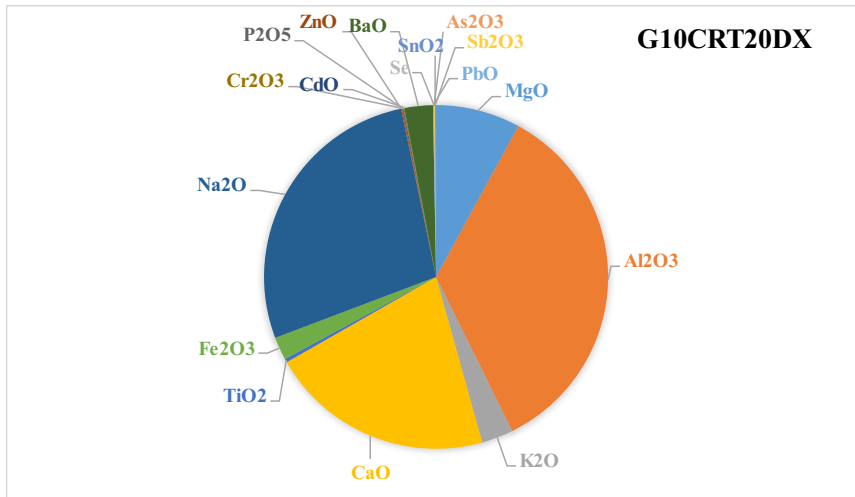**Figure B5.** Oxide content of foam glass made of container glass, 5 wt CRT, and 20 wt dross 64
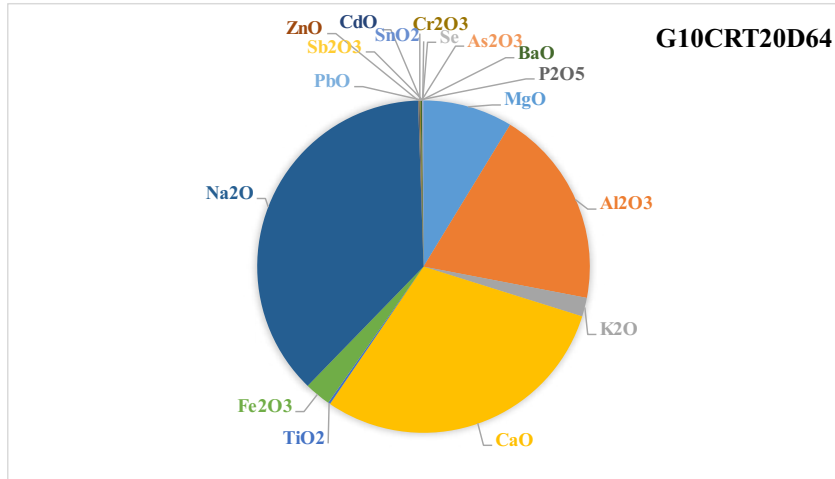
**Figure B6.** Oxides content of foam glass made of container glass, 10 wt CRT, and 20 wt dross 64



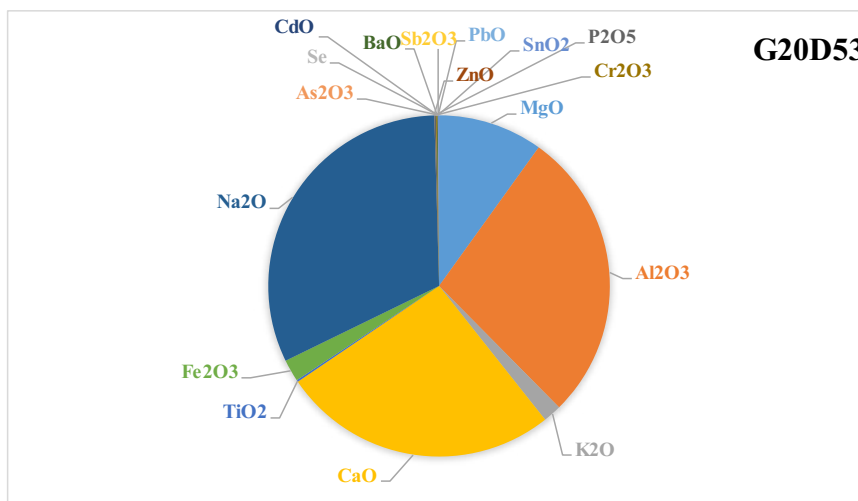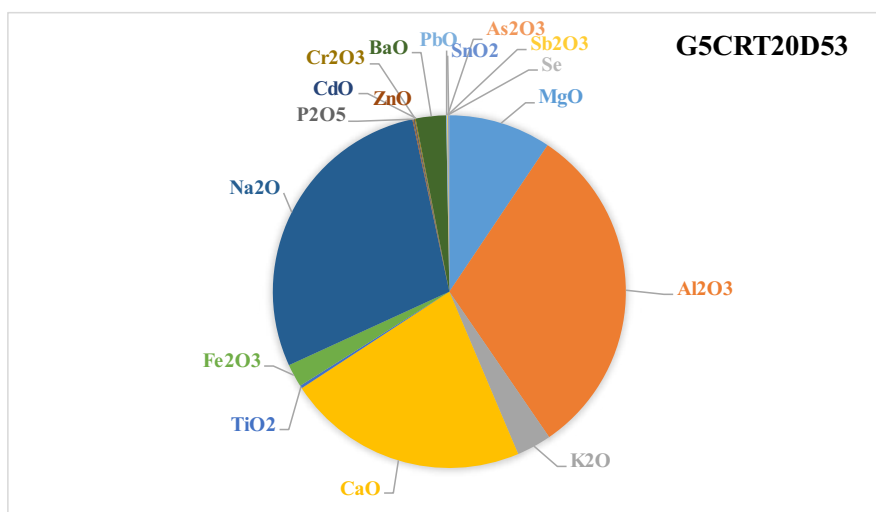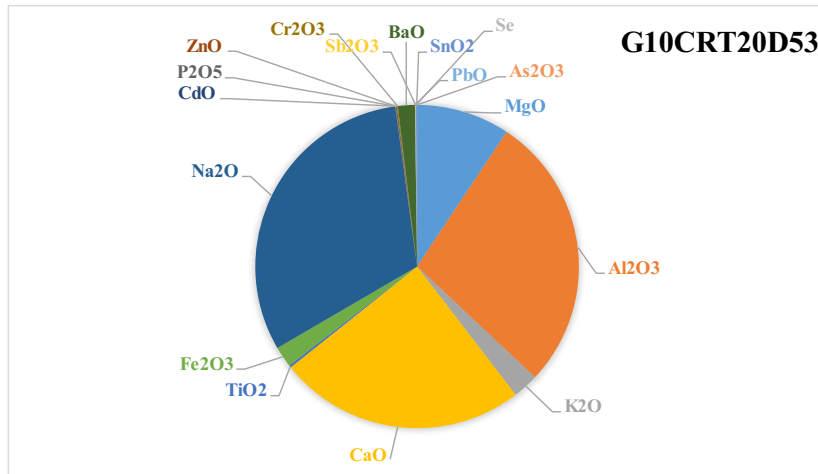**Figure B7.** Oxide content of foam glass made of container glass and 20 wt dross X



**Figure B8.** Oxide content of foam glass made of container glass, 5 wt CRT, and 20 wt dross X

**Figure B9.** Oxide content of foam glass made of container glass, 10 wt CRT, and 20 wt dross X



**Figure B10.** Oxide content of foam glass made of container glass and 20 wt dross 53



**Figure B11.** Oxide content of foam glass made of container glass, 10 wt CRT, and 20 wt dross 53

**Figure B12.** Oxide content of foam glass made of container glass, 10 wt CRT, and 20 wt dross X
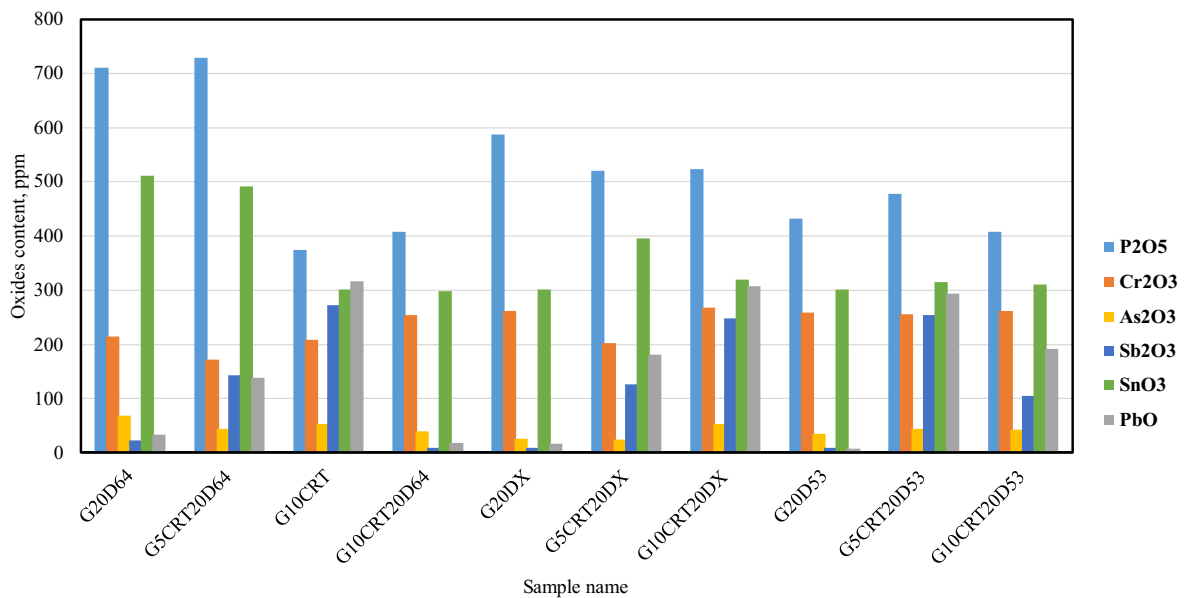


**Figure B13.** Hazardous oxides in the foam glass

**Table B2.** Limit value for non-hazardous waste [105]

| Elements | L/S = 2 l/kg | L/S = 10 l/kg | $C_0$ (Percolation test) |
|---|---|---|---|
| | mg/kg dry substance | mg/kg dry substance | mg/l |
| As | 0.4 | 2 | 0.3 |
| Ba | 30 | 100 | 20 |
| Cd | 0.64 | 1 | 20 |
| Cr | 4 | 10 | 2.5 |

| | | | |
|---|---|---|---|
| Cu | 25 | 50 | 30 |
| Hg | 0.05 | 0.2 | 0.03 |
| Mo | 5 | 10 | 3.5 |
| Ni | 5 | 10 | 3 |
| Pb | 5 | 10 | 3 |
| Sb | 0.2 | 0.7 | 0.15 |
| Se | 0.3 | 0.5 | 0.2 |
| Zn | 25 | 50 | 15 |
| Cl | 10000 | 15000 | 8500 |
| F | 60 | 150 | 40 |
| S | 100000 | 20000 | 7000 |
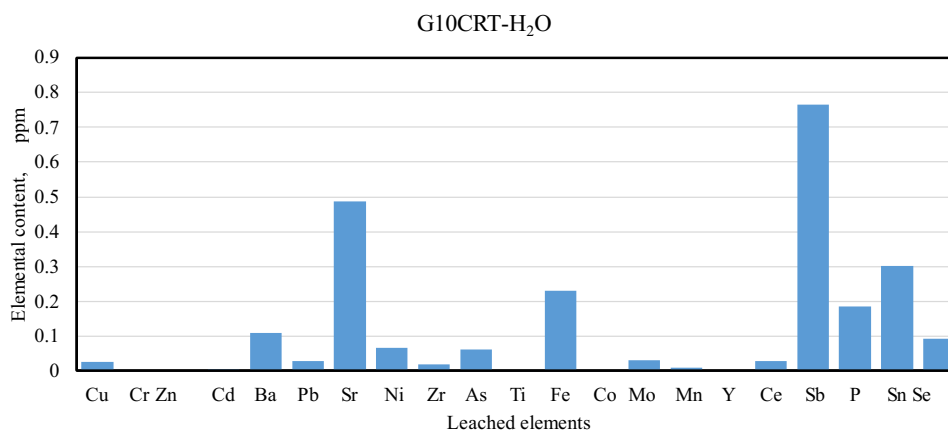


**Figure B14.** The leaching behaviour in water of the sample containing container glass and 10 wt% CRT
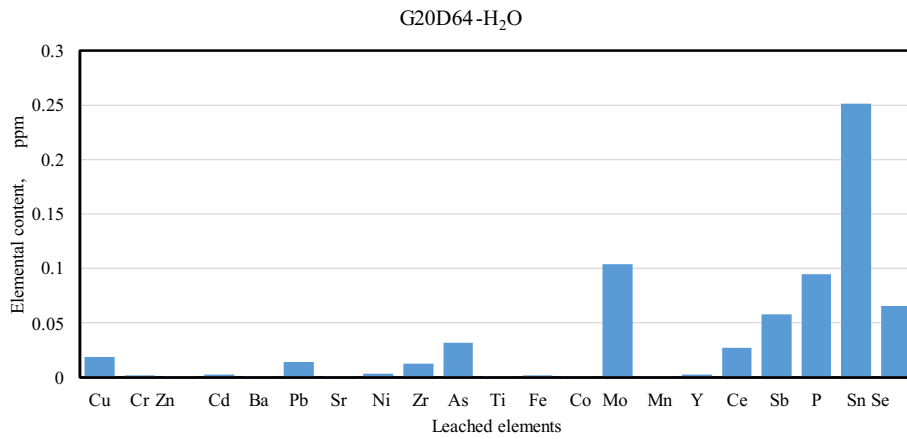
**Figure B15.** The leaching behaviour in water of the sample containing container glass and 20 wt% dross type 64
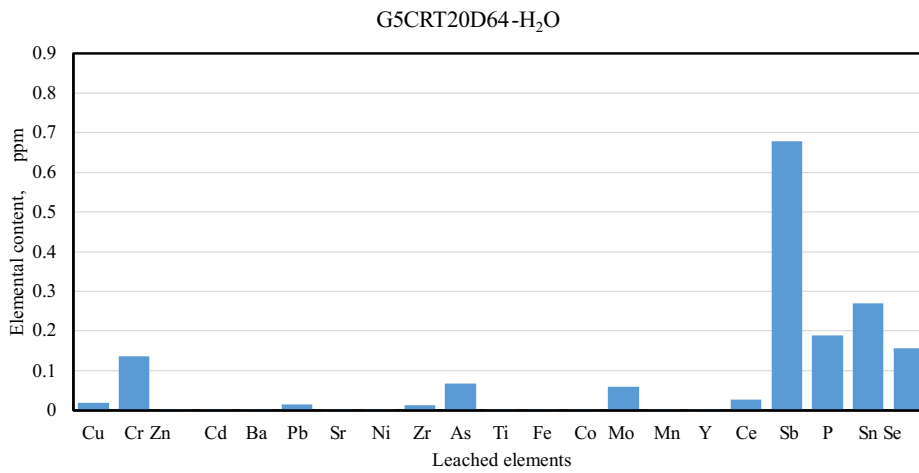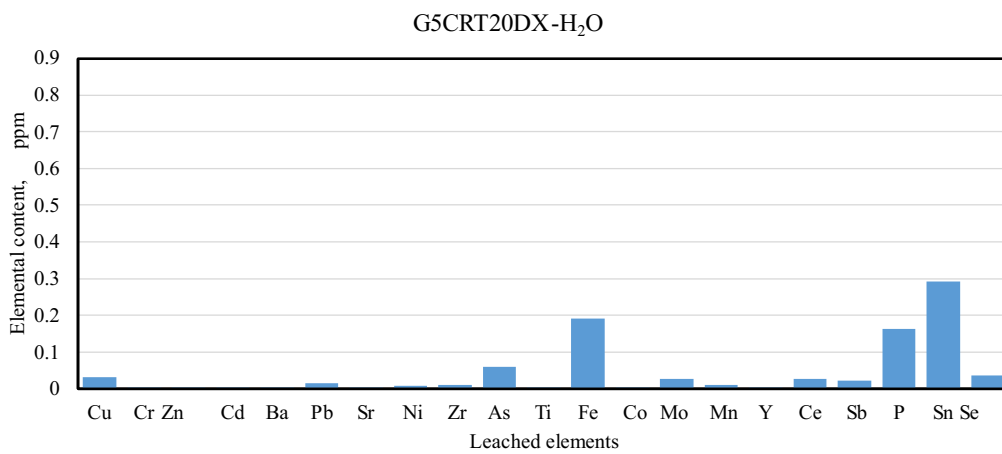


**Figure B16.** The leaching behaviour in water of the sample containing container glass, 5 wt CRT glass and 20 wt% dross type 64
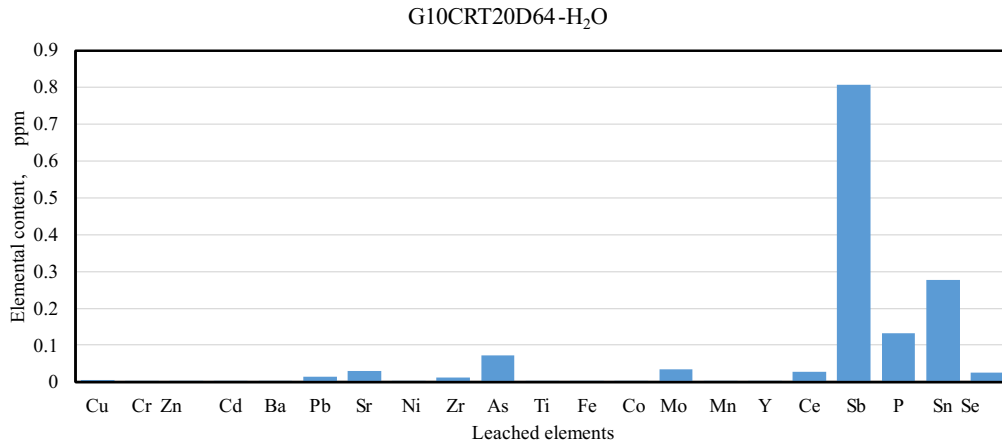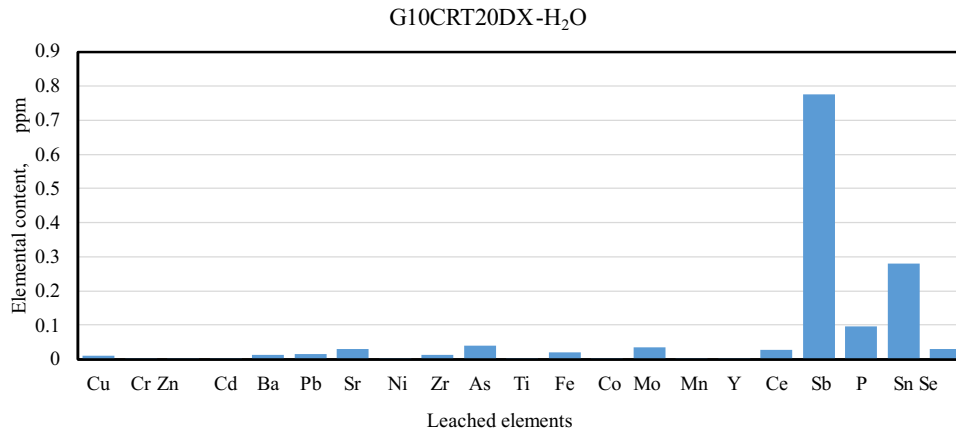
**Figure B17.** The leaching behaviour in water of the sample containing container glass, 10 wt CRT glass and 20 wt% dross type 64
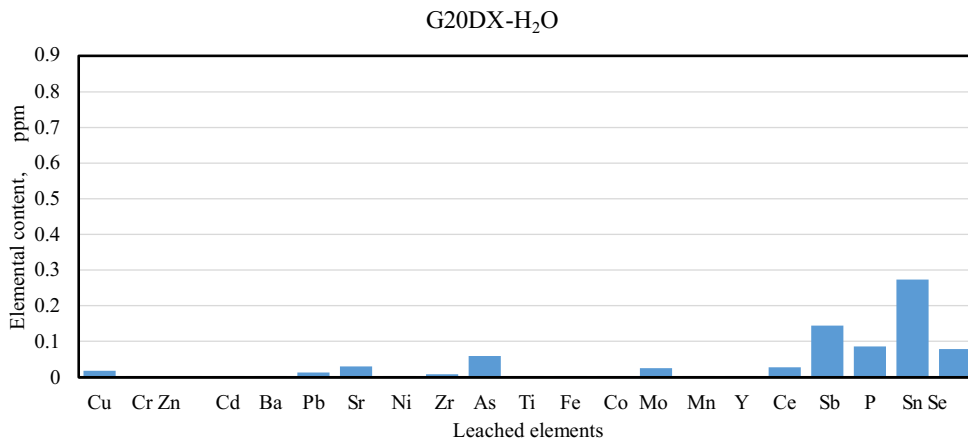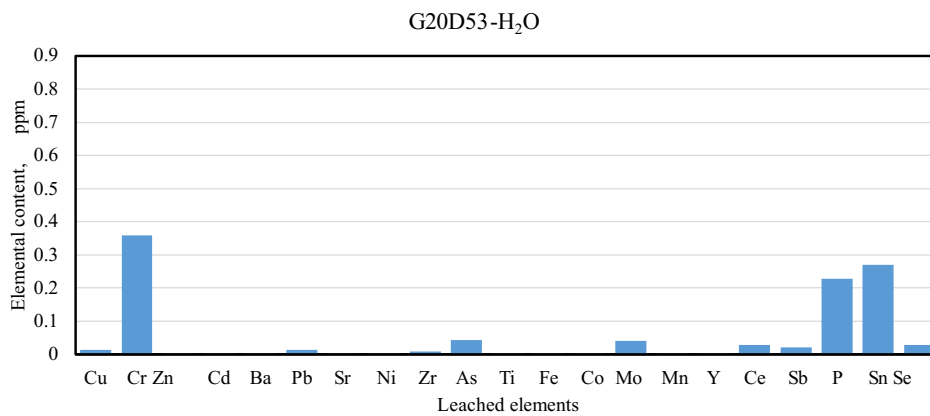


**Figure B18.** The leaching behaviour in water of the sample containing container glass and 20 wt% dross type X
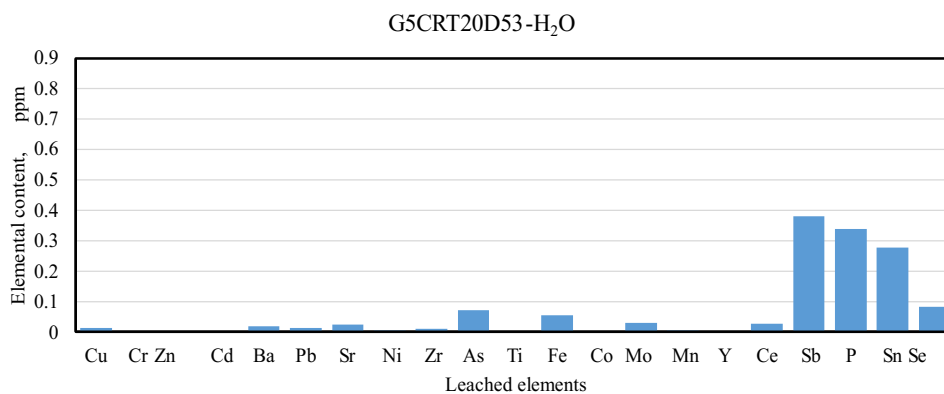


**Figure B19.** The leaching behaviour in water of the sample containing container glass, 5 wt CRT glass and 20 wt% dross type X
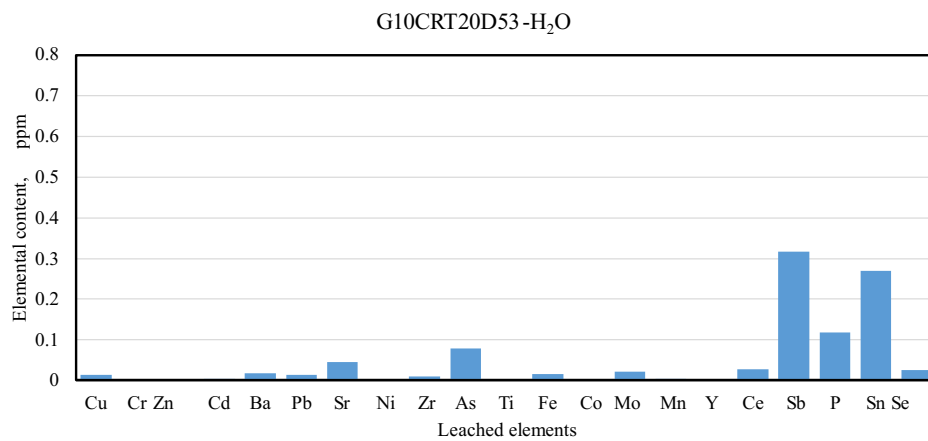
**Figure B20.** The leaching behaviour in water of the sample containing container glass, 10 wt CRT glass and 20 wt dross type X



**Figure B21.** The leaching behaviour in water of the sample containing container glass and 20 wt% dross type 53



**Figure B22.** The leaching behaviour in water of the sample containing container glass, 5 wt CRT glass and 20 wt% dross type 53

**Figure B23.** The leaching behaviour in water of the sample containing container glass, 10 wt% CRT glass and 20 wt dross type 53